FACULTY OF SCIENCE
UNIVERSITY OF COPENHAGEN

New PAT tools for assessing content uniformity, sampling error, and degree of crystallinity in pharmaceutical tablets

PhD thesis 2014 · Solveig Warnecke

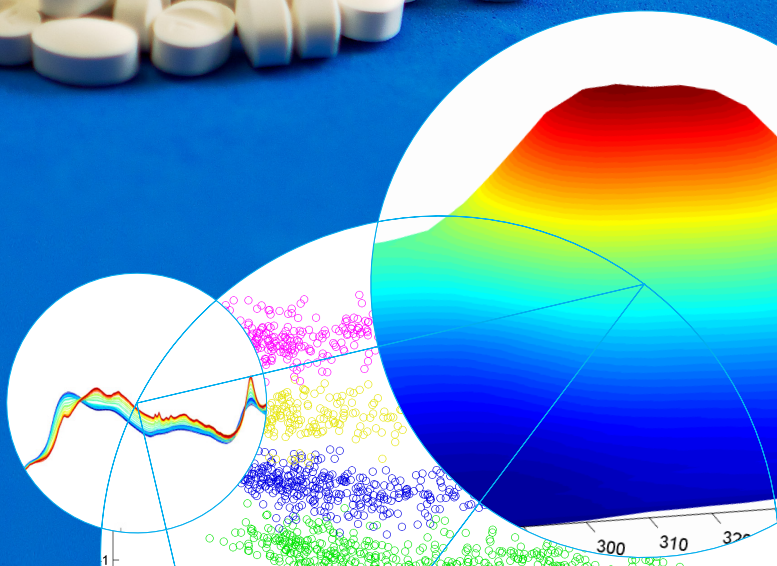

New PAT tools for assessing content uniformity, sampling error, and degree of crystallinity in pharmaceutical tablets

PhD thesis 2014

Solveig Warnecke

Title
New PAT tools for assessing content uniformity, sampling error,
and degree of crystallinity in pharmaceutical tablets

Submission
October 9th 2013

This thesis has been submitted to the PhD School of The Faculty of Science,
University of Copenhagen

Defense
January 6th 2014

Supervisors
Main supervisor:
Associate Professor Åsmund Rinnan,
Department of Food Science, Faculty of Science, University of Copenhagen

Co-supervisors:
Professor Søren Balling Engelsen,
Department of Food Science, Faculty of Science, University of Copenhagen

Morten Allesø, PAT Specialist,
Biologics and Pharmaceutical Science, H. Lundbeck A/S

Opponents
Lecturer J. Axel Zeitler,
Department of Chemical Engineering and Biotechnology,
University of Cambridge, United Kingdom

Erik Skibsted,
Principal Scientist, Novo Nordisk, Denmark

Associate Professor Thomas Skov,
Department of Food Science, Faculty of Science, University of Copenhagen, Denmark

Cover illustration
Tablet picture with permission from Damon Kasacjak

ISBN 978-87-7611-701-6

Printed by SL grafik, Frederiksberg C, Denmark (www.slgrafik.dk)

Preface

This thesis is the outcome of collaborative work between Quality & Technology (Q&T, Department of Food Science, Faculty of Science, University of Copenhagen), and an industrial partner, H. Lundbeck A/S. This PhD study is funded by the Danish Ministry of Science, Technology and Innovation through the QbD consortium (www.qbd.dk). The aim of the studies included in this thesis is to investigate different new PAT tools for pharmaceutical applications.

These studies have given me the opportunity to explore PAT in the pharmaceutical field and expand my knowledge within spectroscopy and chemometrics. During the project I have been in contact with many different collaborators, without them I would not have been able to accomplish my goals.

I will like to thank my supervisors: Åsmund Rinnan, Søren Balling Engelsen from University of Copenhagen and Morten Allesø from H. Lundbeck A/S. Furthermore, I will like to thank the employees at H. Lundbeck A/S at Valby and Lumsås sites who kindly helped with the production of tablets and supporting measurements.

Thanks to Jukka Rantanen and his group Pharmaceutical Technology and Engineering (Department of Pharmacy, University of Copenhagen), for providing expertise and facilities for production of the spray dried material. Special thanks to Jian X. Wu, for his help and support during this project, for many helpful discussions, and finally for proofreading this thesis.

Thanks to Peter Uhd Jepsen and Tianwu Wang (Terahertz Technologies and Biophotonics, Department of Photonics Engineering, Technical University of Denmark, DTU) for help with the terahertz experimental setup and support.

To my colleagues at Q&T, I will send thanks for enjoyable times, talks, and lunches. Great thanks should go to my office mate, Lina Noubariene, with whom I shared many warmhearted talks and discussions.

Furthermore, I will like to thank my family for support, and my brother Christian for acute programming help. Finally, I will thank my husband Damon and our son Erik for their understanding and support during times of hard work.

Solveig Warnecke
Frederiksberg, October 2013

Abstract

The pharmaceutical industry faces considerable challenges due to an increasing complexity of products, greater competition in the generic drug arena, and higher regulatory demands to ensure safe and effective pharmaceutical products. Process analytical technology (PAT) tools can provide knowledge of the pharmaceutical drug, both during development and throughout the production. The usage of PAT tools is encouraged by the regulatory authorities, and therefore the interest in new and improved PAT tools is increasing. The main purpose of introducing Quality by Design (QbD) and PAT in pharmaceutical production is to introduce innovation in the full scale production and to continuously increase the knowledge of the pharmaceutical processes, products, and how they relate to each other, so it is possible to produce pharmaceutical products at a high and consistent quality. This gives benefits to the consumer, the regulatory authorities, and the pharmaceutical manufacturers.

The PAT tools include a wide range of disciplines, including process analyzers (e.g. spectroscopic sensors), multivariate statistical analysis (e.g. chemometric data treatment), process control, continuous improvement, and knowledge management. The real advantage of PAT tools lay in the combination of the different disciplines. This could be spectroscopy-based process analyzer that monitors the pharmaceutical product including latent factors that could influence on the final product quality. Chemometric data treatment can then be used to extract the relevant information from the data, and process control can ensure low variation in the final product quality. This can help to optimize the production, allow real-time product release, and potentially replace the expensive, destructive, and time consuming laboratory testing that is currently the standard practice in traditional pharmaceutical industry.

In this thesis, three spectroscopic PAT tools are investigated, near-infrared-, terahertz-, and fluorescence- spectroscopy. These techniques have been evaluated with chemometrics and theory of sampling. The first study focused on the critical but rather overlooked sampling uncertainty that exist in all analytical measurements. The sampling error was studied using an example involving near infrared transmission (NIT) spectroscopy to study content of uniformity of five batches of escitalopram tablets, produced at different active pharmaceutical ingredients (API) concentrations and at different hardness (compression force) levels. The aim of this study was to investigate the influence of sample orientation, powder segregation, and compression force on the NIT spectra. Therefore, samples were taken at different production time points, at different compression forces, and measured with the spectrometer in different orientations. The study showed that a minimum of 18 tablets from each level of API concentrations (90 spectra in total) were required to establish a robust NIT calibration. Further, it was shown that the spectra from tablets with the scored line facing upwards gave better calibrations than those tablets in which the scored line were facing downwards. However, the largest fraction of the variation between spectra was found when moving the tablet in the tablet sampler. The NIT data was also used to show variable reduction in the API calibration development, which eliminated spectral interference from moisture uptake by the tablets dur-

ing storage. It was possible to improve the prediction error of the quantitative API model considerately by spectral variable selection.

The second study investigated the potential use of terahertz time domain spectroscopy (THz-TDS) to quantify crystallinity in binary mixtures of amorphous and crystalline lactose, and this technique was compared to near infrared (NIR) spectroscopy. THz-TDS gave higher cross validated errors than NIR spectroscopy for both full concentration and low concentration range models.

The third study investigated the use of fluorescence spectroscopy to simultaneously predict two APIs in a tablet formulation: flupentixol (FLU) in low dosage (0.208-0.625 % w/w free base) and melitracen (MEL) (4.17-12.5 % w/w free base). Despite internal quenching between the ingredients and the two APIs, it was possible to establish calibrations using partial least squares regression (PLS) on unfolded fluorescence landscapes with relative errors of 9.1 % for FLU and 4.1 % for MEL, respectively.

Both fluorescence spectroscopy and terahertz time domain spectroscopy are new tools in pharmaceutical applications and the possibilities and limitations, in relation to the abundant NIR spectroscopy, is discussed.

PAT tools can together with Quality by Design contribute to important product and process knowledge that is valuable for optimizing production methods and in the development of new pharmaceuticals.

Sammendrag

Den farmaceutiske industri har store udfordringer i form af øget komplexitet af produkterne, øget konkurrence i forbindelse med patentudløb, samt skærpede myndighedskrav til kvaliteten af lægemidler. *Process analytical technology* (PAT) værktøjer kan give ny viden om lægemidler, såvel under udvikling som i produktionen. Myndighederne opfordrer til at benytte PAT værktøjer, og interessen for implementering af PAT værktøjer er stigende. Hovedformålet med at introducere *Quality by Design* (QbD) og PAT i den farmaceutiske produktion er løbende at hæve vidensniveauet for processerne, produkterne og deres interne påvirkninger, således at det er muligt at producere høj og vedvarende kvalitet. Dette giver fordele til forbrugere, myndigheder og producenter af farmaceutiske lægemidler.

PAT værktøjer omfatter et vidt spænd af discipiner, inklusiv procesmåleudstyr (f.eks. spektroskopiske sensorer), multivariante statististiske analyser (f.eks. kemometrisk databehandling) proces styring, løbende forbedringer og vidensstyring. Den virkelige fordel ved PAT opstår ved kombinationen af de forskellige discipiner. Dette kunne være et spektroskopisk baseret måleudstyr, der overvåger det farmaceutiske produkt inklusiv faktorer, som kunne influere på slutproduktets kvalitet. Kemometrisk databehandling kan derefter benyttes til at ekstrahere den relevante information fra data, og processtyring kan bruges til at sikre en lav variation i slutproduktets kvalitet. Dette kan hjælpe til at optimere produktionen og potentielt erstatte dyre, destruktive og tidskrævende laboratorieanalyser, som på nuværende tidspunkt er standard praksis i den traditionelle farmaceutiske industri.

I denne afhandling er der undersøgt tre spektrosopiske PAT værktøjer: nærinfrarød-, terahertz-, og fluorescensspektroskopi. Disse metoder er evalueret med kemometri og samplingsteori. Det første studie fokuserer på det vigtige, men ofte oversete prøveudtagningsusikkerhed der forekommer ved alle analysemetoder. I studiet demonstreres brugen af den velkendte nærinfrarød transmitans (NIT) spektroskopi til bestemmelse af aktivt indhold i fem produktioner af escitalopram tabletter, produceret med forskellige koncentrationer af det aktive farmaceutiske ingredients (API) og med forskellige brudstyrker (komprimeringstryk). Formålet med dette studie var at undersøge inflydelsen af prøveretningen i instrumentet, pulver segregering, samt komprimeringstrykket på NIT spektrene. Derfor blev der taget prøver ud på forskellige tidspunkter i produktionen, ved forskellige komprimeringstryk, og prøverne blev præsenteret for spektrofotometret i forskellige retninger. Mindst 18 spektre fra hver API koncentrationsniveau (90 spektra i alt) var nødvendige for at skabe en robust NIT kalibrering. Desuden blev det vist, at kalibreringer, der benyttede spektre fra tabletter med delkærven vendt opad gav bedre resultater end hvis tabletterne vendte nedad. Den største spektrale variation blev dog fundet, så snart tabletten blev flyttet i tabletholderen. NIT datasættet blev også benyttet til at vise at variabelselektion kan elimerere spektral inteferens fra vandoptag i tabletterne under lagring af prøverne. Dermed var det muligt at forbedre prædiktionsfejlen på den kvantitative API model betydeligt ved at benytte udvalgte bølgelængdeområder.

Det andet studie undersøger brugen af terahertz tidsdomæne spektroskopi (THz-TDS) til at kvantificerere krystallinitet i binære blandinger af amorft og krystallinsk laktose, sammenholdt med nærinfrarød spektroskopi (NIR). THz-TDS gav højere krydsvalideringsfejl end NIR både i det fulde koncentrationsområde og det lave koncentrationsområde.

Det tredie studie viser hvordan fluorescens spektroskopi kan benyttes til samtidig prædiktion af to APIer i en tablet formulering: flupentixol (FLU) i lav dosis (0.208-0.625 vægt % fri base) og melitracen (MEL) (4.17-12.5 vægt % fri base). På trods af intern *quenching* mellem ingredienterne og de to aktive stoffer, var det muligt at skabe kalibreringer ved brug af *partial least squares regression* (PLS) på udfoldede fluorescenslandskaber med relativ fejl på 9.1 % for FLU samt 4.1 % for MEL.

Fluorescensspektroskopi er et nyt værktøj til farmaceutiske applikationer, hvormed fordele og ulemper, i forhold til NIR bliver diskuteret.

PAT værktøjer kan sammen med QbD give vigtig produkt- og procesviden, som er værdifuld for procesoptimering samt ved udvikling af nye lægemidler.

List of publications included in this thesis

Paper I

S. Warnecke, Å. Rinnan, M. Allesø & S.B. Engelsen, Measurement of active content in escitalopram tablets by a near infrared transmission spectroscopy model that encompasses batch variability.
Journal of Pharmaceutical Sciences (2013), **12**(4), 1268-1280.

Paper II

S. Warnecke, Å. Rinnan, M. Allesø & S.B. Engelsen, Using interval-PLS to eliminate spectral moisture interference from a quantitative near infrared calibration model on pharmaceutical tablets.
Submitted

Paper III

S. Warnecke, J.X. Wu, Å. Rinnan, M. Allesø, F.v.d. Berg, P. U. Jepsen & S.B. Engelsen, Quantifying crystalline α-lactose monohydrate in amorphous lactose using terahertz time domain spectroscopy and near infrared spectroscopy.
Submitted

Paper IV

S. Warnecke, Å. Rinnan, M. Allesø & S.B. Engelsen, Quantification of two active pharmaceutical ingredients in a tablet formulation using fluorescence spectroscopy.
Submitted

Abbreviations and notations

API: active pharmaceutical ingredient
ATR: attenuated total reflection
CQA: critical quality attribute
CMA: critical material attribute
CPP: critical process parameter
CU: content uniformity
DC: direct compression
DoE: design of experiments
DSC: differential scanning calorimetry
EEM: excitation-emission matrices
FLU: flupentixol
FTIR: Fourier transformation infrared
GEE: global estimation error
GI: gastrointestinal
GMP: good manufacturing practice
HPLC: high performance liquid chromatography
ICH: International Conference on Harmonization
iPLS: interval partial least squares regression
IR: infrared
LIF: laser-induced fluorescence
LOD: limit of detection
LOQ: limit of quantification
LV: latent variable
MEL: melitracen
MCC: microcrystalline cellulose
MIR: mid infrared
MSC: multiplicative scatter correction
NCE: new chemical entities
NIR: near-infrared
OOS: out of specifications
PARAFAC: parallel factor analysis
PAT: process analytical technology
PC: principal component
PCA: principal component analysis
PCR: principal component regression
PE: polyethylene
PLS: partial least squares regression
Ppb: parts per billion
RSD: relative standard deviation

RTRT: real time release testing

QbD: quality by design

QbT: quality by testing

QTPP: quality target product profile

RMSEP: root-mean-square-error of prediction

RMSECV: root-mean-square-error of cross-validation

SEM: scanning electron microscopy

SMCC: silicified microcrystalline cellulose

SNV: standard normal variate

TAE: total analytical error

THz: terahertz

THz-TDS: terahertz time domain spectroscopy

TOS: theory of sampling

TPI: terahertz pulse imaging

TPP: target product profile

TPQP: target product quality profile

TSE: total sampling error

XRPD: x-ray powder diffraction

Notations

$\mathbf{X}$ matrix

$\mathbf{x}$ vector

x scalar

$\bar{x}$ average of population

Table of Contents

1 Introduction

1.1 Motivation

The pharmaceutical industry is facing challenges with increased competition due to increased sale of generic products and less capital/resource to invest in the development of new chemical entities (NCEs) [79]. This gives an increased demand for pharmaceutical products to reach the market faster and being more cost effectively produced. The health of the public depends on having access to safe, effective, and affordable medicine. Between 2004 and 2011 there have been reported, on average, one recall per month in the United States [168], which can have implications for the patients and can be very expensive for the manufacturer. Besides the cost of the recall procedure, the company can also lose business due to a tarnished reputation. The pharmaceutical industry is, compared to other industries, behind in production efficiency and quality. IBM [79] reported that for a typical pharmaceutical manufacturer, the reject percentage ranges from 5-10 % compared to 0.0001 % in the semiconductor industry. To ensure the quality of the pharmaceuticals large amounts of resources are used on testing the products. By implementing the appropriate Quality by Design (QbD) approach, a successful top-end pharmaceutical company could reach a level with less than 1 % failure. Thereby the top 30 pharmaceutical companies could save approximately US$10 billion per year [79]. The bottom line is that there is plenty of room for improvement and Process Analytical Technology (PAT) and QbD-based decision-making can pave the way for better efficiency and profit. For a long time, the innovation in pharmaceutical manufacturing and quality assurance has been slowed down due to stringent regulatory constraints, which allowed little room for changes. Unlike many other industries (food, chemical, petroleum, polymer), the pharmaceutical industry is under heavy regulatory scrutiny [153]. However, regulatory initiatives worldwide as the United States Food and Drug Administration (FDA) guidance: "GMPs for the 21st century" [41] and "PAT – A framework for innovative Pharmaceutical Manufacture and Quality Assurance" [43], and International Conference of Harmonization (ICH) published guidelines [74-78] have strongly encouraged the use of PAT, which as a direct consequence, has increased the curiosity for knowledge and usage of the PAT tools [29].

The main purpose for introducing QbD and PAT in pharmaceutical production is to implement consistent product quality disregard of the raw material and process variation. With these techniques it is possible to continuously increase the knowledge of the pharmaceutical processes, products, and how they relate to each other. Then it is possible to produce pharmaceutical products at a high and consistent quality [43]. This should give benefits to the consumer since improved quality and cost competitive products can be released to the market sooner. Likewise, the regulatory authorities should benefit from a simpler documentation system, and finally, it should give the pharmaceutical company a competitive edge in the form of better quality, faster time-to-market, and lower production costs (e.g. lower waste and less scrap).

Pharmaceutical production can roughly be divided into two parts, the chemical synthesis (primary manufacturing) of the active pharmaceutical ingredient (API), and the formulation where the API is converted into the final product (secondary manufacturing). This thesis has mainly focused on the formulation process and to a lesser extent the synthesis process. The usage of PAT tools in the synthesis part of pharmaceutical production is very similar to the usage of PAT in the chemical industry, whereas the formulation part of the production is closer to the challenges in the food industry [153].

During process development or process design, the cost of modifying the design grows drastically with time. This means that if something needs to be changed, it is better that it happens earlier than later in the design phase. Modifications to a process design can, and will often, cause new changes, which can lead to increase in development time, which in turn can lead to longer time-to-market [1]. There is also an extra challenge for the pharmaceutical manufacturer, as a change in existing manufacturing equipment or process can take up to two years to be approved by the regulatory authorizes [79]. Ideally, PAT tools should be implemented during the process development phase for process understanding [43] and later in the full scale production for process monitoring.

1.2 Scope of the thesis

The aim of this thesis is to demonstrate examples of applying PAT tools to pharmaceutical tablet products to determine critical quality attributes (CQA). The PAT tools should potentially be used in a full scale process environment. It is thus important that the method is non-invasive, fast, robust, accurate, selective, and sensitive, which is why the methods will be evaluated from these criteria.

This thesis work has led to four research manuscript/papers which will form the central part of the thesis. **Paper I** looks at the sampling issues when using of the well-established near infrared transmission (NIT) spectroscopy to study content uniformity of five batches of escitalopram tablets produced at different drug concentration and at different hardness (compression force) levels. The aim of this paper was to investigate the influence of sample orientation, powder segregation and compression force on the NIT spectra. Therefore samples were taken at six different production time points, at three different compression forces, and presented to the spectrometer in four different orientations measured in triplicate.

Paper II is a short communication which is a further evaluation of the same NIT escitalopram data set in paper I. The paper shows how variable reduction in the API calibration development can eliminate interference for moisture uptake by the tablets during storage.

Paper III investigates the use of terahertz time domain spectroscopy (THz-TDS) to quantify crystallinity in binary mixtures of amorphous and crystalline lactose. The use of terahertz spectroscopy to quantify low levels of crystallinty is compared to the performance of near infrared (NIR) spectroscopy.

Paper IV demonstrates how fluorescence spectroscopy can be used to simultaneously predict two APIs in a tablet formulation: flupentixol (FLU) in low dosage and melitracen (MEL). Fluorescence spectroscopy is a new tool in pharmaceutical applications and possibilities and limitations, in relation to the abundant NIR spectroscopy, is discussed.

2 Pharmaceutical development and manufacturing

The purpose of drugs is to prevent or cure diseases in humans, and animals. The activity of a drug is the effect on the subject, where the potency is the quantitative effect. Drugs act by interfering with biological processes, so no drug is completely safe [164].

Drug products come in many variations: Liquids (e.g. for injections and cough syrups), semi-liquids (e.g. crème and lotions), and solid dosage form (e.g. tablets, capsules, powders).

The solid dosage forms are the most used delivery forms and can be formulated as hard and soft capsules, chewable tablets or gum, pastille and effervescent tablets (dissolved in water before drinking). Furthermore, tablets can take many sizes and shapes, and come with or without coating, and with or without functional layers. In functional layers, it is possible to control the rate or site of drug delivery, e.g. target the delivery of a drug to a specific organ [4;21].

2.1 Solid state forms

Polymorphs share the same liquid state, but form different crystalline structure in solid forms [12]. It has been shown that about 80 % of active pharmaceutical ingredients (API) have polymorphs [55]. The crystal form with the lowest Gibbs free energy is the thermodynamically most stable form, all other forms are metastable. The most stable form also means the least soluble. There can easily be a 2-4 fold higher apparent solubility of a metastable form than the most stable form [66]. It is important for the pharmaceutical companies to conduct a thorough polymorph screening, as polymorphism can affect properties as dissolution rate, apparent solubility, bioavailability, and manufacturability [26]. Furthermore, it is important to identify the polymorphs for the purpose of protecting intellectual properties.

An amorphous form may have short-range molecular order (i.e. in relationship to neighboring molecules) like the crystalline form, but unlike its crystalline form, it has no long-range order of molecular packing [175]. The amorphous form typically has poor physical stability, but has a much higher apparent solubility and enhanced dissolution. The fact that many APIs are poorly water soluble, has increased the interest for stabilization and formulation of amorphous compounds [173;175].

API solid state can change during processing or storage, which may affect drug stability, dissolution rate, flow, mechanical properties, and ability to mix with excipients. The amorphous form of a drug has the lowest melting point and the fastest dissolution rate, but it is more likely to react or chemical degrade [127].

There are many ways to produce amorphous material; quench cooling of material, rapid precipitation by antisolvent addition, milling, freeze-drying and spray-drying [175]. The stability of amorphous compounds depends on the method of preparation, and therefore there

are different characteristics for poly-amorphous solids [123]. Otsuka et al. [123] found that when producing amorphous indomethacin by quench cooling, a more irregular molecular network was created compared to slower cooling or ball milling production.

The characterization of the solid state form, (e.g. if the API exits as amorphous or crystalline state) can be done by several different techniques that usually observe changes in physical properties as density, viscosity, heat capacity or X-ray diffraction behavior. Often used is the fact that lack of long-range molecular order gives irregular diffraction of X-ray radiation. This will in X-ray powder diffraction (XRPD), be seen as a halo compared to the diffraction pattern of crystalline forms [65]. The quantification limit of crystalline structure by XRPD is usually around 5 % [65]. Another used method for characterization of amorphous form, is the presence of a glass transition temperature (T_g) determined by differential scanning calorimetry (DSC) [65].

Amorphous lactose has quite different physical properties compared to its crystalline form. The compaction behavior of amorphous lactose is improved and that has led to lactose being one of the most popular amorphous materials used in the pharmaceutical industry, in direct compression operations [105;145]. At high humidity, amorphous lactose can absorb water and this leads to the transformation to the more thermodynamically stable α-lactose monohydrate (30 %) and β-lactose anhydrate (70 %), which can result in problems during formulation, processing, and storage [145].

2.2 Tablet manufacturing

Most drugs are formulated as a solid dosage form and the delivery mainly occur by the oral route [96]. Given orally, tablets will undergo disintegration and dissolution followed by absorption through the gastrointestinal (GI) tract. Tablet is one of the most popular solid dosage form due to ease of administration, compliance, low manufacturing costs, and improved chemical and microbiological stability, when compared to liquid dosage forms [21].

Figure 2.1 shows a general overview of a tablet production, where the API is mixed/lubricated with excipients are compressed, coated and packed. If necessary, due to processing problems (e.g. poor flowability) of the API, a granulation step will be performed prior to the mixing with excipients. Furthermore, a milling step to reduce the particle size can also occur prior to the mixing.

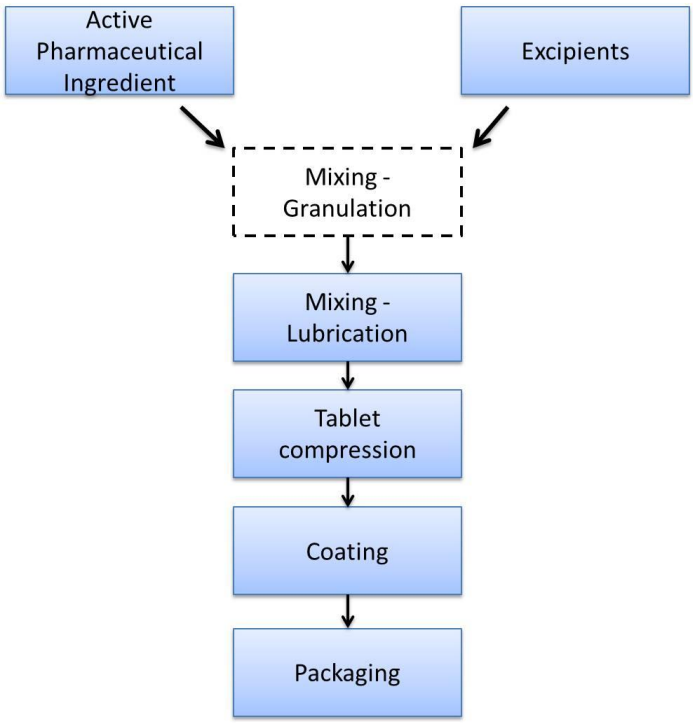

Figure 2.1: Overview of pharmaceutical production of tablet. Granulation will mainly be used if the material does not have sufficient flow and/or compression properties for direct tableting.

2.3 Important characteristics of tablets

The critical quality attributes (CQAs, see chapter 3) for tablets can be uniformity of API content, stability of the API and the formulation, and dissolution [21]. There are a number of factors that can influence these criteria, and some are listed in Table 1.

Table 1: Important factors to pharmaceutical formulation, modified from Lee [96]

Particle shape
Particle size distribution
Solid geometry (packing, density, porosity, void)
Surface characteristics (adsorption, area, surface energy, solubility)
Chemical stability
Dynamics (flow rate, transport)
Dose/drug load
Particle separation
Processing (sieving, sedimentation, grinding, mixing, compaction)

As particle size of the API is reduced, specific surface area is increased, which has a large impact on mixing and API dissolution, and finally impact on the APIs bioavailability [166].

Smaller particles will increase the electrostatic forces and can cause aggregation, whereas larger particles can cause a greater weight variation of the finished tablet. The ideal size range is typically 10-150 μm [96], but this depends on the dose and drug load. The particle size is of great importance to the homogeneity of the powder and finally the tablet. Powders with wide particle distribution are more likely to be heterogeneous. Smaller particles will move through the voids of the bigger particles and migrate to the lower region of the powder mix, also called percolation. Extremely fine particles, on the other hand, will during mixing, be forced upward by turbulent air and form a layer on top. Therefore, wide particle distribution will have a high probability of segregation [96].

The particle size can easily vary in incoming batches (e.g. of excipients). Therefore, there are strict specifications for particle size and distribution of both API and excipients [144]. Particle size can be lowered through milling when it is desired to achieve:

1. higher dissolution rate of a poorly soluble API, by increasing the surface of the particle
2. better possibilities for a homogenous mixture of excipients and API
3. increase flowability

Milling can, though, change the particles, e.g. make them amorphous and thereby change the solubility, stability, and compactiblity [144].

Powder flowability describes how well material is transported through equipment (e.g. through the hopper of a tableting machine). If there is a poor flow in the mix, the feed of the mix into the die will be inconsistence, which will cause higher tablet weight variability, and then lead to failure with tablets out of specification (OOS) on weight or content uniformity (CU) [5]. Smaller particle sizes can lead to problems in filling containers and dies, which can cause high tablet weight variation and unacceptable blend uniformity [96]. Higher particle sizes give better flowabilities, to a certain degree. Free flowing particles, particles typically with particle size of 100-200 μm, can freely move through a container with a narrow orifice [144].

Flowability affects the mixing, granulation, compression, and transportation of powder [5]. There are many factors that affect flowability: purity, crystallinity, electrostatic forces, mechanical properties, density, moisture content, specific surface area, particle-wall interaction, and the particle shape [96]. For example, spherical particles are better flowing than irregular ones. Spherical particles are often obtained by spray drying [8], high shear and fluid bed granulation. Flowing is increased by addition of glidant – such as talc or silicon dioxide, by lowering the friction in the matrix during compression, which improves the tablet dose and mass variation. The powder mixture has to be at least partly coated with the glidant to lower the cohesion of the mixture. The amount depends on the particle size [144].

Cohesion is the binding force between particles, whereas adhesion is binding force between particles and equipment (e.g. the container wall). Typically, particles in the size range from 10-100 μm are weak cohesive, whereas particles < 10 μm can be strongly cohesive. Cohesion depends on environmental conditions and the porosity, as the binding forces increase if the powder is compressed. Cohesive powder will not willingly fill a container, as the binding forces (van der Waals, electrostatic, surface absorbed moisture) are greater than that

of gravity. The van der Waals forces increase with smaller particle size. This results in increased cohesion, which gives less free flowing powder [144].

The hygroscopicity of the material is also very important, as water can cause increased weight and degradation of the API or excipients. Even though water is taken up by the excipient, the water could potential interact with the API, and thereby cause changes in physical stability [96].

2.4 Excipients

It is very rare that an API can be used directly and administrated by itself, therefore excipients are added [89]. The purpose of the excipients is to deliver the API in the right form and dose to the target site [164].

The physicochemical properties as apparent solubility, stability, metabolism, and bioavailability of the API can be varied by the excipients [96].
The main functions of the excipients are to ensure [68]:

1. The drug product has a shape and size that is easy for the patient to handle.
2. That the API is optimally adsorbed by the patient.
3. That the drug has acceptable shelf life.
4. That the drug has acceptable taste and odor.
5. Manufacturability of the API.

In Table 2 is shown an overview of different types of excipients for tablet production, their function, and some examples of excipients. Some excipients can have more than one function, e.g. microcrystalline cellulose (MCC) works as both a diluent, binder and as a disintegrant [21].

Table 2: Excipients for tablet production, their functions and examples [8;21;96].

Excipient	Function	Examples
Filler/diluent	Increase the bulk volume of the formulation	Lactose, sucrose, microcrystalline cellulose
Binder (granulation agent)	To cause agglomeration of the powdered drug and excipients e.g. in the granulation process	Polyvinyl pyrrolidone, starch, cellulose derivates
Anti-adherents, glidant or lubricants	To assist in the smooth tableting process, reduce friction between tablets and die walls	Magnesium stearate, talc, corn starch
Disintegrating agent	To promote the tablet to disintegrate in-vivo.	Starch, sodium starch glycollate, cross-linked povidone, modified cellulose
Coating agent	To improve stability, control release, target release and enhance appearance	Sucrose, film formers, acacia, gelatin, flavors, colorants

2.5 Milling

Milling is often used to reduce the particle size of the material, agglomerates or compacted material. It can be used to increase the apparent solubility of the API, giving a better mixing between API and excipients and enhance the flowability of the material. There exist many

different types of equipment for milling e.g. ball mill, pin mill, jet mill, hammer mill and cryo mill (milling during cooling). The choice depends on the materials mechanical and elastic properties, and the desired properties of the end material e.g. particle size and distribution [144; 116]. Milling can, though, intentionally, or unintentionally, change the crystalline form to an amorphous form [96].

2.6 Mixing or blending

The purpose of mixing is to ensure that all dosage units get equal amounts of API. It is not completely possible to get the exact same amount in practice, but the aim is to get as low a variation as possible [144]. Mixing of powders is more difficult than mixing of liquids (of similar polarity) and will never become as homogenous as liquids [144].

Most pharmaceutical powders consist of mixtures of materials with different physical properties; particle size, particle shape, density, and surface area. This can lead to segregation, where particles with similar properties tend to collect together in the same section of the powder. When a powder prone to segregation is mixed, the powder will first become more homogenous, but with extended mixing time it will deblend [96]. Even though, powder blending is a routine operation, it is not always simple [153]. Powder mixing is dependent upon several parameters including: blender type and design, scale and properties of the constituents as particle size distribution, particle shape, density, cohesion, and electrostatic charge [48;114].

In general, it is more difficult to obtain a uniform mixing with a low API content [96]. It is more efficient to mix components with good flow properties e.g. for direct compression. There is, though, a risk of fractioning upon emptying the mixing equipment. The risk is lower when using API and excipients of similar particle size distributions, and thereby avoiding percolation. In general, the more cohesive a powder is, the more difficult it is to mix [96]. Another approach, though, is to produce an ordered mixture, where a small amount of cohesive material (≈1 %) is mixed with a free flowing carry powder with a particle size (> 100 μm) often lactose or corn starch. Van der Waals forces will make the small cohesive powder particles adhere to the carry particles [144]. This technique can be used with poorly soluble API, that can be coated on water-soluble carrier particles to improve the solubility [143].

2.7 Direct compression

The simplest way to produce tablets is by direct compression (DC), which is the most cost effective manufacturing process and less stressful to ingredients in terms of heat and moisture [21]. The API is mixed with the excipients that form the compression mix. The mix is placed in a hopper (loading container) on top of the tablet press and fed into the tablet station. The tablet station consists of an upper and a lower punch and a die that will receive the mixture. The upper and the lower punches come together in the die, and the compression force will then compress the powder blend into a tablet [16]. There are two types of tablet presses, the rotary press that can produce from a few to many thousands of tablets/min and the eccentric

tablet press that can produce from 50-130 tablets/min [50]. The eccentric press, that is a single punch tablet press, is usually used for development purposes, where smaller batches are needed [131]. The rotary press has a number of punch- and die- sets that move in a circle [131]. The upper and lower punches in the rotary press exert pressure on the mixture at the same time, which gives a more even hardness compared to the eccentric press [50].

The ingredients are required to have good flowability to allow proper filling of the die, and be easily compacted. The term "compactibility" refers to the ability of a formulation to give a tablet with specified hardness. Diluents for direct compression are often specially designed and undergo additional processing to improve flowability and compression. An example of this is amorphous lactose that can be produced by spray drying, but the amorphous state can contribute to reduced physical stability [8;21]. These specially designed excipients are usually more expensive, but the higher cost is compensated for by the lower production cost of a DC operation. So therefore, DC is usually the preferred method if possible [144]. Segregation in the hopper is a known issue which can lead to a non-uniform product often with large mass and content variation. As the dies are filled by volume and not by weight, different density in inhomogeneous mixture, will lead to different mass of the tablets [5]. Greater attention must be paid to the API content uniformity in a DC formulation compared to a granulation compression mix with a similar API loading. If there is no interaction between the API and the excipients, there is a risk of segregation during handling and tableting [16]. Ordered mixing can also be a solution to the segregation issue in DC, and has shown good result with API loadings down to 0.1 % [16].

2.8 Granulation: wet and dry

If it is not possible to produce tablets by direct compression, a granulation, either wet or dry is often chosen. The main purpose of granulation is to increase the particle size and to (ideally) fix the blend state of the API in the excipients. This is done to prevent segregation and improve the flow properties and compaction characteristics of the powder [21].

In wet granulation, water or an organic solvent will be added to form liquid bridges between the particles, followed by a drying process [96]. During the drying process, many interrelated parameters influence the quality of the outcome. This could be the design of the equipment, inlet temperature, granulation fluid volume and rate, particles flow rate, and the humidity of the environment [46].

The dry granulation processes is usually divided into slugging and roller compaction. These methods can be used if the mixture is moisture or heat sensitive and has poor flow properties [50]. If the powder is compressible but does not flow well, slugging may be used [50]. In slugging, the powder is compressed in a slowly operating machine with large dies. In roller compaction, the powder is processed and compressed between two heavy-duty rollers, and emerges as a compressed ribbon. Compressed material from the slugging and roller compression are then milled to obtain a uniform particle size distribution [50]. Dry binder (powder) can be added to enhance the granulation process.

2.9 Coating

Not all tablets are coated, e.g. drug intended for local action in the GI tract may be left uncoated [21], but most tablets have added coating. Coating material is added for protecting the drug from the environment (moisture, light, and air) and increase thereby the shelf life of the product. It can also be used to mask taste, or improve the product identity and appearance. Furthermore, it can be used to control the release of the API, the controlled-release formulation [8;96]. There exist different types of coating; sugar coating, film coating and compression coating [8].

2.10 Validation of tablet batch production

During the production, tablet weight variation, and tablet hardness are often used parameters for process control. After the production, the tablet batch will be validated according to regulatory guidelines. This often includes test for tablet height, weight and its variation, hardness, dissolution, content uniformity (CU), and impurities [96].

The dissolution test is an in-vitro dissolution rate test that shows how quickly a drug is dissolved in a given solvent. Dissolution tests can be an indicator of in-vivo bioavailability [96]. The dissolution of a drug depends on many factors; the particle size, the specific surface area, crystal polymorphism, solubility, molecular size, salt formation, pK_a, hydration, wetting and surface tension. Furthermore, formulation factors and processing parameters can also be important for the dissolution [96].

Typically a large weight variation precludes good CU. Variation in CU often comes from either a non-uniform distribution of the drug substance, segregation of the powder mixture or granulate during the manufacturing process or tablet weight variation.

The requirement for CU according to European Pharmacopoeia (Ph. Eur; 2.9.6 [23]) is that 10 dosage units must conform within ± 15 % of the label claim. Additional test is performed if one unit is outside these limits.

3 Quality control, PAT, and QbD

Quality for pharmaceuticals is, by the International Conference on Harmonization (ICH), defined as "The suitability of either a drug substance or drug product for its intended use. This term includes such attributes as the identity, strength and purity" [77]. In the pharmaceutical industry there is a significant interest in the new paradigm "Quality by Design" (QbD), and this is often compared to the traditional "Quality by Testing" (QbT) [20;174]. QbD follows the notion that quality cannot be tested into the product, it needs to be built into the product, as stated by the ICH Q8 guideline [77] and FDA´s PAT guideline to the industry [43]. This means that quality has to be considered already when the product is developed. QbT is based on the testing of every batch (but not every sample) to ensure the proper quality at the end of the process. QbD is, on the other hand, relying on analysis of process and product quality during production, so that the quality of the end-product can be predicted. This can, in some cases, ultimately result in release without further testing, called real-time release testing (RTRT). Table 3 shows a comparison of the current, traditional QbT approach with a future desired, enhanced QbD approach. For QbT, a combination of fixed (and inflexible) manufacturing steps and extensive testing of the finished product, against the specification, determine the quality of the product. This often leads to a higher failure rate and more scrap, where the root cause is not understood [174]. IBM reports [79], that it is possible to improve the quality of a product to a minor degree by increasing the testing frequency. Further improvements, however, require that the product and process are designed with quality in mind. Sometimes, the manufacturer has not fully scrutinized how drug substances, excipients and manufacturing processes affect the quality. This is one of the essential points in QbD, where extensive research is done throughout the development of the drug. It is here that, relationships between the formulation and manufacturing are established and sources of variation identified.

One QbD approach for evaluating, understanding, and refining the manufacturing process could be as follows: First, it is important to identify the target product profile (TPP), which can be thought as the "user interface" of the product [98]. That includes defining the quality target product profile (QTPP or sometimes called target product quality profile (TPQP) [98]) as it relates to quality, safety and efficacy, considering many factors (e.g. the route of administration, dosage form, bioavailability, strength, and stability [77]). Further it involves identifying the critical quality attributes (CQA). CQAs are physical, chemical, biological, or microbiological properties that must be controlled to ensure the quality of the product [174]. Then it is important to identify the critical material attributes (CMA) and the critical process parameters (CPP). CPP are process inputs that have a direct and significant influence on CQA. Interactions between CQA and CPP should be understood so that CPP can be varied to compensate for changes in raw material quality [174]. Risk assessment can be used to identify the most critical CMAs, CPPs and CQAs. Quality risk management can be used at different stages during process development and manufacturing implementation [74;78].

Design of experiments (DoE) is a tool for understanding the influence of parameters on a CQA. In the pharmaceutical production, raw materials (e.g. particle size or particle shape), and process variables (e.g. speed and time) are the input variables and the CQA as dissolution characteristic, blend uniformity etc. is the response. This is used to find the design space for the process. Design space is the multidimensional combination and interaction of input variables and process parameters that have shown to assure a specified quality [174]. Inside the design space is the control space (or normal operating ranges), wherein the process should be run. The control space is usually defined with upper and lower limits for each input variable (raw material attributes and process parameters). There should be an established control strategy for how to describe and justify the quality, preferably a risk -and science- based strategy [20;74;104]. Process control is the active changing of process based on the result of on-line process monitoring. Any deviation from normality will trigger the system to apply changes so that the process is brought back on track [174]. Under the QbD, process understanding and process control provides sufficient evidence that the batches meet the specification if tested [174], which should be stated in the control strategy together with the control of raw materials [106]. Finally, product lifecycle management and continuous improvement is also part of the QbD strategy and a quality system is recommended by ICH (Q10 [76] and Q11 [78]).

Table 3: Comparison of current and future desired QbD approach (modified from ICH Q8 [77] and McCurdy [104]).

Aspect	Minimal approach or QbT	Desired QbD approach
Pharmaceutical development	Empirical, typically univariate experiments	Systematic, multivariate experiments
Manufacturing process	Locked down, validation on three batches, focus on reproducibility	Adjustable within design space, continuous verification within design space, focus on control strategy
Process control	In process testing for go/no-go, offline analysis	PAT utilized for feedback and feed forward in real time
Product specification	Primary means of quality control, based on batch data	Part of overall control strategy, based on product performance
Control strategy	Mainly by intermediate and end product testing	Risk based, control shifted up-stream, real-time release
Lifecycle management	Reactive to problems and out of specification (OOS), post-approved changes needed	Continual improvement enabled within design space

Process Analytical Technology (PAT) are systems for designing, analyzing, and controlling manufacturing through timely measurements of critical quality and performance attributes of raw and in-process material and process with the goal to ensure final product quality [43]. PAT implements important tools focusing on improving process understanding and knowledge. Hence, the use of PAT to assist in the implementation of QbD is highly recommended. In their strategic plan of advancing regulatory science from august 2011, FDA promotes the use of QbD and PAT approaches, to ensure manufacturer's ability to maintain consistent quality. It is encouraged to use PAT to monitor and control processes instead of just testing products [42].

The ultimate goal of PAT is a better fundamental scientific understanding of manufacturing processes [29]. In QbD regime, PAT plays a crucial role in design, analysis and control of

manufacturing processes based on timely in-line, on-line and at-line measurements of CQAs with the goal to ensure the final product quality [29]. Figure 3.1 shows the difference between in-line, on-line, at-line, and finally, off-line measurement in a production. In-line analysis measures on the product stream itself, on-line measured on a diverted stream, which may be let back to the process, at-line is measured on a sample that is removed from the stream, whereas off-line is typically measured in a laboratory remotely placed from the process both in time and location. The biggest differences between PAT and classic laboratory analysis are the speed of analysis, which opens the opportunity to live feedback and the elimination of manual sample handling and often operator error [56]. Therefore, the real advantages of PAT tools are first realized when the process is monitored in-line or on-line, as this will give the opportunity to act on the results [150].

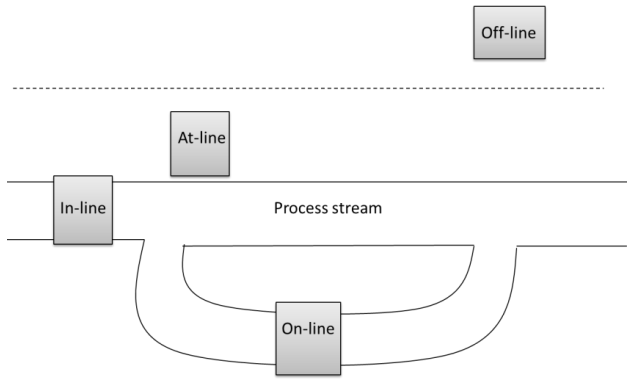

Figure 3.1: Illustration of in-line, on-line, at-line and off-line analysis at a process stream. Off-line analysis is often performed in a remotely laboratory and not necessarily at the same time as the production is running.

PAT tools can be divided into four groups [43]:

- Multivariate tools for design, data acquisition and analysis
- Process analyzers
- Process control
- Continuous improvement and knowledge management tools

According to a review of Pomerantsev and Rodionova [135] from 2012, NIR spectroscopy accounts for more than 60 % of the published PAT studies. Of the multivariate/chemometrics tools, partial least squares (PLS) regression and principal component analysis (PCA) dominate the picture and account for 45 % and 20 % respectively.

In this thesis, only the process analyzers: NIR-, terahertz-, and fluorescence- spectroscopy, and the multivariate/chemometric tools: PCA, PLS, and PARAFAC will be discussed. This will also include some pre-processing techniques and variable selection.

Furthermore, theory of sampling (TOS), the issue of whether an analysis is representative of the sample/lot, will be discussed.

4 Multivariate data analysis – chemometrics

Multivariate data analysis or chemometrics is in practice a necessity, when dealing with high throughput spectroscopic data, especially if the objective is to gain the full value of these methods. Some of the basic principles will be explained here with a few examples.

4.1 Principal component analysis

In a principal component analysis (PCA), the largest variation in a dataset is found. The data is decomposed into a new set of variables called principal components (PCs). The PCs are composed of two sets of data: the scores (**t**) and loadings (**p**) with the scores referring to spectral variation and the loadings representing the spectral contribution to each PC. After calculating the PCs the difference between the explained variance and the original data is the residual (**E**) [38]. The residual will decrease with the number of PCs. The additional explained information decreases with the number of PCs, therefore it is typically the first 2-3 PCs that are of most interest.

The matrix, **X**, that could be spectral data, is explained by the scores, **t** and the loadings, **p**, and the residuals, **E**:

$$\mathbf{X} = \mathbf{t}\mathbf{p}' + \mathbf{E} \qquad 4\text{-}1$$

Figure 4.1a shows an example of a PCA score plot of NIR spectra from escitalopram tablets (4-12% w/w) from paper I & II. Figure 4.1b shows the corresponding loading plot. The loading plot show which variables that describe each principal component, and thereby for explaining the variation in the data.

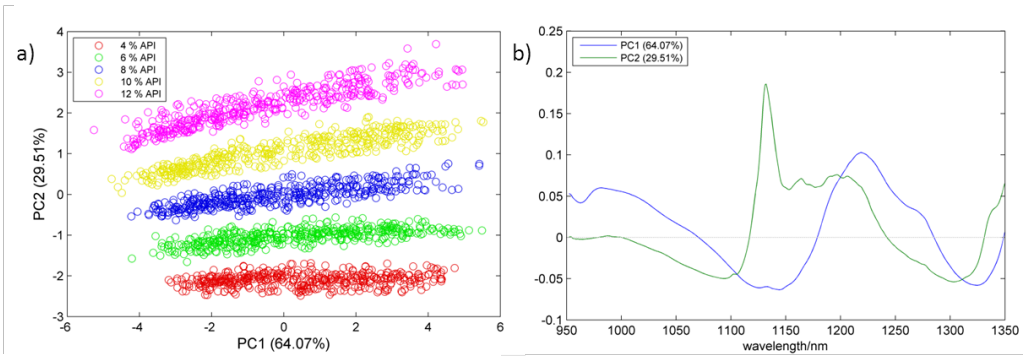

Figure 4.1: a) PCA score plot of NIR spectra of escitalopram tablets with 4-12 % (w/w) API. b) corresponding loading plot.

4.2 Partial least squares regression

Partial least squares (PLS) regression is a two-block regression method based on estimated latent variables (LV) that require an **X** block (e.g. spectral data) and corresponding **y** data (e.g. chemical data). The purpose of the PLS regression is to build a linear model predicting the desired characteristic (**y**) from a measured spectrum (**X**). It can be written as:

$$\mathbf{y} = \mathbf{X} \cdot \mathbf{b} + \mathbf{E} \qquad 4\text{-}2$$

where, **b** is the regression coefficient and **E** is the residual. It is desired to maximize the covariance between **y** and **X** and to lower the residual.

The root-mean-square-error of cross validation (RMSECV) is an estimate of how good the model is. RMSECV are calculated as follows:

$$\mathbf{RMSECV} = \sqrt{\sum_{\mathbf{i=1}}^{\mathbf{N}} (\mathbf{y_i} - \hat{\mathbf{y}}_\mathbf{i})^2 / \mathbf{N}} \qquad 4\text{-}3$$

where y_i is the measured y (e.g. chemical reference method), $\hat{y}_i$ is the predicted value (e.g. spectral prediction), and N is the total number of samples.

The optimal number of LVs is usual found by the minimum or breakpoint in RMSECV-curve. It is desired to minimize the complexity of the model and use as few LV as possible. Afterwards, a test set can be used for testing the model. Then a root-mean-square of prediction (RMSEP) is calculated in the same way as for the RMSECV.

4.3 Pre-processing of spectral data

Pre-processing of spectral data is frequently used to improve the calibration methods and enhance the prediction-model performance [176]. Often, it is desired to decrease the influence of various signal sources that are not related to the chemical or physical information by the raw spectra. This could for example be information from instrumentation, light scattering, particle-size distribution, packaging density, and effect of tablet face and position in relation to a probe beam [138]. Furthermore, influence of standard blisters, bottles, and other packag-

ing material can also be removed by pre-processing methods [138]. Centering is an important pre-processing of spectral data prior to multivariate evaluation for quantitative analysis [163]. Basically, the mean spectrum is found and subtracted from every spectrum.
Rinnan et al. [137] divide the most used pre-processing techniques for NIR spectra into two categories: scatter correction methods and spectral derivatives. Standard normal variate (SNV) correction and multiplicative scatter correction (MSC) both belong to the first category of pre-processing techniques. In SNV correction, for each wavelength, on an individual spectrum basis, the variation in slope and offset are removed [7]. For MSC each spectrum is corrected with a reference spectrum. This could be the average of the sample set [49]. In practice, for NIR spectra, the two methods give very similar results [137]. Figure 4.2 shows an example of how pre-processing of the spectra with SNV makes the chemical changes in the spectra more obvious. In this case, it is binary mixture of amorphous and crystalline lactose analyzed by NIR from paper III.

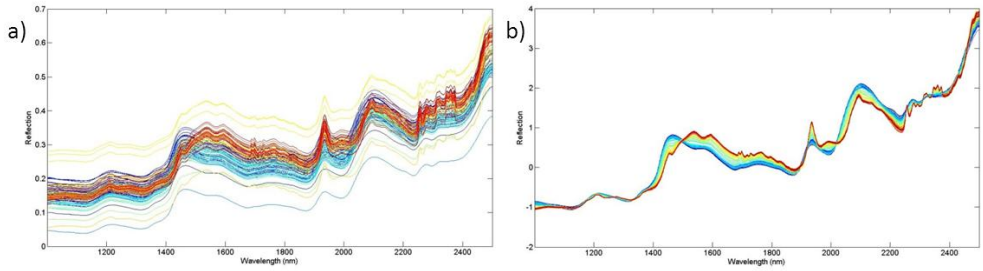

Figure 4.2: a) Raw NIR data of amorphous (blue) and crystalline (red) lactose. b) SNV treated NIR spectra (from paper III) .

The other category of pre-processing methods is derivatives of the spectra. Derivatives have the ability to remove additive and multiplicative effect from the spectral data. Figure 4.3 illustrates an example of a Gaussian peak (blue line), with added baseline (green line), and with added baseline and multiplicative effect (red line). First derivative removes the baseline whereas second derivative removes the baseline and the linear trend [137]. In practice, before applying derivatives to the data, smoothing and fitting into a low-order polynomial within a data window is often used in pre-processing methods (e.g. Savitzky-Golay [115]).

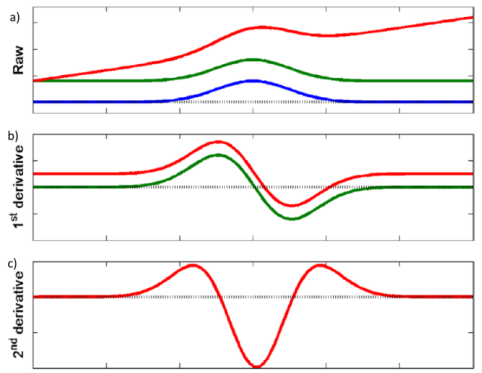

Figure 4.3: Gaussian peak (blue) added baseline (green), and added baseline and multiplicative effect (red). a) raw data b) first derivative c) 2nd derivative (from Rinnan et al. [137]).

For pre-processing of NIR spectra, Rodionova and Pomerantsev [138] recommend using SNV or MSC, whereas application of derivation should be done with care as this may add noise to the data. In general, Rinnan et al. [137] recommend that the pre-processing should maintain or decrease the effective model complexity.

4.4 Variable and subset selection for improvement of regression models

In spectral data, not all information is important for quantitative models (e.g. prediction of API content). Sometimes, selection of only some variables can be an advantage for the prediction [176]. There exist many different techniques for variable selection. However, here only interval partial least squares regression (iPLS) will be described. iPLS is an extension to PLS that create local PLS models on subintervals of the full-spectrum region, and thereby can focus on important spectral regions and remove interferences from other regions [122]. Local models are compared to the full-spectrum, global model mainly by RMSECV. The forward stepwise selection method is the simplest, where first all intervals are tested individually and the interval with the lowest error is chosen. Then the intervals are tested in combination with this selected interval, and intervals are added until the RMSECV increases by introduction of new intervals [122]. An alternative method is the backward interval PLS, where data is also divided into a number of intervals, and models are created each time, with one interval less until RMSECV increases [95]. Forward selection tends to provide more parsimonious calibration models as fewer variables/regions are retained in the final models. In this thesis, only forward selection iPLS has been used. Figure 4.4 illustrates an example of iPLS on unfolded fluorescence data of pulverized tablets predicting melitracen (MEL) from paper IV. Each interval is an excitation wavelength and it is obvious that including only 4 of the 18 intervals give lower RMSECV than the global model.

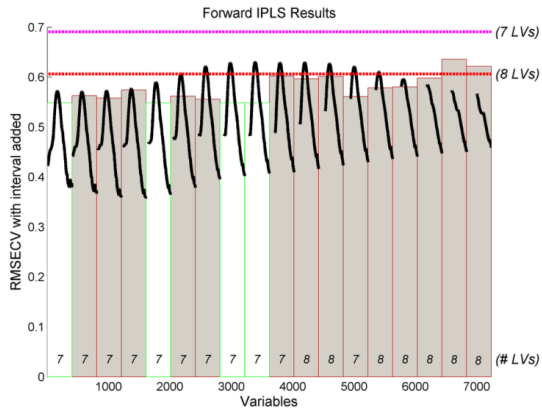

Figure 4.4: interval PLS (iPLS) of unfolded fluorescence spectra of pulverized tablets predicting melitracen (data from paper IV). The green intervals are the one chosen with the lowest RMSECV. The pink line and the red line show the RMSECV for global model for 7 LVs and 8 LVs, respectively.

4.5 Tensor analysis of spectroscopic landscapes - PARAFAC

PARAFAC is a generalization of PCA to higher order arrays, often used for three-way (e.g. fluorescence landscape) data. PARAFAC is more constrained and less flexible than e.g. unfolded two-way PCA, and PCA will therefore fit the data better than PARAFAC. An important advantage of using multi-way methods instead of unfolding methods is that the estimated models are more robust and easier to interpret [13].

PARAFAC creates unique models, and similar to PCA, loadings will also be obtained, although there will be a set for each dimension. These loadings can be used to read the chemistry, which is an advantage over the unfolded PCA. In contrast to PCA, all the factors are calculated simultaneously, which makes it vital to determine the right number of factors. A good way of judging the number of factors for PARAFAC is by split-half validation, where the data set is spilt in two and the loadings from the models should, due to the uniqueness of PARAFAC, be similar [13]. Another tool for judging how many factors to use in a model is to look at the core consistency factor, which should be close to 100 % [14].

5 Theory of Sampling (TOS)

On a macroscopic level, all lots may seem very homogeneous, but at a microscopic level, most lots are not homogeneous. Only (completely dissolved) solutions are fully homogeneous, and even that statement is debatable [57]. For solid material this phenomenon is more pronounced and especial for pharmaceuticals due to differences in particle sizes and shape, flowability and density.

The purpose of sampling is to take samples that are representative for the lot or production. This is, though, not as easy as it sounds due to the complex nature of the real world [27]. As it is very rare that the whole lot can be analyzed, mass reduction is needed. Sampling from a lot can be seen as large mass reduction and should be a major part of quality control [57].
The purpose of sampling can be divided into two parts:

1. How are the samples taken from the lot – are they representative of the lot?
2. How much/many samples are needed to describe the lot?

Those two issues are closely related as it is possible to some extent to compensate for the representativeness by increasing the number of samples e.g. at a very inhomogeneous lot, but this is rarely the most efficient approach.
For correct sampling the following two statements should be fulfilled:

1. All parts of the entire population/production lot should have the same (non-zero) probability ending up as a sample.
2. Everything that is not part of the population or production lot should have zero probability to end up in the sample (no pollution of the sample).

If this is fulfilled there should be no systematic error also called bias [60].

Sampling can be divided into three different types [57;152];

1. Grab sampling. This is the common used “take a spoonful from the top of the lot” sampling, that is often based on what is “a suitable size” and conveniently accessible. Unless the lot is perfectly homogenous or is remained well mixed, this way of sampling does not give a representative sampling of the lot.
2. Splitting of the lot. The lot is split into a certain number of fractions and one or more fractions are used in analysis or for further mass reduction. This way of sampling occur in many variations and can be done so the end sample will be representative of the lot.
3. Incremental sampling. This is when more samples are taken from a lot and is the preferred method for a production line.

Strictly speaking, all lots are three dimensional or four-dimensional if including time. However, from a sampling point-a-view it is possible to define samples in a certain way that

dimensions may be ignored [152]. The remaining dimensions are called the sampling dimension and it is important to decide how samples should be taken. The internal connection between the fragments defines the optimal sampling strategy. Zero-dimensional sampling can be used at discrete objects (population) that are independent from one another (non-ordered/no autocorrelation). This condition is met if the whole lot is taken or the whole lot can be mixed [57;58;130]. One-dimensional sampling can describe long objects (e.g. a cable) or series of ordered units (e.g. a process stream). Here, there is typically a distinct autocorrelation/internal order (spatially, physically or chronologically) [130]. Two-dimensional sampling can explain a flat object (e.g. a piece of paper), where the thickness is small compared to the two dimensions of its surface. A three-dimensional sampling will typically represent a bulky lot where sample cannot cover any dimensions fully (e.g. an ore body) [58;130]. The sampling theory covers sampling from zero- and one-dimensional issues, where higher dimensional sampling issues need to be transformed into zero-or one-dimension (e.g. by sampling from transportation at a conveyer belt [130]).

A way of sampling is to withdraw many smaller samples/increments and combine them to a bigger primary sample. From this primary sample, the mass has to be reduced one or more times, until the right size for the analysis is achieved. The mass reduction has to follow the same principle, that all the material should have the same probability to end up in the final sample [39]. In the literature there are some examples of how this can be done depending on the materials size and consistency [128].

In a process stream, it is crucial to the sampling that the whole process stream is withdrawn at once. A tool placed vertically to “cut” the stream must have parallel sides. Otherwise, the process material will have an unequal probability of being withdrawn [152]. Figure 5.1 shows examples of proper sampling (a) and b)) and incorrect sampling (c), d), and e)).

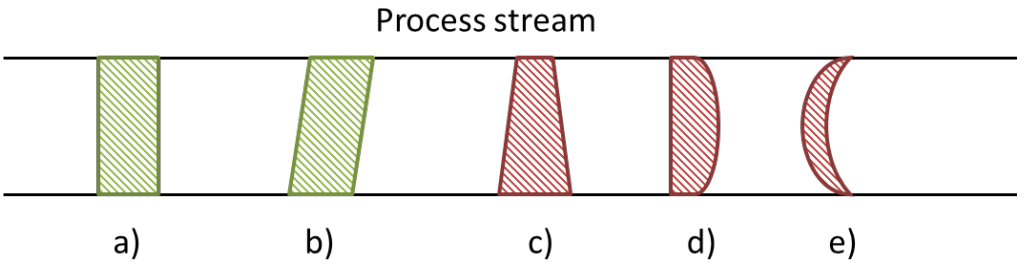

Figure 5.1: Sampling from a process stream. a) and b) will be considered correct sampling, whereas c), d) and e) represents incorrect sampling

During processing of powder and especial during transportation, segregation is a problem and the main factors are differences in particle size, shape, and density [166]. Figure 5.2 shows an example of a process stream with different size particles. Segregation can occur due to the differences in particle size, where the small particles tend to drop immediately after the belt, whereas the bigger particles tends to travel a bit further away [134]. A different example is

shown in Figure 5.3, where the segregation happens due to density differences of the particles. In both cases, a way of withdrawing a representative sample will be by taking the full process stream within a given time frame.

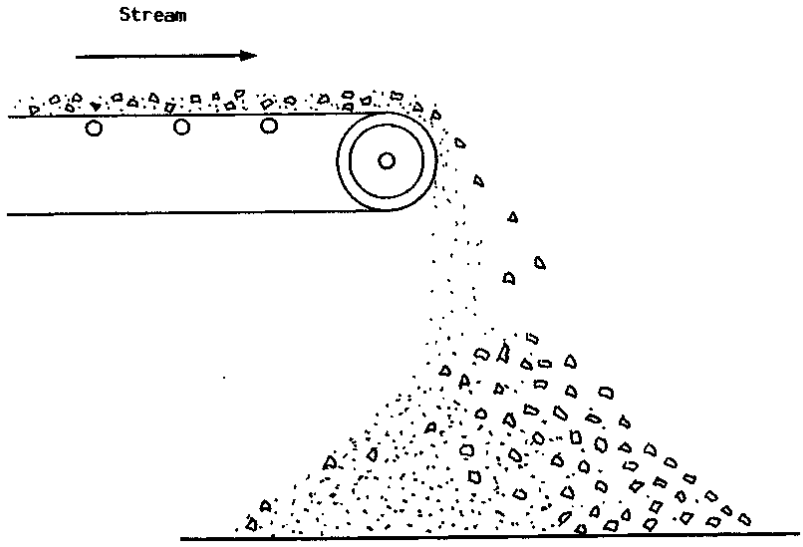

Figure 5.2: Segregation of fine particles from larger fragments in the same density class (from Pitard [134]).

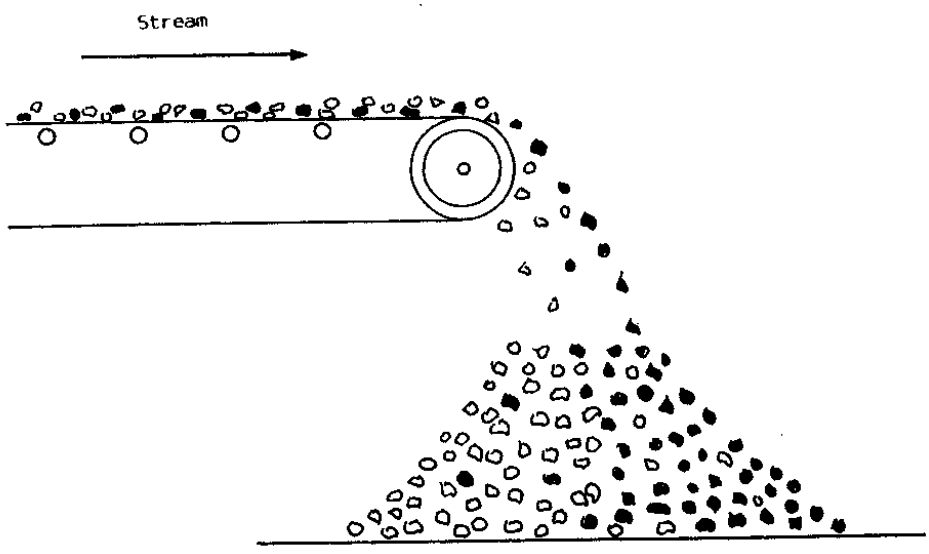

Figure 5.3: Segregation of dense fragments from lighter ones in the same size fraction (from Pitard [134])

As segregation is a known problem in direct compression tablet manufacturing, this was investigated on a smaller scale with the sampling study of the tablet production of escitalopram in paper I. The assumption was, if there were problems due to segregation, there would be substantial API content variation between tablets samples at different process time points. Figure 5.4 shows the high performance liquid chromatography (HPLC) variances calculated over six tablets taken at the same time point, 1 through 6. For each time points there are five batches (API loads). There is no evidence of segregation, as the variances for time point 5 and 6 are not larger than time point 1 and 2.

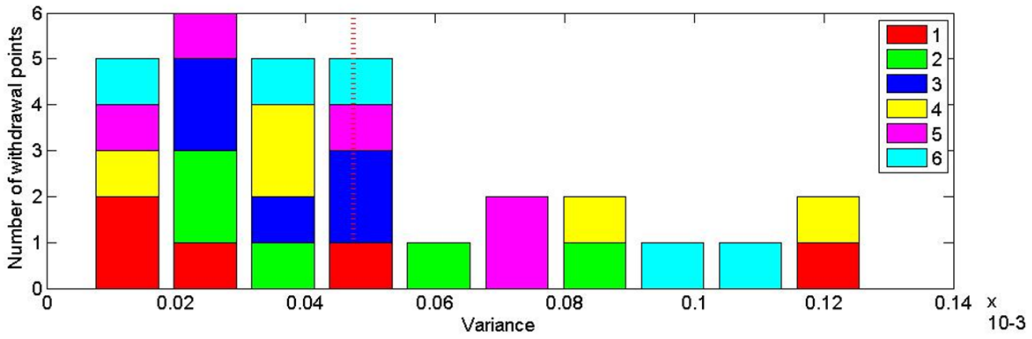

Figure 5.4: HPLC variances (x 10^{-3}) based on six individual tablets for five batches of of escitalopram tablets from six time points during production (in total 30 withdrawal points). The red line shows the average value of all the time points.

The other sampling issue, regarding the amount of sample to be representative for a lot, takes a more statistical approach, but can of course not be separated from the sampling method. The true variation, σ, of the mass is only known if the whole lot is analyzed. This is rarely the case; therefore σ is estimated as the standard variation, s, or the variance, s^2. The larger part of a lot that is analyzed, assuming through correct sampling (no systematic error), the closer the estimate, s, comes to true value σ. If the number of samples, n, is increased the standard error of the mean becomes smaller. The variability of $\bar{x}$, also called the sampling distribution of the mean, can be calculated as follows [108]:

$$\boldsymbol{standard\ error\ of\ the\ mean} = \sigma/\sqrt{n} \qquad 5\text{-}1$$

Knowing the variance of the lot and assuming it follows a Gaussian distribution, having a specification of maximum 5 % error, e the number of samples needed can be found from the following equation [69]:

$$\boldsymbol{n} = \boldsymbol{t^2 s_s^2 / e^2} \qquad 5\text{-}2$$

where t is found in a student t-test table for n-1 samples.

Figure 5.5 shows a statistical uncertainty of the ratio between the estimated and the true standard deviation as a function of the number of samples on a logarithmic scale [144]. It is assumed that the lot contains much more than 100 samples in total. From Figure 5.5 it can be

seen that the benefit of increasing the sample number from 10 to 30 samples, in terms of higher certainty of the result, is much larger than increasing the samples number from e.g. 80 to 100 samples.

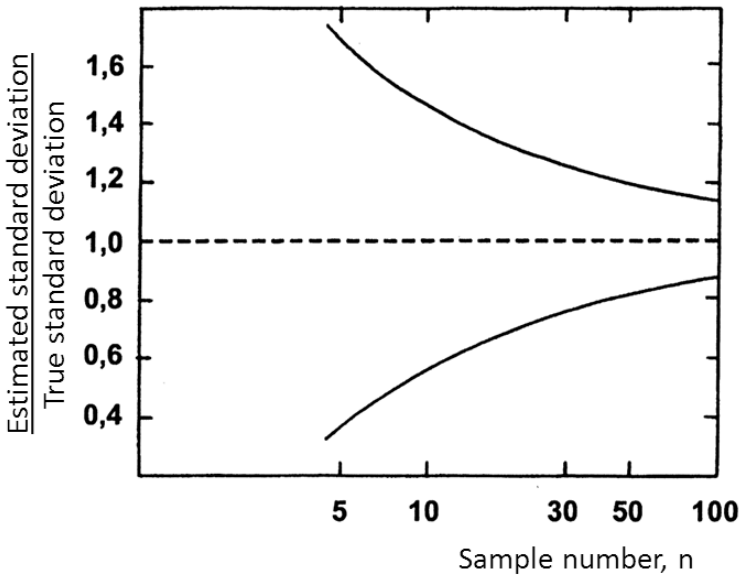

Figure 5.5: Uncertainty of the standard deviation as a function of number of taken samples, n, with 95 % confidence intervals (modified from Schæfer [144]).

Overall variance s_0^2 is the sum of the variance of the analytical procedure s_a^2 and the variance of the sample operation s_s^2 [69]:

$$\boldsymbol{s_0^2 = s_a^2 + s_s^2} \qquad 5\text{-}3$$

These are also sometimes referred to as global estimation error (GEE), total sampling error (TSE) and total analytical error (TAE) in sampling language. Variances are additive, which is also used in sampling study in paper I. Here the variances were used to show that the largest variance in the spectra came from the dislocation of the tablet in the auto sampler (see paper I, Figure 5). This is probably due to smaller changes in the path length (thickness of the sample) and scatter of the NIT beam.

To see a process of tablet production (one-dimensional) as individual units (zero-dimensional), it is necessary to investigate the variance over the production. This can be done with a variographic analysis, where 60-100 samples are taken out at specific intervals over the whole production. Here differences between adjacent time points and time points with greater separation can be calculated, and trend line shown. This is an excellent tool for seeing the variance of the production (the sill). If there is a large difference between samples taken in the beginning and in the end of a production, samples from more than one withdrawal points are needed to describe the production lot. It is also possible to detect drifts or cyclic

variation during the variation. Furthermore, it is also possible to find the lowest possible error (the nugget effect), which will be the estimated variation between two samples taken at the same time [59]. If, however, the production is large, more samples could be taken within a certain interval e.g. an hour to see the local variation. If samples are only taken out at one point or very close to each other, they are in sampling terms, basically the same sample, and therefore only describing that part of the production. One has to be sure that the production is not varying if only one sample (or 10 taken at the same time) should describe the whole lot of e.g. 1.000.000 samples. From a variographic analysis the number of samples can be found, as well as the sampling strategy; random selection, random stratified selection, or sampling to a fixed interval with semi-random starting points [37;129;130]

In this thesis, the analytical errors due to different rotation of tablet were analyzed. This gives an indication of the best sample presentation in the instrument and how many samples are needed to create a PLS calibration (see more in Section 6.2 Infrared spectroscopy and paper I). It can, though, not determine whether the withdrawn samples are representative for the whole production batch. For that purpose, a variographic analysis is needed.

6 Rapid analysis by spectroscopy

Spectroscopic sensors are key PAT tools as they can provide rapid analysis of sample and process stream composition [120] in an industrially robust form requiring little regular maintenance [53]. Thus far, most spectroscopic PAT sensors have been based on optical spectroscopy which will be summarized briefly in the following.

6.1 General about spectroscopy

Light can either be described as a stream of photons or as an electromagnetic wave. The energy of the photons is

$$\boldsymbol{E = h * \nu} \tag{6-1}$$

where h is the Planck constant ($h = 6.626 \cdot 10^{-34}$ J s) and ν is the frequency of light. The light velocity in vacuum C and the wavelength λ are related by

$$\boldsymbol{\nu = C/\lambda} \tag{6-2}$$

Thus, the energy of the electromagnetic waves is directly proportional to the reciprocal wavelength.

Figure 6.1 shows an overview of the electromagnetic spectrum, ranging from radio wave, over microwave, terahertz, infrared (IR), NIR, visible light, UV, to X-ray, and gamma rays with decreasing wavelengths [157].

Describing light as an electromagnetic wave, it can be written as

$$\boldsymbol{A(\varphi) = A_0(\varphi)\, e^{i(\omega t - \delta)}} \tag{6-3}$$

where A is the amplitude, ω is the circular frequency, t the time, δ the phase angle and φ the polarization angle [73]. The circular frequency can be expressed by the wavelength λ and the refractive index n:

$$\boldsymbol{\omega = C/\lambda\, n} \tag{6-4}$$

Equation 6-3 applies to light in a non-absorbing medium. In case of absorbing medium, equation 6-3 has to be modified by replacing the refractive index n by its complex form n^*:

$$\boldsymbol{n^* = n + i\kappa} \tag{6-5}$$

where n and κ is always non-negative.

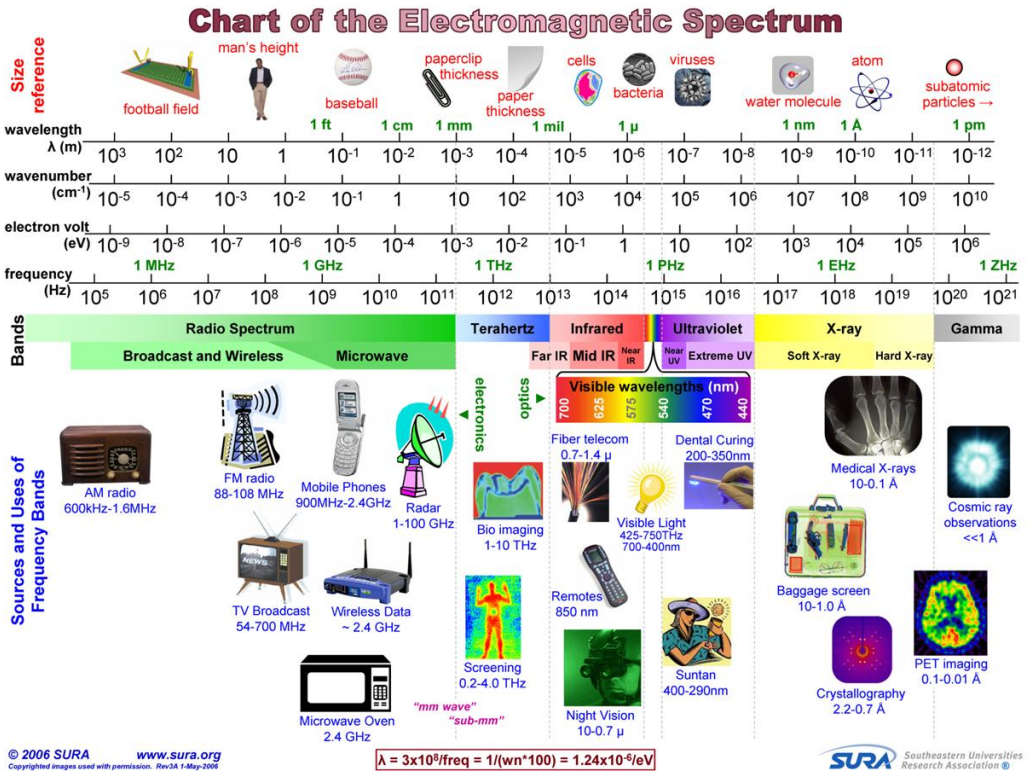

Figure 6.1: Electromagnetic spectrum (modified from SURA [157])

Electrons can exist in different energy states within molecules. The lowest energy state is called the ground state, whereas higher energy states are called excited states. At room temperature, normally electrons will be at their ground state. If a sample is stimulated with energy in form of e.g. heat or light, some analyte may undergo a transition to the excited state. This can provide information of the analyte by measuring the electromagnetic radiation emitted when it returns to the ground state or by measuring the amount of electromagnetic radiation absorbed or scattered as a result of excitation [151].

Atoms, ions and molecules can only exist in certain discrete states with definite amount of energy. They can absorb or emit an amount of energy exactly equal to the energy difference between the states. This energy can be described as:

$$\boldsymbol{E_1 - E_0 = h\nu = hC/\lambda} \qquad 6\text{-}6$$

where E_1 is the energy of the higher state and E_0 the energy of the lower state, ν the frequency and λ the wavelength. C and h are the speed of light and Planck constant respectively [151]. Figure 6.2 show a schematic overview of absorption and emission of photons between states for IR, NIR and fluorescence (see description in later sections).

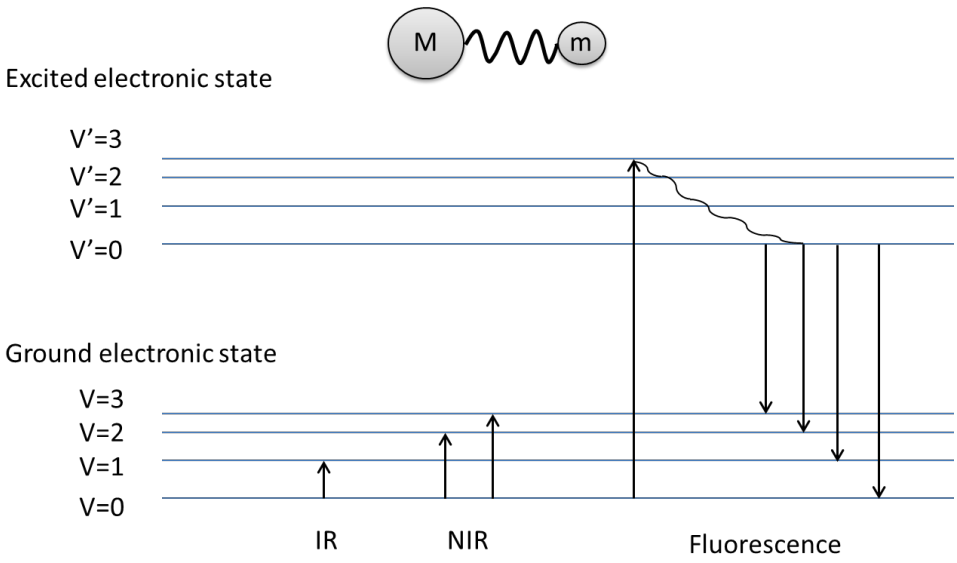

Figure 6.2: IR and NIR absorption and fluorescence (modified from De Beer [29]).

The Lambert Beer law can then be written from Equation 6.6:

$$\boldsymbol{I = I_0 e^{\varepsilon c l}} \qquad \text{6-7}$$

where ε is the molar absorption coefficient, c the concentration of the absorbing compound, and l is the path length of light within the absorbing medium. The Lambert Beer law is usually written in its logarithmic form:

$$\boldsymbol{\log(I_0/I) = A = \varepsilon c l} \qquad \text{6-8}$$

where A is the absorption [73].

When interacting with a sample, incoming light (I_0) may partly be reflected at the interfaces (I_R), it may be scattered (I_S) and absorbed by the sample (I_A), and the rest will be transmitted (I_T) [154]:

$$\boldsymbol{I_0 = I_A + I_T + I_R + I_S} \qquad \text{6-9}$$

Figure 6.3 shows the different outcome of the incident light when it meets a sample. It is possible to measure the reflected light (I_R), the scattered light (I_S) and the transmitted light (I_T), but not the absorbed light (I_A) directly. As the absorbed light is most informative about the chemistry of the sample that would typically be calculated from the measured light. Most

setups will only have one detector, so therefore it is desired to keep the other light intensities to a minimum, e.g. scattered reflected light should be kept low when measuring the transmission. This is often done by sample preparation, but it is not possible to completely neglect this and that will lead to a measurement error [154]. Scattering by molecules with dimensions significantly smaller the wavelength of the radiation is called Rayleigh scatter (same wavelength as the original light). Whereas, with large particles scattering can be in different direction and is called Mie scattering [151]. When measuring light that is scattered in all directions, it is usual called diffuse reflection.

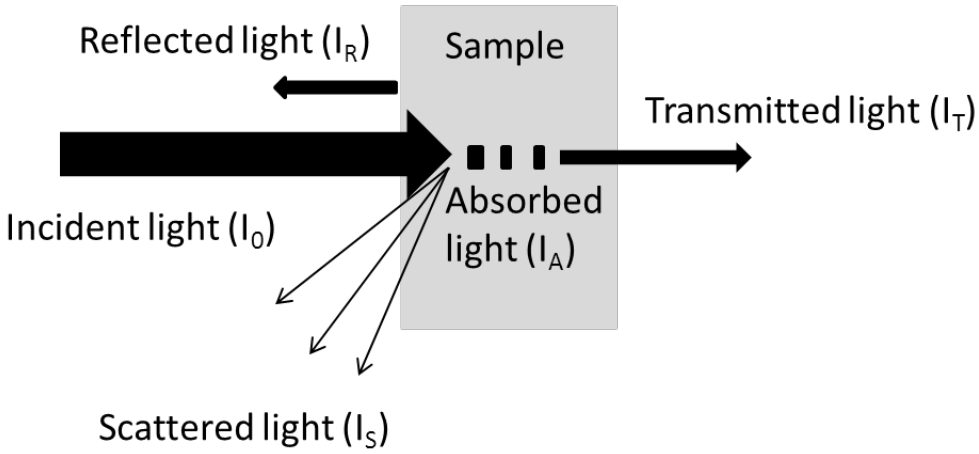

Figure 6.3: Energy balance of incident upon interacting with a sample (from Steiner [154]).

A typical measuring setup could be: light is sent out from light source e.g. a laser, and will be split into different wavelengths by e.g. a beam splitter or a monochromator, afterward it hits the sample and the part that is transmitted or reflected will be measured by the detector (see Figure 6.4). The wavelength splitting can also happen after the light has passed through the sample (post-dispersive).

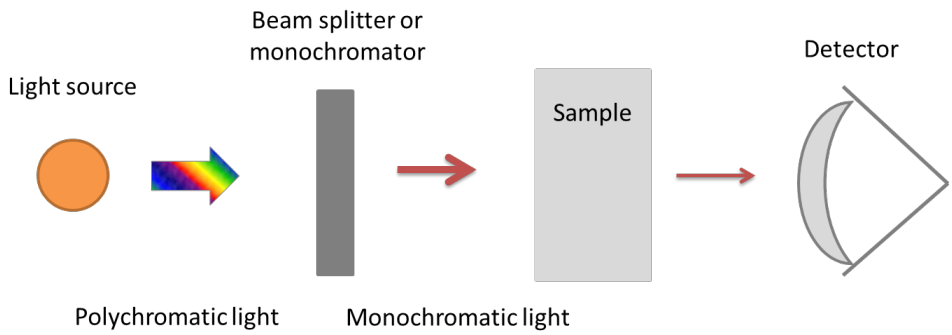

Figure 6.4: Measuring principle of transmission spectroscopy. Light comes from a source, divides into different wavelengths, over time hits the sample, and the transmitted light will be measured by the detector.

6.2 Infrared spectroscopy

Mid-infrared (MIR) covers the radiation from 4000-400 cm^{-1} and interacts with the fundamental molecular vibrations. Near-infrared (NIR) covers the wavenumber range from MIR and up to the visible region (12,500-4000 cm^{-1}, 800-2500 nm) [149]. Absorption bands NIR are the result of interaction between the light and molecular vibrational overtones and combination tones. Thus in MIR and NIR spectra of chemical compounds can be observed as a consequence of molecular vibrations. If having a simple diatomic oscillator; the vibrational frequency ν can be correlated with molecular parameters by [149]:

$$\boldsymbol{\nu = 1/2\pi\ \sqrt{f/\mu}} \qquad 6\text{-}10$$

where the force constant *f* reflects the strength of the bond between m and M and the reduced mass μ is given by

$$\boldsymbol{\mu = mM/(m + M)} \qquad 6\text{-}11$$

The vibrational frequencies are very sensitive to the structure of the investigated compound.

Vibrational energy may only have certain discrete values called energy levels that are given by

$$\boldsymbol{E_{vib} = h\nu(v + ½)} \qquad 6\text{-}12$$

where *h* is Planck's constant, ν is the vibrational frequency and v is the vibrational quantum which can only have the integer values 0, 1, 2, 3…[11]. At room temperature most molecules exist at the ground vibrational (v=0). The transition from v=0 to v=1, called the fundamental transition, dominates the infrared absorption spectrum.

However, molecules are not ideal oscillators. Due to anharmonicity, the vibrational energy is not equally spaced, that means that there is not exactly the same distance between fundamental transitions and the 1st overtone and the 2nd overtone. For the anharmonic oscillator, the frequencies of the overtones absorption are not exactly 2, 3, …

The occurrence of MIR bands requires a change in the dipole moment μ during vibration or rotation [151]. If a frequency exactly matches a natural vibrational frequency of a molecule, absorption of the radiation takes place [151]. Most molecules absorb IR radiation except molecules with no net change in dipole moment (e.g. simple diatomic molecules such as O_2, N_2 and Cl_2). The most intense MIR band can be traced back to polar groups (e.g. C-F, Si-O, C=O, and C-O) [149]. The vibrations can be divided into stretching and bending. In stretching there is a change in the interatomic distance, whereas the bending there is a change in the angle between the bonds [142]. Furthermore, combination bands can also be seen, when a photon excites two vibrational modes simultaneously. This gives bands that are approximately the sum or difference of the two fundamental frequencies [151].

Absorption in NIR region require - in addition to a change in dipole moment - a large mechanical anharmonicity of the vibrating atoms [11;149]. Thus in NIR, it is mainly X-H stretching vibrations (CH, OH, and NH) that dominate the spectrum, whereas the most intense MIR fundamental absorptions are rarely represented in the NIR frequency range [149].

Most of the X-H fundamentals absorb at wavenumbers between 4000 and 2000 cm^{-1}, so the 1st overtones appear in the NIR frequency range. The polar groups of many of the fundamental absorptions in MIR usually absorb at wavenumbers < 2000 cm^{-1}, which means that their 1st overtone still occur in the MIR region. Due to the intensity loss, which is approximately a factor of 10 for each step from the fundamental to the next overtone, the absorption intensities of these functionalities are negligible by the time they occur in the NIR range [11;149]. The bonds involving hydrogen, the lightest atom, vibrate at high energy and with a large amplitude when undergoing stretching motions, and therefore carry the most intensity. The NIR region is dominated by absorption associated with $X\text{-}H_n$ functional groups. These absorptions arise from the overtones of fundamental stretching bands or combinations involving the stretching and bending modes of vibration of such groups [11].

A molecule containing N atoms will have (3N-6) vibrational degrees of freedom (3N-5 for linear molecules) and the same number of fundamental vibrational frequencies of the molecule [11]. The transitions have to have a connection to a change of dipole moment to appear in the infrared spectrum. In practice fewer bonds are observed due to several phenomena: (1) symmetry in the molecule, which does not create a change in dipole moment, (2) that the energy of two or more vibrations are identical, (3) that the absorption is too low to be detected, or (4) that the vibration energy is outside the range of the instrument [151]. In polyatomic molecules, the anharmonicity causes not only the appearance of overtones but combination bands as well [11].

Figure 6.5 shows an example of near infrared transmission (NIT) and IR spectra of toluene that is often used as a solvent in API production. In the figure it is shown how C-H bond vibrations (C-H stretch at 2965 cm^{-1} and C-H aromatic at 3042 cm^{-1}) are mirrored in the NIT spectra as 1st overtone between 1640-1750 nm and again as 2nd overtone between 1120-1220 nm. In this case, the 1st overtone would not be useful for quantification, as the detector seem to be saturated due to very long path length. The band in-between the fundamental band and the first overtone and again between 1st overtone and 2nd overtone are combination bands.

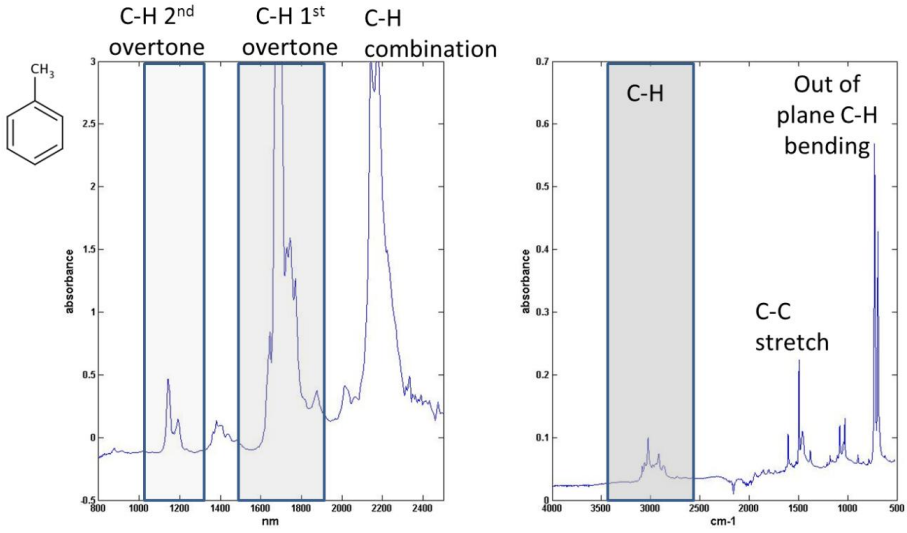

Figure 6.5: NIT and IR spectra of toluene, as an example of mirroring of bond vibrations from IR to NIR wavelengths.

NIR radiations result in the excitation of overtones and combination modes of vibrations. These absorptions are weaker in nature and therefore longer cell path length (e.g. mm or cm for liquids) is needed for NIR compared to MIR (often in μm). This can be an advantage, as process stream often include particles that can block narrower cells [53].

NIR radiation can be transmitted through relatively cheap fibers, which means that instruments can be installed remotely from the process stream, This is very convenient for a hazardous or dusty production area [53]. The development of NIR with light fiber optics coupled with specific probes has increased the purposes in processes. The sample preparation is typically easier for NIR than e.g. IR [149]. Furthermore, NIR instruments are robust and relatively cheap, which has also been important to the popularity of NIR.

NIR absorptions are typically broad, therefore individual components of mixtures overlap considerably. Due to the capability of chemometrics to resolve or find hidden and overlapping NIR peaks of components, the usefulness of NIR has increased tremendously [53]. NIR spectroscopy requires reference analysis of the samples to build up calibrations and to maintain the established calibration [149]. Because of the complexity of NIR spectra, typically many samples are required for creating a calibration depending on the application [140].

In NIT, due to often thicker sample path lengths, it is mainly 2^{nd} and 3^{rd} overtone band (short wavelength part of the spectrum) that can be used. These are much weaker than first overtone, but this is compensated for by the longer effective path length compared to reflection analysis [107]. The useful range of wavelengths of the spectra depends on the thickness of the sample among other parameters. Corti et al. [22] found that for a 4 mm thick diphenhydramine tablet the useful range was up to 1400 nm in transmission mode. For trans-

mission analysis, a limited wavelength range is useful due to too high absorbance. Merckle et al. [107] found that analyzing tablets in diffuse reflectance 1100-2500 nm were useful, whereas only 700-1300 nm in transmission. In paper I a similar wavelength limitation was found analyzing escitalopram in transmission mode, and only wavelengths up to 1350 nm were useful. Studies from Thosar et al. [165], Gottfries et al. [52], and Ito et al. [82] showed that calibrations for transmission measurements performed better than calibrations for reflectance measurements. This is probably due to increased sampling volume and therefore a reduction of the sampling-related heterogeneity.

In pharmaceutical applications there are many examples of NIR for process and development of pharmaceutical products [29]. In the following only some examples for each type of application are mentioned. NIR spectroscopy offers a wide range of in-line and at-line transmission and diffuse-reflection probes designed the measurements of liquids and solids [149].

NIR allows rapid and non-destructive analysis of bulk material [11]. Therefore it is useful as quality control on incoming materials, where the material is compared to a spectral library through a discriminant analysis (e.g. PCA with limits on distances) [101]. NIR is a rapid method that can measure remotely with fiber optic probes, which makes it possible to identify raw material in warehouses through closed polyethylene bags as incoming quality control [139].

Using NIR spectroscopy to measure API dosage uniformity

For determination of API, Han and Faulkner [64] found excellent correlation (R>0.99) of the API SB 216469-S in concentrations 0-6 % (w/w) to NIR reflectance in tablets of 5, 10 and 20 mg, both as powder after blending, as core tablets during compression, after film coating and in clear blister packaging. Merckle and Kovar [107] found that for acetylsalicylic acid (ASA) in three different effervescent tablet formulation with a concentration between 8.7-17.4 % (w/w), the relative error of prediction was between 2.21 and 3.13 %. Dyrby et al. [36] found for escitalopram tablets between 4.8 – 9.1 % (w/w) analyzed by NIT, RMSECV values between 0.21-0.289 % (w/w) depending on the pre-processing procedure. This is very much in line with the findings on the same API and similar formulation used in the study from paper I. Here it was possible to achieve calibrations for escitalopram within the concentration 4-12 % (w/w) at a RMSECV of 0.25-0.35 % (w/w).

Using NIR spectroscopy to inspect powder blending

The CU measurement, often done by HPLC, is based upon the API, but the uniformity of the excipients can also influence end-product quality, which can be analyzed by e.g. NIR [153]. In the 1990s, Sekulic et al. [146] were among the first ones reporting on successful monitoring of powder blend using NIR probe. Since then, many studies have been reported using NIR for determining the end-point of the mixing of powders [29].

Using NIR spectroscopy to measure moisture content in solid forms

In the NIR range water has specific bands centered around 1950 nm (OH stretching and HOH bending combination) and 1450 nm (1^{st} overtone of OH stretching + 1^{st} overtone HOH bending), and at 970 nm (2^{nd} overtone OH stretching), which has been very useful in the study of water in various samples [11;142].

Drying can be a critical part of the production of API or granulate, but it may also be a potential bottleneck in the process. The quality of the product depends on the drying conditions, and online monitoring of the moisture or solvent content can be of great importance to increase product quality as well as production efficiency [15]. Normally the drying process is stopped either at a specific time, temperature or at a certain degree of moisture. NIR can be used to determine this end point of drying and have the timely advantage over traditional methods as weight loss of drying in oven or Karl Fischer titration. If the production has to wait for clear signal from the laboratory to stop the drying process or if the drying time is fixed, the quality of the product may vary, due to overdrying and potential formation of undesired decomposition products [15].

Han and Faulkner [64] showed a good correlation between loss-on-drying (water) and NIR reflectance for granulation mixture taken out during fluid bed drying. Furthermore, Rantanen et al. [136] also showed how NIR could be used to monitor moisture level during fluidized bed granulation. Frake et al. [46] found that NIR could be used not only to monitor the moisture content during granulation, but also for monitoring the particle size growth of the granule. Therefore, they concluded that NIR is an excellent PAT tool for process control and the use that can lead to more stable process and quality. In 2005, Green et al. [54] point at a very valuable point not only for NIR analysis during wet granulation, but for all in-line analysis and production sample, the issue of proper sampling. They introduced a modified NIR probe with reference sample device, and found that the way the reference sample were taken compared to the NIR had large impact on the ease to develop a calibration. Furthermore, they emphasize the importance of having a representative sample for the process rather than aiming for a low error compared to the reference method, as the reference sample can be incorrect compared to the dynamic in the process.

In the context of determining moisture in solid application, a water gradient in the data from paper I was found and investigated in paper II. Figure 6.6a shows the score plot of PCA on NIT on escitalopram tablets, which is also showed in paper I colored by API concentration (and in Figure 4.1a). In this figure the coloring is according to the day of analysis. The chronological trend in the scores reveals, an uptake of water by the hygroscopic filler silicified microcrystalline cellulose (SMCC) [141]. This interpretation is in agreement with the loading plot (Figure 6.6b) where the first loading (blue line) has a water absorption peak at 950-1100 nm, corresponding to the 2^{nd} overtone O-H stretching of water, and a characteristic 1^{st} overtone combination peak at around 1200 nm. The measurements were carried out over the time period of two months (15 days of analysis), and the tablets were stored at room temperature in NIR vials.

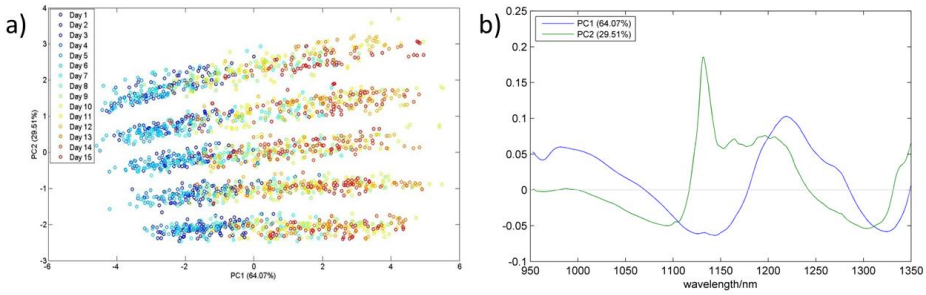

Figure 6.6: a) PCA score plot of NIT spectra of escitalopram colored according to day of analysis. b) Corresponding loading plot

In order to investigate how the water uptake will affect a calibration model, PLS models built on day 1-9 of analysis were calculated and (test set) evaluated on the spectra from day 10-15 of analysis. Figure 6.7a shows the PLS calibration model of the full spectral range (952-1350 nm) model for the calibration set (day 1-9) and the test set (day 10-15) using three LVs. RMSECV obtained is 0.320 % (w/w) and RMSEP is 0.417 % (w/w). Figure 6.7b shows a PLS model on a reduced spectral range (1118-1137 and 1272-1296 nm, found by iPLS) on the same calibration and test set using three LV. Using the optimal spectral range selected by iPLS, the RMSECV is reduced to 0.244 % (w/w) and the RMSEP to 0.236 % (w/w), which are close to the calibration results obtained with all the spectra in paper I (RMSECV 0.251 % w/w). These results demonstrate, that through variable selection, the model for API concentration is not only improving, but also that it becomes unaffected by the interfering water uptake.

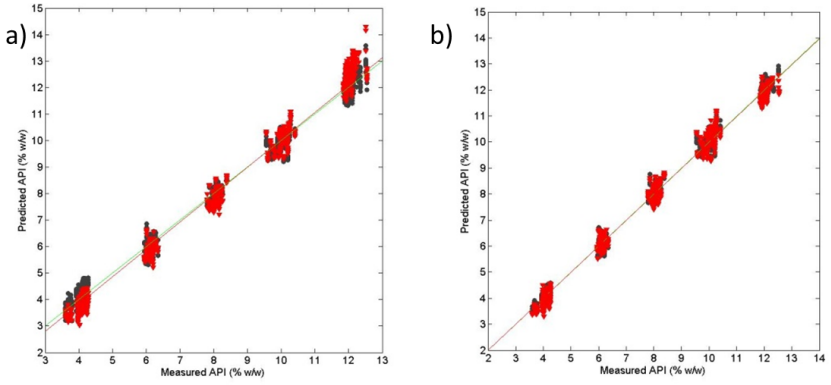

Figure 6.7: PLS calibrations on escitalopram tablets divided into calibration set (black), day 1-9 and validation set (red), day 10-15. a) Spectral range used from 952-1350 nm, RMSECV is 0.308 % (w/w) and RMSEP is 0.332 % (w/w). b) Calibration on spectral ranges 1118-1137 and 1272-1296 nm, RMSECV is 0.244 % (w/w) and RMSEP is 0.236 % (w/w). There are used three latent variables and SNV and mean centering of the spectra.

Using NIR spectroscopy to study crystallinity and polymorphism of excipients and API

Polymorphs differ in the way the molecules are packed into the crystal lattice, and often have differences in the hydrogen bonding. Differences in hydrogen bonding can be seen as a shift in the fundamental bands in the mid-IR, and as overtones and combinations band in the NIR range [28]. Luner et al. [100] found that NIR relative accurately determined different forms in binary powder mixtures of sulfathiozole, sultamethoxazole, ampilicillin and, lactose (α- and β-form). Davis et al. [28] found that NIR during granulation could quantify the transformation rate of γ-glycine to α-glycine at different drying techniques. Furthermore, Dreassi et al. [35] found that it was possible to classify four different polymorph forms (three crystal forms and the amorphous form) of chenodeoxycholic acid by NIR.

Fix and Steffens [45], Gombás et al. [51], and Nørgaard et al. [121] all modeled on mixtures between crystalline and amorphous lactose. In the study from paper III, calibrations for crystallinity in binary mixtures of crystalline and amorphous lactose were performed. The spectral areas used for the lower concentration calibration were mainly in the area 1870-2014 nm (O-H combination band, 1900-1980 nm [121]) and, to a lesser extent, 1537-1560 nm (O-H 1^{st} overtone) and the area around 1200 nm, probably due to C-H 2^{nd} overtone [51]. This gave a RMSECV of 0.2 % (w/w) for 0-10 % crystallinity, which are in line with the findings of Fix and Steffens [45], who found RMSECV of 0.537 % (w/w) for 0-10 % lactose.

Other relevant NIR applications

NIR has also been used to predict particle size and hardness of tablets [101]. Furthermore, NIR is also widely used for identification of genuine drug compared to counterfeit-drug. This is an increasing problem, especially as counterfeit products become more sophisticated [138].

Robust calibration development for PAT applications

There are many definitions of calibration "robustness" in the literature [177]. In this thesis, robustness of a multivariate calibration is referred to as its stability to remain unaffected by small but deliberate introduced variations. This will indicate its reliability during normal use, and the definition is similar to the definition by ICH [75] and by Zeaiter et al. [177].

Most routine processes under normal operation conditions will not provide the data required for developing calibrations for quantification [32]. Blanco and Peguero [10] describes that the success in developing accurate NIR calibrations relies on having large enough calibration sets that cover the characteristics of the samples of future prediction. For expanding the range of the calibration there exist different approaches. Construction of calibrations using laboratory powder mixtures is a simple way to obtain a sufficient calibration range. However, this might not succeed for production sample predictions, as properties from the production process are missing [107]. Spiking powdered production tablets with excipient or API, will to some extent include the physical properties of the production tablets. It will, however, be better to build the calibration on intact tablets on the desired calibration range [107]. NIR calibration should be carried out with samples whose physical properties correspond to those of the samples to be determined [107]. Blanco et al. [9] found that due to small changes in

physical properties during the manufacturing process, at least three production samples were needed in the calibration set of lab samples, to obtain a good prediction of future production samples. When spectral variation is caused by other parameters than the predicted (e.g. external variation in temperature), it can be included in a global model or only spectral areas that is not heavily influenced by the external variation can be chosen [158]. The latter approach is similar to the example with the water uptake in the escitalopram (Figure 6.7b), where only spectral areas not majorly influenced by the water were chosen.

The ICH guideline Q2A [75] recommend for calibration purposes, at least to expand the API concentration range to ± 20 % of the nominal value. Blanco and Peguero [10] recommend to expand calibration design with ± 5 % around of each excipient to account for potential differences in production and to minimize correction, all in order to ensure robustness. Furthermore, Xiang et al. [172] emphasize that it is important to break the internal correlation between the constituents and most important between the API and the excipient. Otherwise, the model may be built on variation that is not related to the API, and if this relationship is different in future samples, the prediction might fail.

In order to investigate in more detail how compression force during tableting influences the API calibration, a calibration setup with spectra from the different time points in paper I were used. Tablets from four of the six time points were produced with a hardness, H_{medium}, close to 85 N (time point 1, 2, 5 and, 6), whereas tablets at time point 3 were produced at hardness, H_{low}, of 70 N (low hardness, but within specifications), and tablets at time point 4 were produced at hardness, H_{high}, of 100 N (high hardness, but within specifications). These calibrations were produced on randomly selected spectra from five time points and evaluated on the last time point. There were no restrictions in sample position, but only first replicates were used. The selections of spectra were performed 100 times. First the calculations were done based on the API concentration in mg/tablet and then afterwards in % (w/w). Figure 6.8 shows the RMSEP from models with 1 to 30 spectra from each concentration level (mg/tablet). The results for the models containing more than 30 spectra for each API concentration level are not shown as these do not differ significantly from the model with 30 spectra. At the first point on the graph (x-axis), only one spectrum from each batch (five spectra in total) is used for each calibration. Therefore, the average and the standard deviation of RMSEP for the 100 calibrations are high, which means that the calibrations build on one spectrum per batch are not reliable. The average RMSEP decreases as the number of spectra increases. Furthermore, the standard deviations between the 100 calibrations also decrease with the sample size. This is as expected, as increasing the calibration set optimally also should provide a more stable model, and the variation between similar models should decrease. The RMSEP curve seems to flatten out or converge when using more than 10-20 NIT spectra per API level. This is much in line with different analysis of the same data (paper I), that showed that minimum 90 spectra or 18 per API concentration were required to get a robust calibration. From Figure 6.8 it is clear that the RMSEP for 20 spectra for time point 3 (H_{low}) is higher than for the other time points. Time point 1, 5, and 6 are the lowest and time point 2 and 4 are mediocre. Noticeably, the PLS prediction does not perform well on tablets of low hardness, i.e. high porosity (time point 3), when there are no such tablets included in the calibration set. This could be due the fact that the tablets with low hardness are higher

than the remaining tablets, and more of the light from the beam will be either absorbed or scattered due to higher degree of internal voids [25]. The opposite does not seem to be the case for tablets of high hardness, i.e. low porosity (time point 4). This could probably be due to the difference in porosity between the three hardness level (H_{low}, H_{medium}, and H_{high}: 23 %, 19 %, and 17 %), and that there is a large difference from H_{medium} to H_{low} compared to H_{medium} to H_{high}.

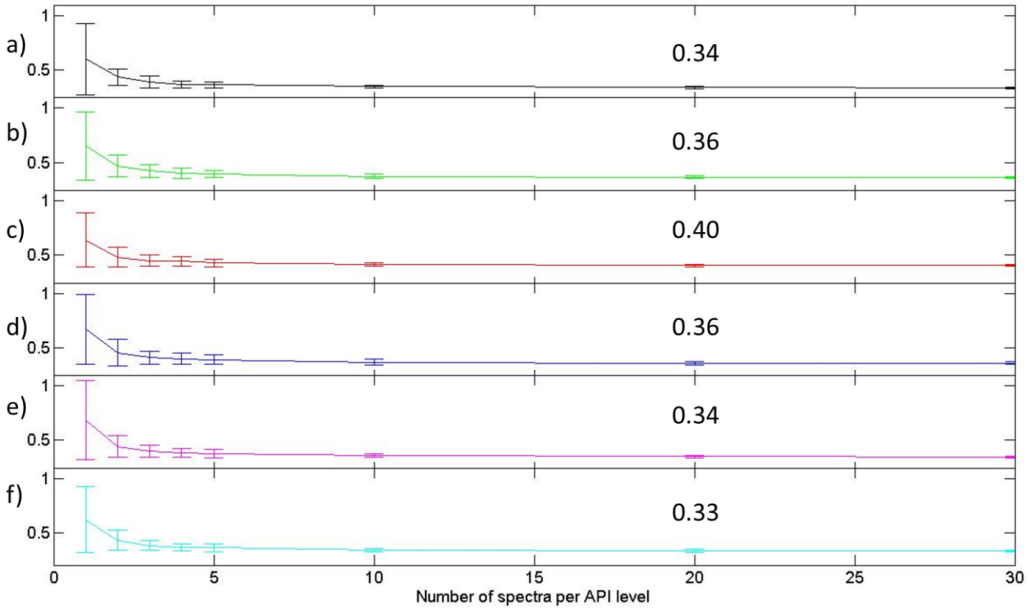

Figure 6.8: Number of spectra used to creating the calibration from each API level, RMSEP values are calculated in mg/tablet. The calibrations are created on five time points and validated on the last time point. RMSEP mean ± standard deviation for calibrations evaluated with spectra from time point 1 to 6. Between 1-30 NIT spectra from each API concentration randomly selected 100 times from all directions are used for calibration and calculation of standard deviation (only first replicates). Three latent variables (LVs) are used and the spectral areas of 1018-1086, 1063-1070, 1104-1129, and 1139-1156 nm are included. a) time point 1, hardness 85 N, b) time point 2, 85 N, c) time point 3, 70 N, d) time point 4, 100 N, e) time point 5, 85 N, f) time point 6, 85 N.

However, if the models were calculated on weight corrected API values (% w/w) the picture looks a little different. In Figure 6.9 is shown the results from the models calculated from API in % (w/w). As one tablet weight is approximately 125 mg, the weight corrected results are approximately 20 % lower than the results in mg/tablet, and can therefore not be compared directly. Figure 6.9 reveals no difference between the RMSEP at 20 spectra for time point 3 (H_{low}) and the other time points. With the weight corrected results, there are no significant differences between the hardness levels H_{medium} and H_{high} or H_{low}. In paper I it was shown though, that calibrations made on the samples from H_{medium} gave poorer predictions on H_{low} tablets than H_{high} tablets. The reasons for the different findings can be due to different selection method in spectra and spectral range.

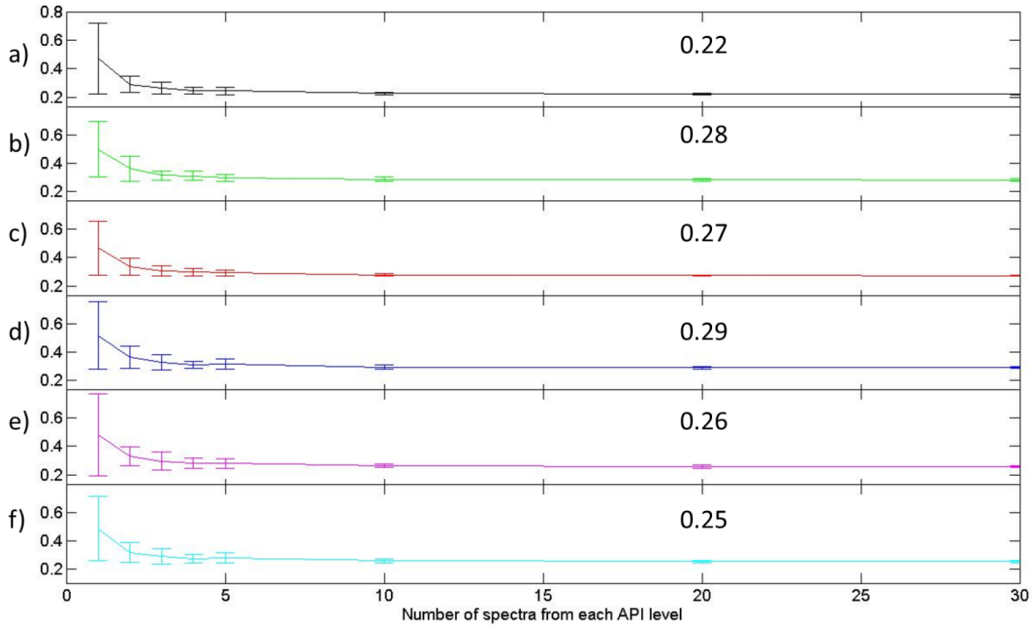

Figure 6.9: Number of spectra used to creating the calibration from each API level, RMSEP values are calculated in % (w/w). The calibrations are created on five time points and validated on the last time point. RMSEP mean ± standard deviation for calibrations evaluated with spectra from time point 1 to 6. Between 1-30 NIT spectra from each API concentration randomly selected 100 times from all directions are used for calibration and calculation of standard deviation (only first replicates). Three latent variables (LVs) are used and the spectral areas of 1018-1086, 1063-1070, 1104-1129, and 1139-1156 nm are included. a) time point 1, hardness 85 N, b) time point 2, 85 N, c) time point 3, 70 N, d) time point 4, 100 N, e) time point 5, 85 N, f) time point 6, 85 N.

When constructing calibrations, it is important to incorporate variation that potentially could be met in future sample. Usually, it is a compromise of including sufficient information but not make it overly broad, as the model will often perform poorer. An example of what will happen if too little variation is built into the calibration is shown in Figure 6.10. PLS models on NIT on escitalopram tablets (from paper I) were performed with all samples (2160 individual spectra), averaging over spectral replicates (3 replicates → 720 spectra), averaging over tablets turning with the scored line facing down (3 rep · 2 down → 180 spectra), averaging over tablets turning with the scored line facing up (3 rep · 2 up → 180 spectra), averaging over tablets turning both up and down (3 rep · 4 up/down → 180 spectra), averaging over tablets taking from the same time point, tablet replicates, (3 rep · 4 up/down · 6 tablets → 30 spectra), and averaging over tablets taking from the same batch (3 rep · 4 up/down · 6 tablets · 6 time points → 5 spectra). The RMSECV is calculated by taking out a time point at the time (1/30 of data) and in the last model one concentration at the time. The "RMSEP" values are not independent results as it is obtained by predicting all the individual spectra. RMSECV decreases when using fewer spectra until a certain point, 30 spectra is the minimum, whereas the 5-spectra model gives a higher RMSECV. When validating with all the individual spectra, the "RMSEP" stays at the same level (~ 0.28 % w/w) except at the 5-spectra model, where it doubles to ~ 0.57 % (w/w). This means that at this point too much information has

been averaged out and is no longer part of the calibration, which negatively affects the prediction. This information includes differences between the time points and the pressure, which is the main cause for the models to decrease in performance.

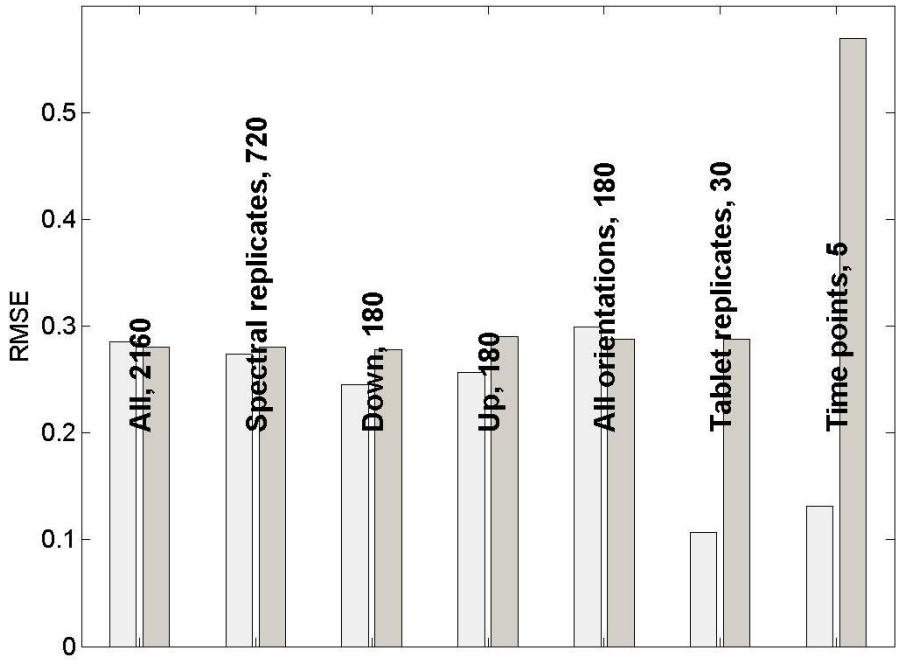

Figure 6.10: PLS models of API in escitalopram tablets analyzed by NIT with HPLC as reference. RMSECV (white) and "RMSEP" (grey). Three LVs are used and the spectral areas of 1126-1132 and 1287-1295 nm are included. Values are calculated in % (w/w).

Presentation of the sample to the NIR instrument

When a sample is going to be analyzed it is important to know what difference it makes if the tablet is analyzed facing up or down, especially if the analysis is on-line. In reflection NIR analysis, Laasonen et al. [90] found that the two faces of a tablet gave different spectral information when analyzing and decided to use an average of spectra from both faces. The difference was due to higher compression force in the upper punch than the lower punch, leading to a variation in tablet density and therefore a spectral difference. Ito et al. [82] compared reflection and transmission spectra for tablets of different thickness, shapes and also including embossing and scored line. The second derivatives of the reflection spectra were affected by all the variation, where the second derivatives of the transmission spectra were mainly affected by the shape and thickness of the tablet. It was possible to create quantification API calibration models that could predict despite all the variability, however additional 6 LV were needed. The models based on transmission spectra performed better than the reflection model. Further, for reflection mode, it was recommended not to measure the face of the tablets that was embossed or had a scored line.

One of the aims with the study from paper I, was to show the difference of the sample presentation in the NIT instrument. As the samples are tablets with a scored line and two letters on the front side, it was possible to turn the tablet four different positions where position 1 and 2 were facing upwards (away from the light beam) and 3 and 4 face downwards (towards the light beam). For the setup there were five API concentration levels, six time points and six tablets from each time point.

To test the difference between turning the tablet upwards and downwards in the tablet auto sampler, up to 30 spectra from each API level were selected either turning up (position 1) or down (position 3). Five time points were used for the calibration and the last time point was used for prediction and gave RMSEP and a standard deviation for RMSEP (only one RMSEP for 30 spectra). The random selection of the spectra was repeated 100 times except for the case with all 30 spectra included. The results (% w/w) are summarized in Figure 6.11 for the six time points. It is seen that there are differences in the models containing tablets facing upwards and downwards. For all time points except time point 4 (H_{high}), the models, including only the tablets measured downwards, are inferior to the upwards models. This is probably due to higher light scattering when the tablets are facing the light source, and therefore giving higher deviation in the transmission. This is closely related to findings of Cournoyer et al. [25], that observed differences between the the two sides of the tablets with different embossing. When comparing all the models of tablets turning upwards with the models of tablets turning downwards, there are no significant difference (p=0.38) on the RMSEP-values. However, comparing the models from the normal level of hardness (H_{medium}) the RMSEP-values of the upwards facing samples are significant lower than the models including the downwards facing samples.

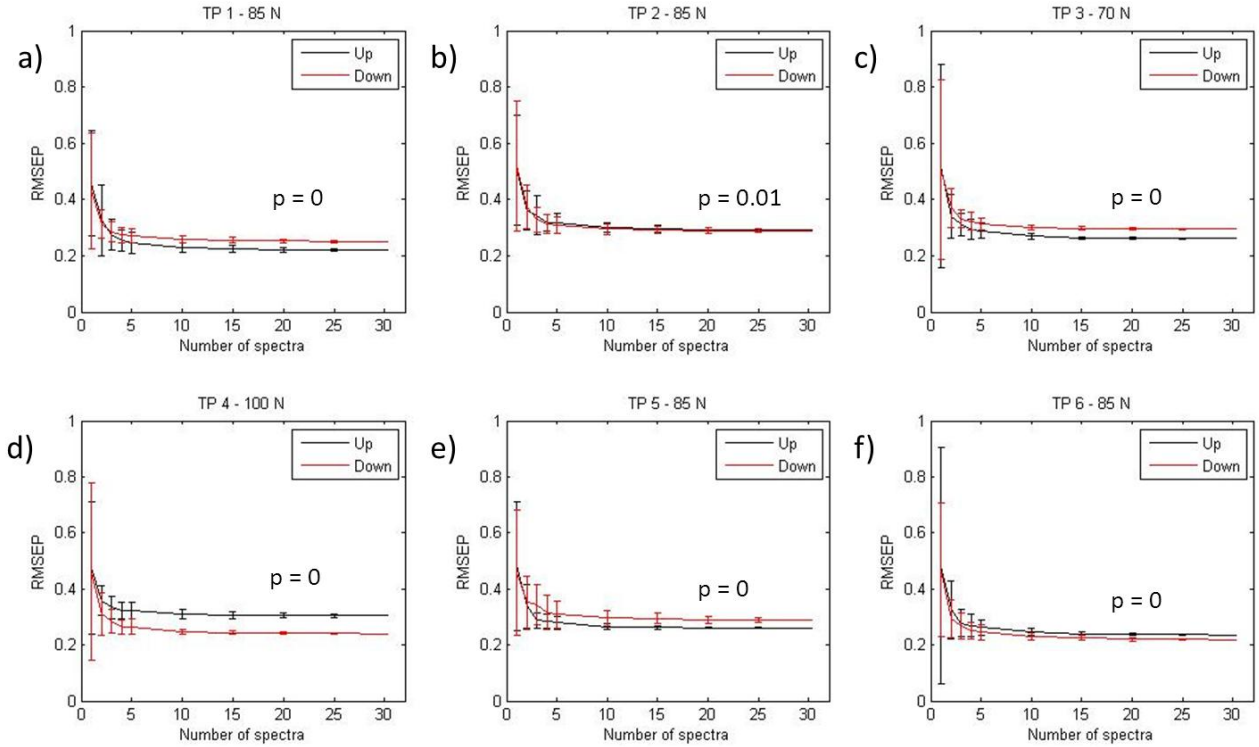

Figure 6.11: Number of spectra per API concentration level to create calibrations. RMSEP mean and standard deviations (100 random selections) for calibrations evaluations at time point 1 to 6 for tablet facing upwards and downwards. The p-levels are from ANOVA test between up and down of calibrations containing 20 spectra at each API level.

Perspective for NIR usage for pharmaceutical solid applications

There still exist some challenges within sampling and sample presentation in the NIR instrument. Tablets that have scored lines or are embossed etc. may be more difficult to analyze in an on-line application. It could be interesting to consider analyzing the powder in the moment it is fed into the die of the tablet press but before compression. The analysis would then be done on the powder in reflection mode, and this could potentially lead to scatter problems depending on particle size distribution. However, Pfizer is currently showing progress with the installation of a NIR probe in the force feeder of a rotary tablet press [62].

NIR can, besides performing the actual predictions, also provide more knowledge of the tablet process. An example is when there are differences between upper and lower punches in a rotary press, which could have an effect on the dissolution of the tablet, as the porosity is different in the upper and lower part of the tablet. This may seem like a minor issue, but in a layered tablet with different functionalities, this may be of higher importance.

Regarding the challenges of creating robust calibrations, Pieters et al. [133] propose a different approach that works over longer time and includes more production variation. This is to include prior knowledge from spectra of API and excipients and use this to extract intra- and inter-batch variability by orthogonal projection. In this way, more spectra but fewer reference samples are needed to build calibrations that encounter the process variation. Hansen et al. [67] demonstrated how external factors from cheese production can be removed from spectral data by orthogonalization. Both these approaches could be relevant to pharmaceutical tablet productions as many reference samples are usually time consuming and costly to prepare.

6.3 Terahertz spectroscopy: a new PAT tool in the pharmaceutical industry

The terahertz (THz) region of the electromagnetic spectrum is usually defined to be 0.1-10 THz (3.3-333 cm^{-1}) [132]. The THz region is positioned between microwave and radio frequencies on one side and IR and NIR region on the other side (see Figure 6.1). The THz region is often called the "THz gap" due to a recognized lack of efficient, coherent light sources and detectors in this region [132]. However, during the last decades terahertz spectroscopy has undergone dramatic changes, including increased amount of development and commercialization within the terahertz pulsed spectroscopy and terahertz pulsed imaging [44;148].

In the following is described a setup of a terahertz time domain spectroscopy (THz-TDS), which is often called terahertz pulse spectroscopy. A general setup of a THz-TDS system is shown in Figure 6.12 [47]. In order to generate electromagnetic energy in the THz range, the duration of the electromagnetic oscillation must be within the picosecond or femtosecond range, therefore a femtosecond laser is often used [184]. A pulse from the femtosecond laser is divided by a beam splitter (BS) into a probe beam and a pump beam. The pump beam goes to THz emitter and generates a single-cycle of THz radiation. This THz pulse is then transmitted through the sample and collected by the THz receiver (detector). In the meantime, the probe beam is passed through a variable time delay before passing to the THz receiver [47]. By varying the time delay of the probe pulse, the point where the pulse is sampled changes and the detector records different values as a function of time delay. When mapping the electrical field of the THz pulse by the time delay, a THz waveform is found. A waveform is found for the reference and for the sample. In transmission mode, the reference could be the sample cell without the sample. In reflection mode it could be a high reflecting metal mirror [126]. Through Fourier transformation of the waveform, the amplitude and the phase can be found [47;184].

In THz-TDS, the electric field, *E*, is obtained and is dependent on time, *t*. The time dependent electric field, *E(t)*, is transformed into a circular frequency space, *E(ω)*, using Fourier transform such as [126]:

$$\boldsymbol{E(\omega) = \int E(t) e^{-i\omega t} dt} \qquad 6\text{-}13$$

Both amplitude and phase information can be directly recovered as a signal directly proportional to the electric field of the terahertz pulse, rather than just the intensity [182]. Due to the fact that there is both a real and complex part it is possible to extract both the amplitude and the phase [126].

$$\boldsymbol{E_{Sample}/E_{Reference} = |\tau|\, e^{-i\varphi(\omega)}} \qquad 6\text{-}14$$

where φ is the phase and $|\tau|$ is the complex transmission. In the Fourier transmission often a filter is used to smooth the data. Several methods can be used to remove noise when transforming the waveform into a suitable time-domain response, e.g. a Gaussian filter function to remove both high and low frequency noise [132].

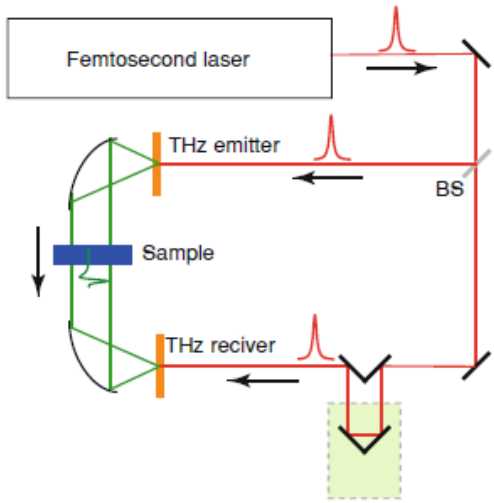

Figure 6.12: Measuring principle of THz time-domain spectroscopy, BS: beam splitter (from Freeman et al. [47]).

The following is an example of the conversion of the time-domain waveform to the amplitude or power spectrum and further to the absorption spectrum (data from paper III). Figure 6.13a shows the waveforms of amorphous lactose and crystalline α-lactose monohydrate and a Teflon reference cell used in paper III. Figure 6.13b shows the corresponding power spectra and Figure 6.13c the absorption spectra for the amorphous and crystalline lactose sample.

The reflective index is proportional to the density of a medium. As it is often a porous material that is measured, it will be a combination of the refractive index of the material and air (air is included in the porous material), which will be the effective refractive index [85]. Juuti et al. [85] also found that with terahertz spectroscopy it was possible to monitor the porosity of flat-faced acetate tablets.

The absorption spectrum of the THz radiation is directly related to the three-dimensional arrangement and low frequency motions of all the atoms in a molecule, so it is sensitive to the molecule's interaction with its environment [169]. The vibrational characters of the normal modes in the THz region consist primarily of external motions (rotations and translations) and global internal motions (torsions) that are governed by the intermolecular contact specific to the crystalline system [156]. The vibrational motions of modes less than about 50 cm^{-1} are almost purely external in nature, while higher energy modes consist of mixed inter- and intramolecular motions [88]. In contrast to MIR and NIR, the THz region is dominated by intermolecular vibration corresponding to motions of larger molecules or phonon modes (Figure 6.14). These phonon modes only exist in materials with periodic structure. This is often seen as crystal fingerprints, therefore terahertz spectroscopy is excellent for characterization the crystalline properties of solid material, as the phonon lattice modes are probed directly [148].

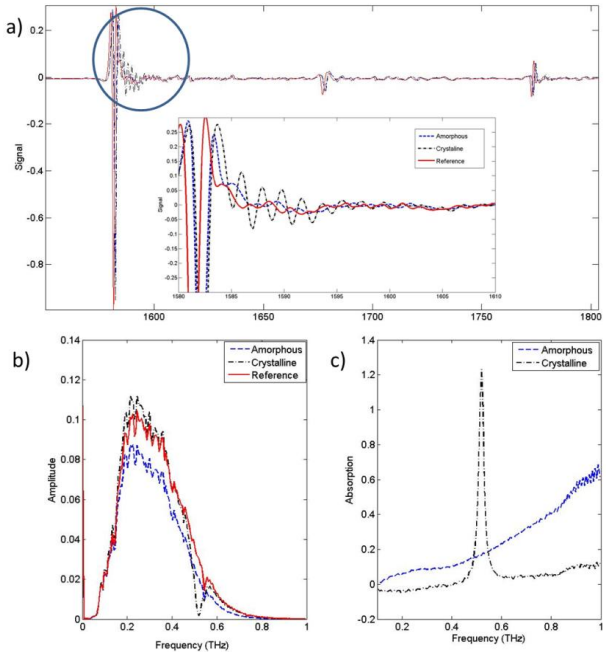

Figure 6.13: a) Terahertz time domain waveform of pure amorphous and crystalline lactose and reference (Teflon) cell. b) amplitude or power spectra of amorphous and crystalline lactose, and reference. c) absorption spectra of amorphous and crystalline lactose.

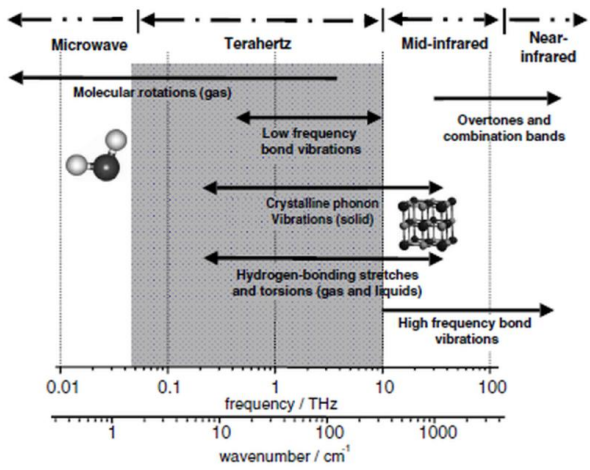

Figure 6.14:The THz region and molecular transitions in the electromagnetic spectrum (from Pickwell and Wallace [132]).

Many amorphous compounds are transparent or semitransparent, whereas many crystalline compounds have characteristic spectral features in the terahertz region [148]. Crystalline

compounds have sharp spectral features that arise from inter-molecular vibrational modes of long-range order, controlled by non-covalent bonds between the molecules. The lack of long-range symmetry in amorphous compounds means that the sharp features are not present in the spectrum, but absorption is monotonously increasing absorption at higher frequencies [132;156]. Crystalline APIs have unique phonon modes and different polymorphic forms have different terahertz spectra [160]. Furthermore, absences of distinct modes in liquid crystalline and amorphous form of pharmaceuticals have been demonstrated, which is likely to be due to the lack of order in these compounds [155]. Otsuka et al. [123] found, though, that different amorphous forms of indomethacin, due to different methods of preparation, had different pattern in the THz range. Analysis with XRPD could not see the different polyamorphous solids, since they all had similar X-ray diffraction patterns. In Table 4 are shown some examples of studies with terahertz spectroscopy used to distinguish between crystalline, hydrates and amorphous forms.

McIntosh et al. [105] could, by terahertz spectroscopy, follow the crystallization of amorphous lactose due to high humidity. Furthermore, Zeitler et al. [178] found that hydrate and anhydrate forms of α-lactose, carbamazepine, piroxicam, and theophylline showed very different THz patterns. Similar findings were presented by Liu et al. [99] who investigated hydrate and anhydrous forms of caffeine, theophylline, D-glucose and ampicillin. The water occupies certain positions in the crystalline lattice by forming hydrogen bonds or coordinate covalent bonds with the anhydrous molecule, which results in different crystalline forms for the hydrate and the anhydrate [99]. As there are van der Waals interactions and hydrogen bonds with vibrational frequencies in the THz range, terahertz spectroscopy is an excellent tool for detecting water [132] and probably also monitoring pharmaceutical purity regarding water [6]. Therefore, THz-TDS is in general highly affected by humidity [162].

Ikeda et al. [80] found that changes in polymorphism of both carbamazepine and tolbutamide can be detected earlier by second derivative of terahertz spectrum than by XRPD. They confirmed that terahertz spectroscopy is one of the more highly sensitive analytical methods for determination of pharmaceutical polymorphs [80].

Terahertz spectroscopy is shown to be an effective tool to characterize and follow the kinetics of solid transformations [148]. This includes detecting changes due to temperature changes in polymorphic forms for carbamazepine [179;181] and sulfathiazole [180]. Zeitler et al. [182] found that phase transformation can be seen by terahertz spectroscopy. Even though, no distinct features were observed in the THz range, thorough analysis leads to differences between glassy and rubbery state of amorphous carbamazepine.

Nishikiori et al. [119] could quantify L-tartaric acid in L- and DL-tartaric acid mixture. It was not possible to observe differences on L-or D-tartaric acid, due to the fact that the intermolecular vibrations and phonon frequency are the same for L- and D-tartaric acids. However, both intermolecular vibrations and phonon frequency of DL-tartaric acid were different from those of L- or D- tartaric acid. The quantification method of L-tartaric acid improved by using PLS instead of a single peak at 1.09 THz.

Wu et al. [169] analyzed with terahertz spectroscopy theophylline and excipients in tablets with variation in concentrations, production methods (wet granulation and direct compression) and tablet hardness. For predicting the content of the tablets, three different approaches

were used to evaluate the spectra; characteristic peak uni-variate method, superposition method (addition of spectral information), and multivariate method (principal component regression, PCR, and PLS). The outcome was that multivariate data analysis outperformed the other methods. Furthermore, terahertz spectroscopy was suggested to pick up on some of the physical information, such as the tablets processing history, hardness level or whether the tablets were manufactured by wet granulation or direct compression [169]. For theophylline and MCC better correlation were obtained for tablets with the same nominal hardness compared to the cases with tablets of different hardness values [169]. A similar discovery was made with hardness level and NIR in article I (see more in Section 6.2 Infrared spectroscopy).

Since the radiation energy that interacts with the sample is less than at other radiation frequencies (e.g. NIR or mid-IR radiation), the likelihood of damage of the sample by radiation will be lower [171]. In fact, the ultrashort pulses of electromagnetic radiation are approximately 1 million times lower power than X-ray photons [162]. Terahertz has a better sensitivity and dynamic range compared with far-IR Fourier transform spectroscopy at frequencies under 3 THz [63]. Furthermore, Han et al. [63] found that terahertz spectroscopy have a five times higher signal to noise ratio than FT-IR in the same range. At high frequencies, above 5 THz, far-IR Fourier transform performs better.

The influence of particle size on terahertz measurements

THz utilizes longer wavelengths than both NIR and mid-IR, and is therefore less influenced by scatter from particles [171]. However, the effect of scattering cannot be completely ignored particularly for granulated materials with particle sizes in the terahertz radiation [148]. The particle size that could disturb the terahertz radiation with scatter, changes with the wavelength and is around 300 μm for 1 THz and around 75 μm for 4 THz [159;170]. Shen et al. [147] found that sucrose samples above 250 μm had anomalous spectral features and showed very little uniformity between samples. Furthermore, nonabsorbing polyethylene powder with different particle size (< 50μm to > 200 μm) were investigated. It turned out, that overall scatter increased with the third powder of the particle size in the range from 50-250 μm. Strachan et al. [156] on the other hand, found that PE up to 80 μm could be used without scattering problems. In general it is recommended to minimize the effect by either using finely milled powder or compress powder into a pellet-like compact. Alternatively, averaging over multiple measurements over a large sample area is also a possibility [147].

Table 4: Examples of studies by terahertz spectroscopy of polymorphic, amorphous and hydrate forms.

Researchers and references	System studied	Outcomes	Limitations
Taday [160] 2003	Polymorphic identification of ranitidine hydrochloride form 1 and 2 in powder and in tablets	Possible to identify the two forms. In tablets different spectral profile above 1.5 THz due to different excipients.	
Taday [159] 2004	Quantifications, acetylsalicylic acid and paracetamol in presence of lactose and cellulose using PLS	RMSECV of 2.85 % for paracetamol (0-67 %), 3.90 % for aspirin (0-67 %), 3.65-4.3 % for lactose (0-58.7 %)	
Strachan [155;156] 2004, 2005	Polymorphic forms of carbamazepine, enalapril maleate, crystallinity of fenoprofen calcium and indomethacin	RMSECV values between 0.35-2 %. LOD 0.69-4 %, LOQ 2.1-12.1%	
Liu et al. [99] 2007	Hydrate and anhydrous forms of caffeine, theophylline, D-glucose and ampicillin	Could identify the hydrate and anhydrate forms	
Zeitler [178] 2007	Hydrate and anhydrate of α-lactose, carbamazepine form I, III and dehydrate, piroxicam form I and monohydrate, theophylline anhydrate and monohydrate	Could identify all forms both at 90 K and 293 K, sharpest peaks at 293 K	
Otsuka [124] 2010	Quantification of mefenamic acid form I in miture with form II 0-100 % in 10 % increase. Different pre-treatment of data used.	SEC down to 8.6 % with 2nd derivative and mean. No mixture with PE	Up to 7 LV are used to create the models
Chakkittakandy [18] 2010	Polymorphic forms of mannitol in freeze-dried droplets	Could identify different forms due to different settings for the freeze drying	Best separation of the forms happened between 2.5- 6 THz, many systems will not be able to measure in that range
King [88] 2011	Identification and quantification of two polymorphic forms of diclofenac acid	Could quantify the two forms at 78 K, and also calculate the theoretical peaks with density functional theory	The samples had to be cooled to 78 K to obtain nice separation in the two forms
Hisazumi [70] 2011	Theophylline anhydrate mixes with theophylline monohydrate, MCC and Magnesium stearate (0, 25, 50, 75, 80, 90, 100 %)	Could quantify anhydrous form with RMSECV 2.89 % using 3 LV	
Takeuchi [162] 2012	Crystalinity of trehalose dihydrate (0, 25, 50, 75, 100 %). Prediction of trehalose dihydrate microspheres	Nice correlations for crystallinity at 3 different peaks (R^2 =0.9992-0.9998)	Predictions of the microspheres gave 3 different answers (2.39-4.73 %), and water vapor may be causing these differences.

Figure 6.15 shows terahertz spectra of crystalline lactose monohydrate (Pharmatose 50M, 80M and 110M, DMV Fonterra, Goch, Germany) with three different particle sizes and distributions. The crystalline lactose peaks at 0.53 and 1.36 THz are obvious, which are also identified by Allis et al. [2]. As the particle size increases, the background gets higher especially at higher frequencies, which may make quantification in the lower range of crystallinity more difficult. It can further be observed that the peak at 0.53 THz is not significantly influenced by the particle size.

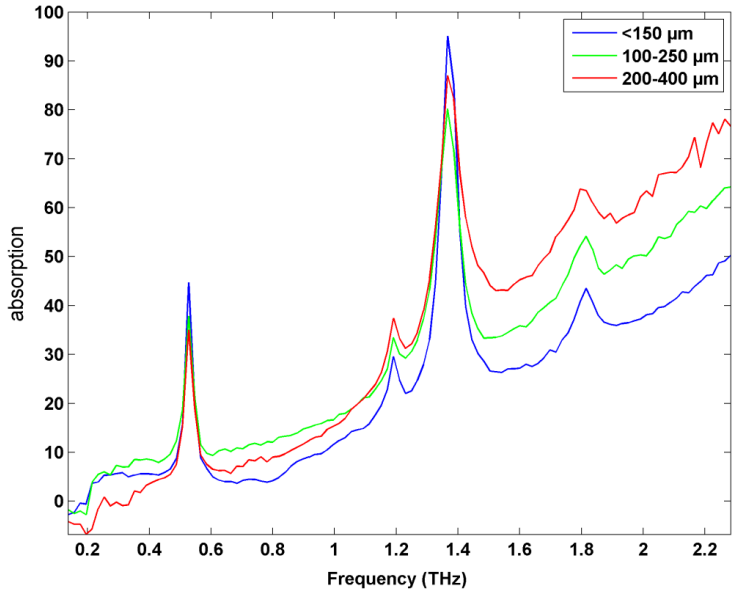

Figure 6.15: Terahertz spectrum of crystalline α-lactose with 3 different particle sizes, <150 µm, 100-250 µm, and 200-400 µm.

Increasing the terahertz information by sample dilution with polyethylene

In terahertz transmission spectroscopic experiments, it is often desirable to keep the amount of sample to a minimum in order to maximize the spectral bandwidth of the instrument, which without dilution results in a sample thickness down to 0.2 mm [125]. This can cause multiple reflections from the pellet-air interfaces, causing the signal to bounce back and forth in the sample (the etalon effect or Fabry-Perot effect). In the time domain, this is seen as echoes of the main peak [34;105;125], and the effect manifests itself as oscillations in the measured transmission spectra. Therefore, samples often need to get diluted to avoid exceeding the limits of the dynamic range of the systems [84;125]. High-density polyethylene (PE) fine powder is often added in concentrations ranging from 25-96 % of the total sample [2;155;156;160;170]. Ultrahigh molecular weight PE is a good binder and is nearly transparent with a rather frequency independent refraction index of 1.53, in the terahertz region [167]. When adding PE to the sample, the dynamic range of spectrometer can be fully exploited,

while the ticker sample results in a larger separation in the time domain of etalon echoes, which are then easy to remove by standard time windowing procedures [105;125]. The drawback of adding PE is that it makes it less applicable for in-line production analysis. Furthermore, there will be larger errors when handling and diluting samples. Wu et al. [170] reported that when preparing a disk sample for analysis, disk drying time, disk composition, and particle size could influence the intensities and peak positions of the terahertz transmission spectra.

In the terahertz spectroscopy study (paper III), the lactose samples were not diluted with PE. This led to lower spectral dynamic range and most likely also to saturation when the lactose samples contained between 90-100 % crystallinity.

There have only been reported a few studies that quantify the limit of detection (LOD) and limit of quantification (LOQ) of terahertz quantification of different polymorphic forms in mixtures. Strachan et al. [156] found for carbamazepine form I in 0-10 % (w/w) mixtures with form III, LOD of 1.2 % and LOQ of 3.7 %, when calculating from the deviation of the samples with lowest concentration. For enalapril acetate form I in 0-10 % (w/w) mixtures with form II, they found LOD of 0.69 % and LOQ of 2.1 %. For detection of crystallinity, Strachan et al. [156] found for 0-100 % crystalline indomethacin in binary mixture of amorphous and crystalline indomethacin, LOD of 1.1 % and LOQ of 3.2%. For crystalline fenoprofen calcium 0-100 % the LOD was 2.7 % and LOQ was 8.2 %. In the terahertz spectroscopy study (paper III), models on binary mixtures of amorphous and crystalline lactose were created on samples containing 0-10 % crystalline material. The terahertz model had a RMSECV of 0.30 % (w/w), and LOD and LOQ of 0.8 % (w/w) and 2.4 % (w/w) respectively.

For another application using terahertz spectroscopy, Ma et al. [102] found for thiabendazole, a white powder, mixed with PE 0-50 % (w/w), variable selection for terahertz spectroscopy worked very well. With moving window PLS (interval size 9) the RMSEP was lowered to 0.36 % (w/w) (3.75 % relative error) compared to 0.75 (9.6 % relative error) obtained by PLS on the full spectra, 0.3-1.6 THz with 72 intervals.

Kawase et al. [87] detected spectral differences in THz-TDS on three different types of medicine (Amlodin OD, Basen OD and Gaster D) due to aging when analyzing samples before and after expiration dates. Even though, there was seen unevenness between tablets from same batch, the differences between old and newer batches were larger. The tablets were also tested on XRPD, but no changes could be detected.

Using terahertz spectroscopy in reflection mode

Most terahertz spectroscopic measurements are done in transmission mode, but some are performed in reflection mode [83]. Reflection configurations can be useful when studying opaque samples as large solid dosage forms or tablets in packages [147;148]. Hisazumi et al. [71] used terahertz reflectance spectroscopy for quantification of drug substance in tablets of mixture of mannitol and sodium salicylate. Due to the use of an aluminum mirror, the reflection intensity was enhanced. In double layer tablets with the top layer consist of mannitol, sodium salicylatein the range from 8.1-13.5 % (w/w) could be detected with a RMSEP of 1.4 % relative error in 3 mm thick samples. They also found that with the enhanced reflection

intensity it was possible to analyze at least 5 mm thick samples. Furthermore, they mention the option that in a tablet press, the lower punch can be used as a mirror and therefore in-line monitoring is possible. They concluded, though, with their setup that 256 scans are needed for standard deviation to reach a plateau, and this will take 2 sec, which is still too slow for current tableting production speeds [71].

Attenuated total reflection (ATR) has also been used in the THz range. Newnham and Taday [118] found ATR very useful for fast screening of many small samples, as only 1 mg is needed, which makes it very useful for development purposes. This could be a solution for avoiding dilution of the sample with PE [148].

Terahertz pulse imaging (TPI) is a technique where the time domain waveform of the reflection is obtained at several points. Two or three dimensional spectroscopic imaging of samples can also be obtain in addition to spectroscopic information [162]. TPI has shown promising results using the THz waveform for analyzing the thickness of a coated dosage form [61;103;183]. Taday et al. [161] found that by analyzing tablets with TPI, they could not only measure the average thickness but also the distribution of the coating during manufacturing. This is not only very useful within quality control, but also as a development tool. Analysis time in TPI with 200 μm step sizes (spatial resolution of 250 μm, axial resolution of 38 μm) of a 7-mm large tablet is about 20 minutes [161].

For modified or controlled release, which require more control on the tablet coating layer thickness, TPI could be very valuable [171]. Real time monitoring of tablet coating process has been established. The technique has, though, limitations to low coating thickness [171]. However, TPI is a non-destructive method compared to a direct method that is often used, scanning electron microscopy (SEM), where it is necessary to cut the tablets to obtain cross-section pictures [171].

Ho et al. [72] used TPI to identify scale up problems going from laboratory (4 kg) scale batch to pilot batch (20 kg). This included significant differences in dissolution profile, which they could assign to differences in the density of the coatings. From the TPI waveforms of the tablets, prediction models to the mean dissolution time were performed [72].

The future of terahertz spectroscopy in PAT applications

It is possible from the time-domain waveforms, to determine the thickness or relative thickness of samples [85]. It is possible, that this could improve the calibrations performed in paper III. However, due to lack of resources, this was not performed.

For analyzing tablet on-line there might potentially be a challenge with the path length as many tablets are concave shaped. However, this could potentially be solved by analyzing on either powder or alternatively prepressed powder inside the tablet press. The suggestion from Hizasumi et al. [71] using the lower punch as a mirror, could then be an option.

Terahertz spectroscopy is a fast method (i.e. the terahertz spectra used in article III were obtained as average of 10.000 scans over 100 sec, which means that 1 scan takes approximately 10 ms). It is therefore possible to lower the time of analysis, but the amount of scans needed for a proper determination have to be determined, similar to the 256 scans Hizasumi et al. [71] found for reflection spectroscopy.

Even though terahertz technology has been known for some years, no studies of quantifying the amount of API in real world solid dosage forms have yet been published [148]. The main reason for this is probably due to the price of the terahertz equipment. For the moment, terahertz instrumentation are bulky, energy consuming, and most important of all very expensive.

The so called “THz gap”, occupies the void between the electronic devices (e.g. radiofrequencies transmitters/receivers) on the one side, which are typically using low cast, small device technology, whereas on the other side are the optical based systems (e.g. fiber optics devices), which are more bulky and expensive. Within electronic devices, the desire for faster responding equipment (e.g. fast data transfer) will drive the development, and utilization of the THz frequencies. Within cancer research there is also high interest for terahertz technology as studies have shown differences between healthy and cancer infected skin, mainly due to the differences in water absorption between tumor and normal tissue [132]. Furthermore, security scanning, along with communication technology, drives the innovation for cheaper terahertz devices. Pharmaceutical application will probably not be the main target for development of terahertz instrumentations, as it is still missing core benefits that are not already provided by other and cheaper techniques. However, if the price of terahertz instrumentation enters an affordable range or unique benefits are discovered, there can be potential uses within pharmaceutical quality control, both during development and throughout the manufacturing process.

6.4 Fluorescence spectroscopy as a PAT tool

Fluorescence spectroscopy monitors the radiation from components in a sample that has previously been excited by a radiation source [53]. Figure 6.2 shows a simplified version of fluorescence. Absorbed light excites a molecule, fluorophore, from the ground state to electronically exited state. When it returns to its ground electronic state, emission of fluorescent light will occur. The emission will occur at longer wavelengths (lower energy) than the excitation, and the difference (energy loss) is called the Stokes shift, and is typically in the range from 10 nm to 150 nm [31]. Due to the Stoke shift, emission signals can be detected against a negligible background assuming there are no interferents, which leads to superior sensitivity and low detection limit, as compared to other spectroscopic methods [31]. Fluorescence spectroscopy is highly sensitive as it can analyze down to parts per billion (ppb), and in low concentration, the fluorescence signal is proportional to the concentration of the fluorophore [81]. One characteristic for fluorescence spectroscopy, is that the emission spectrum is independent of the excitation wavelength, also known as the Kasha's rule [94].

Fluorescence typically occurs from molecules with aromatic, cyclic, or closed ring structure, or highly unsaturated molecules [31]. Furthermore, highly conjugated molecules are often fluorophores as well as molecules with rigid planar structure, but the wavelength is often related to the size of the chromophore [81]. Environmental factors such as temperature, solvent, pH, and the presence of other compounds influence the fluorescence properties of a molecule [31]. The fluorescence signal can be reduced by the presence of interferences called quenchers. This quenching can happen in different ways (e.g. dynamic quenching that requires contact between the excited fluorophore and the quencher). Another form of quenching is static quenching, where the fluorophore and the quencher form a complex, and only the unbound fluorophore gives fluorescence [81]. Furthermore, Förster quenching, or energy transfer between molecules, can happen without collisions. The donor fluorophore will excite and the emission light will be taken up by the acceptor, which might use the energy to excite and emission light at a different wavelength [151].

APIs often consist of substituted aromatic and heterocyclics molecules. Many of them may therefore fluoresce at the proper wavelength [91], while most excipients (lactose, starch, etc.) do not fluoresce or only to a smaller degree [31;93]. Cellulose has, however, shown weak fluorescence properties, that may be a problematic interferant in some situations [17]. When there is only negligible interferents, fluorescence spectroscopy should be very suitable for very low API concentration applications, where other technologies (e.g. NIR) provides inadequate detection [31]. Despite this fact, only a few applications in pharmaceutical fluorescence spectroscopy PAT studies have been made [135] compared to the food area [19].

When analyses are performed at multiple excitation wavelengths in combination with multiple emission wavelengths excitation-emission matrices (EEM) can be obtained [81]. Recently, the measurement of EEM was proposed together with chemometric methods for analysis of pharmaceutical formulations [3]. Furthermore, a few studies have been conducted on pharmaceutical tablets or powders both in low concentration range (down to 0.5 % w/w) and up to 20 % (w/w) [33;109-112] usually with the RSD in the range of 2-12 %.

Figure 6.16 shows EEM landscapes of 36 batches of tablets (each landscape is the average of three pulverized tablets) containing two different types of API, melitracen (MEL) and flupentixol (FLU) from paper IV. The explanation of the experimental design is found in paper IV, but it can be mentioned that FLU is added in a low concentration (0.208-0.625 % w/w free base) where MEL is added in 4.17-12.5 % (w/w free base). The landscapes are cropped to eliminate Rayleigh scatter (excitation equal to emission wavelength) and Raman scatter (at emission higher than excitation) by cutting off everything up to 20 nm higher than the excitation wavelengths. The top left of Figure 6.16 is the placebo tablets without any APIs. Samples in the first left column include no FLU, and samples towards the right have an increase in concentration of FLU. The samples in the top row include no MEL, and there is an increase in MEL concentration downwards. The placebo landscape shows minor fluorescence despite its lack of API. This could be due to fluorescence from some of the excipients; corn starch, MCC, hydroxypropylcellulose or hydrogenated vegetable oil, that all have shown minor fluorescence (results not shown). It is not necessarily the excipient itself that has fluorescence properties, but could be due to minor impurities from the production. This has been seen within production of sugar which in itself does not have fluorescence properties. Due to minor impurities, it was possible to distinguish between sugar products produced at different factories by fluorescence spectroscopy [113]. The first left column of Figure 6.16, which only include MEL at increasing concentrations, show weak but increasing fluorescence at excitation 310 nm and emission 350 nm. The top row, which only include FLU at increasing concentrations displays increasing fluorescence at excitation 280-350 nm and emission around 400 nm. When both APIs are present, the fluorescence from MEL is not visible and part of the fluorescence from FLU (excitation 280-300 nm, emission 400 nm) seems to disappear due to quenching [94] between the two molecules or their excipients. In the formulation MEL is used as melitracen hydrochloride, and ionic chloride is like other halogens, known to be a quencher [151]. Together with each flupentixol molecule, are added two hydrochloride molecules, but melitracen is added in approximately 20 times the concentration of flupentixol. It is therefore possible, that the chloride from the MEL addition is quenching the FLU signal. It is also possible that energy transfer, or Förster quenching [151] is occurring as FLU excites light in the range of MEL's emission around 350 nm.

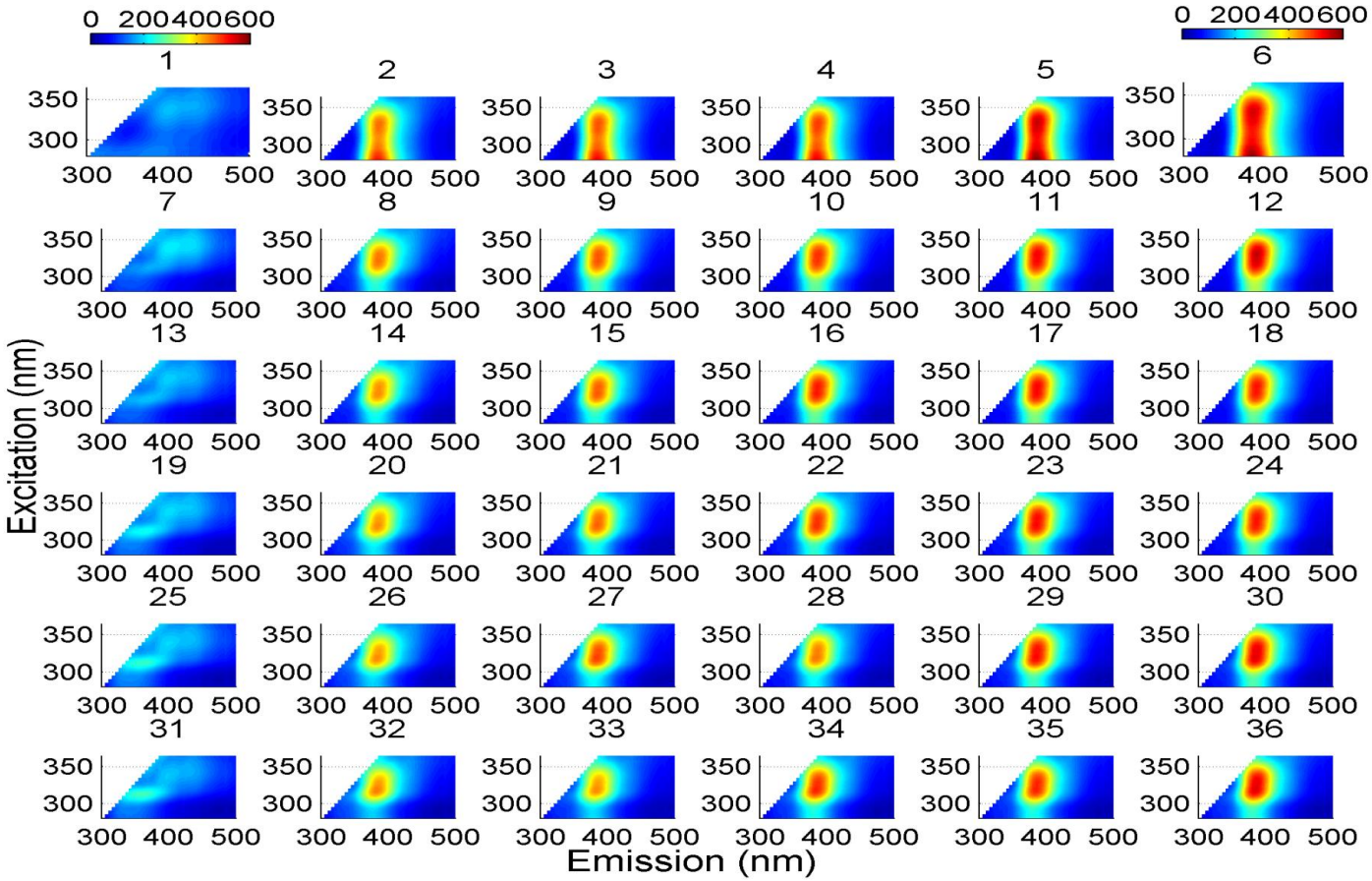

Figure 6.16: Emission-excitation matrix (EEM) of tablets (average of three pulverized) from 36 batches including two APIs, MEL and FLU. Top left landscape is placebo tablets. The tablets in the top row are not containing MEL, and the concentration of MEL is increasing in descending direction. The tablets in the left column are not containing any FLU and the concentration of FLU is increasing towards right.

For fluorescence spectroscopy there can be problems with selectivity, if the sample matrix has more fluorescent components with overlapping bands. Furthermore, specificity can be a problem in the determination of fluorescent drugs [86]. Applying PLS to the fluorescence data have in several cases, helped avoid using time consuming separation techniques [30;86;111;117]. A different method to overcome the problem with emission overlapping peaks, is to use first derivative synchronous fluorescence, where the difference between excitation and emission is kept constant during measurement. Karim et al. [86] used first derivate synchronous fluorescence to simultaneously determine acetylsalicylic acid and caffeine. Another approach is to use the second-order advantage of the EEM with e.g. PARAFAC [3;40;97].

Figure 6.17 shows the loadings for two split-half PARAFAC models on fluorescence landscapes of tablets with two types of API (from paper IV). The split-half division is performed so samples from the same batch belong to the same set. The placebo samples are very different from the remaining samples and are therefore included in both set, as otherwise the models will be very different. It is obvious that the two models are very similar and perform well, despite core consistency values of 0. There are four factors used, and a comparison between the loadings in Figure 6.17 to the landscapes in Figure 6.16 can be made. The red and green loading seem to explain MEL, and to some degree the placebo landscape. The blue loading seems to explain FLU. The black loading possibly explains FLU, when it is present by itself. A four factor PARAFAC model containing all the samples gives very similar result. Second order prediction, where the PARAFAC scores are used as input to a PLS model [13] has also been tried. At least five factors were needed to give a linear relationship between the APIs and the scores from the PARAFAC analysis. However, the five factor models in split half analysis did not show consistent results, therefore only four factor model is reported here. Due to necessity for trilinearity in the data for PARAFAC to work optimally, the RMSECV are higher than the RMSECV obtained from the unfolded PLS (U-PLS) models shown in paper IV (0.076 % w/w for PARAFAC and 0.038 for U-PLS for FLU, and 1.06 % w/w and 0.34 % w/w for MEL). It should be noticed that only regular PARAFAC analysis has been performed.

So far, only a few studies have been conducted using fluorescence spectroscopy for on-line measurements in the pharmaceutical industry, but the possibilities are promising [3;33;91-93]. Lai et al. [92] developed a laser-induced fluorescence (LIF) sensor for on-line monitoring of powder blend homogeneity for triamterene down to 0.1 % (w/w) in lactose matrix with less than 5 % RSD. Later, Lai and Cooney [91] found a limit of detection below 0.02 % (w/w) on a similar setup. In 2004, Lai et al. [93] simulated a production line and applied a LIF sensor with a measurement rate of up to 3000 tablets per minute.

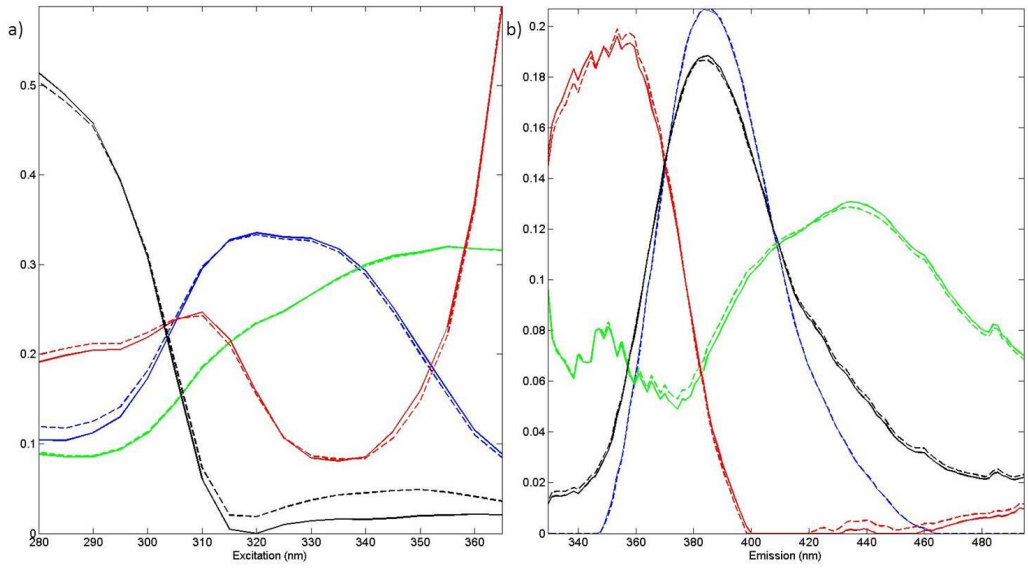

Figure 6.17: PARAFAC loadings for fluorescence landscapes of tablets including two APIs divided into two set (split half) a) excitation mode b) emission mode. There are used four factors.

The future of fluorescence spectroscopy in PAT applications

For the particular application used with two APIs, it could be interesting to explore the interaction between the two APIs and their excipients and the quenching in more details. This could be done by producing tablets with MEL granulate in very low levels up to the normal level together with FLU and inspect the influence on the quenching. The response should be proportional to the concentration added.

For the fluorescence study shown here, the sample presentation in the instrument could be optimized, so the analysis would be completely non-invasive and perform the analysis directly on the tablet.

For the purpose of tablet manufacturing, fluorescence spectroscopy has the potential for quantifying API in low concentrations if the background matrix is not too fluorescent. For fast on-line analysis, there would be need for fewer wavelengths and properly also lower resolution, which can decrease the analysis time from 7-8 min down to 90 sec or maybe less. Another purpose for process fluorescence spectroscopy could be detection of degradation products, as they are usually present in very low amounts. The requirement is, though, that degradation product should be fluorescent and differ from the API that most likely also will be fluorescent.

7 Conclusions and perspectives

In this thesis three different spectroscopic PAT analyzers have been described: NIR, terahertz and fluorescence spectroscopy. They all show great potential as PAT analyzers, but it is no wonder that NIR counts for over 60 % of the studies published within pharmaceutical applications [135]. NIR is a mature technique; whereas both fluorescence and terahertz spectroscopy are still in their "childhood", especially terahertz spectroscopy. Fluorescence and terahertz spectroscopy both have their limitations. For fluorescence spectroscopy the linear concentration range and multiple quenching phenomena can be troublesome, whereas terahertz spectroscopy's biggest challenge is the lack of affordable equipment.

This thesis only touches some of the available techniques for PAT analyzers as well as chemometrics. There exist many other promising technologies: Raman spectroscopy, FTIR spectroscopy, UV spectroscopy, to mention a few. Each pharmaceutical application has to be individually evaluated and the best fit technique should be chosen. It should, however, not just be evaluated only for the sake of analyzing a given quality or as a return on investment, but also globally as a return of process knowledge and understanding.

It is important that the data achieved turns into knowledge gain; otherwise the PAT projects are likely to fail. One way of succeeding is by gathering a PAT team [32], that among other include a chemometrician/data analyst, an organic chemist, a pharmacist, an analytical chemist, a process engineer as well as production staff members. Production staff members know the process and will feel ownership over the PAT installation after the project is over and successful installed. This is important; as many forget that the work is not over once the PAT installation is done. PAT installations need updates and maintenance, not in the same extent as chemical analysis in the laboratory, but it is still important to verify that the prediction is still what it needs to be also after longer periods of running time [76].

In order to succeed with a PAT project and a QbD approach it is important, as with any other new working habits, to have full support from management. This can be a challenge, as QbD and the benefits by choosing the QbD path, are not always understood fully by other than the technical/scientific personal. Sometimes unrealistic expectations to the direct return of investment are formed [32], and therefore the PAT project may be called a "failure". Often, PAT should be utilized as tools for process understanding and an investment in processes in the future, rather than a quick fix on problems here and now. PAT cannot solve everything, but it may help to design the next product and processes with quality and flexibility in mind.

An applied approach within PAT projects is to use the PAT analyzer during the development and optimization of the process to monitor it, and maybe in combination with DoE, to identify the CQAs and CPPs. Once the design space is established, the PAT analyzer is moved to a different project (or simply removed). This will not give the benefits from long time monitoring of the pro-

cess. However, it is a cost effective approach to optimize on the process, as only few PAT analyzers, that are typical expensive in purchasing, are needed for several production facilities. Another approach, also used several places in the industry, is to have long fibers from one instrument that can measure at several points in the processes. This will give the benefit of lower cost per sampling point, even though the instrument might be a large investment.

Within sampling there are still many challenges. First, comes the understanding of sampling practice and what influence poor sampling does to the results. Many are unaware of this issue. The ideas are all very simple, but there are many people who don't think about them, or take this huge uncertainty into account when setting up an analysis. Furthermore, the challenge is increased by the fact that not many correctly designed sampling tools are available. Many tools and even PAT sensors only sample a smaller part of the stream or process, and are thereby not giving all parts of a batch even probability to get analyzed. Therefore, there are still a lot to do in this area, and it is vital for process understanding and PAT to keep this in mind when trying to monitor a process.

An example of the lack of interest for sampling can be seen in a tablet production. It must be essential here to show that not only are the 10 or 20 samples taken out from a batch in compliance, but they are also representative for the whole lot. It could be done by a variographic analysis, where variation over the batch is tested.

The newest guideline from Ph. Eur. (2.9.47) [24] recommends to analyze up to 100 samples in a spectroscopic analysis. When this is done by a non-invasive spectroscopic technique, and if it is done as in-line or on-line analysis, no samples will be lost in the process.

Another issue with sampling is that the withdrawn sample from process often is different from what is measured with PAT tools in- or on-line in the process. The same issue exists for reference analysis where the whole sample is often dissolved, whereas for fast spectroscopic analysis, only a part of the sample is analyzed. This will lead to challenges in the development of calibrations. It can partly be solved by focusing more on replicates of the same sample at different spots/mixing in-between measurements, compared to having many scans at the same spot. One important issue is that the error of the spectroscopic technique probably is smaller than the error of the reference methods, which is much smaller than the error of the actual sampling.

The pharmaceutical manufacturing industry is known to be a conservative and regulatory strict business, where every decision involves high stakes. Unfortunately, there is also a tendency to see incoming raw material as constant, and therefore no reason to monitor it. Further, problems of complex matters might be approached in a univariate way even though a multivariate solution could be more appropriate. Nevertheless, there is also lack of knowledge of QbD and PAT, especially in the management. This is where the collaboration across different technical disciplines is important (e.g. process understanding, data treatment, product understanding, product development, and knowledge sharing). QbD and PAT are very broad fields and nobody can be an expert in all the disciplines that are involved.

Many pharmaceutical companies are, although, moving slowly towards more use of spectroscopic PAT tools for raw material and process control, as well as designing with quality in mind. There is also a smaller trend of moving towards continuous manufacturing processes, which also increase

the need for process monitoring and control. More continuous manufacturing in pharmaceutical processes is also a topic that get more attention within the regulatory authorities [42].

Individualized medicine, where the treatment is a customized dosage for the patient, is still far away, but it will probably become a reality. Then the need for more flexible production systems is even greater, and PAT and QbD will be appropriate and necessary tools to achieve this.

QbD will continue to improve the way risk is approached and it will increase the understanding and control of the manufacturing processes. In addition to increasing quality, it will help the pharmaceutical industry to reduce development and manufacturing cycle times as well as costs in the process. QbD will, probably in combination with other tools as Lean and Six Sigma, be the prospective leading tool for designing, manufacturing and controlling the pharmaceutical products.

8 Reference list

[1] T.T. Allen, Introduction to engineering statistics and Six Sigma: Statistical quality control and design of experiments and systems, Springer-Verlag, London, 2010.

[2] D. Allis, A. Fedor, T. Korter, J. Bjarnason, E. Brown, Assignment of the lowest-lying THz absorption signatures in biotin and lactose monohydrate by solid-state density functional theory. Chemical Physics Letters 440 (2007); 203-9.

[3] J.C. Alves, R.J. Poppi, Simultaneous determination of acetylsalicylic acid, paracetamol and caffeine using solid-phase molecular fluorescence and parallel factor analysis. Analytica Chimica Acta 642 (2009); 212-6.

[4] A.K. Anal, Controlled-released dosage forms. in: S.C. Gad, editor. Pharmaceutical manufacturing handbook: production and processes. John Wiley & Sons, Inc., Hoboken, New Jersey, 2008.

[5] G. Andrews, D. Jones, H. Zhai, O.A. Diak, G. Walker, Effect of grinding in pharmaceutical tablet production. in: S.C. Gad, editor. Pharmaceutical manufacturing handbook: production and processes.Wiley & Sons Inc., Hoboken, New Jersey, 2008.

[6] P.B. Balbuena, W. Blocker, R.M. Dudek, F.A. Cabrales-Navarro, P. Hirunsit, Vibrational spectra of anhydrous and monohydrated caffeine and theophylline molecules and crystals. The Journal of Physical Chemistry A 112 (2008); 10210-9.

[7] R.J. Barnes, M.S. Dhanoa, S.J. Lister, Standard normal variate transformation and de-trending of near-infrared diffuse reflectance spectra. Applied Spectroscopy 43 (1989); 772-7.

[8] J. Berggren, G. Frenning, G. Alderborn, Compression behaviour and tablet-forming ability of spray-dried amorphous composite particles. European Journal of Pharmaceutical Sciences 22 (2004); 191-200.

[9] M. Blanco, J. Coello, H. Iturriaga, S. Maspoch, C. delaPezuela, Quantitation of the active compound and major excipients in a pharmaceutical formulation by near infrared diffuse reflectance spectroscopy with fibre optical probe. Analytica Chimica Acta 333 (1996); 147-56.

[10] M. Blanco, A. Peguero, Influence of physical factors on the accuracy of calibration models for NIR spectroscopy. Journal of Pharmaceutical and Biomedical Analysis 52 (2010); 59-65.

[11] L. Bokobza, Origin of Near-Infrared absorption bands. in: H.W. Siesler, Y. Ozaki, S. Kawata, H.M. Heise, editors. Near-Infrared spectroscopy. Principles, instruments, applications.Wiley-VCH, Weinheim, 2002.

[12] H.G. Brittain, Polymorphism and solvatomorphism 2005. Journal of Pharmaceutical Sciences 96 (2007); 705-28.

[13] R. Bro, PARAFAC. Tutorial and applications. Chemometrics and Intelligent Laboratory Systems 38 (1997); 149-71.

[14] R. Bro, H.A.L. Kiers, A new efficient method for determining the number of components in PARAFAC models. Journal of Chemometrics 17 (2003); 274-86.

[15] J. Burgbacher, J. Wiss, Industrial applications of online monitoring of drying processes of drug substances using NIR. Organic Process Research & Development 12 (2008); 235-42.

[16] B.A.C. Carlin, Direct compression and the role of filler-binders. in: L.L. Augsburger, S.W. Hoag, editors. Pharmaceutical dosage forms, tablets. Informa Helthcare USA, New York, 2008.

[17] A. Castellan, R. Ruggiero, E. Frollini, L.A. Ramos, C. Chirat, Studies on fluorescence of cellulosics. Holzforschung 61 (2007); 504-8.

[18] R. Chakkittakandy, J.A. Corver, P.C. Planken, Terahertz spectroscopy to identify the polymorphs in freeze-dried mannitol. Journal of Pharmaceutical Sciences 99 (2010); 932-40.

[19] J. Christensen, L. Nørgaard, R. Bro, S.B. Engelsen, Multivariate autofluorescence of intact food systems. Chemical Reviews 106 (2006); 1979-94.

[20] R.P. Cogdill, J.K. Drennen, Risk-based quality by design (QbD): a Taguchi perspective on the assessment of product quality, and the quantitative linkage of drug product parameters and clinical performance. Journal of Pharmaceutical Innovation 3 (2008); 23-9.

[21] B.R. Conway, Solid dosage form. in: S.C. Gad, editor. Pharmaceutical manufacturing handbook: production and processes. John Wiley & Sons, Inc., Hoboken, New Jersey 2008.

[22] P. Corti, E. Dreassi, G. Ceramelli, S. Mattii, Near infrared transmittance analysis for the assay of solid pharmaceutical dosage forms. Analyst 124 (1999); 755-8.

[23] Council of Europe, European pharmacopoeia. Strasbourg, 2007.

[24] Council of Europe, General Chapter 2.9.40 Uniformity of Dosage Units. European Pharmacopeia. Strasbourg, 2012.
[25] A. Cournoyer, J.S. Simard, L. Cartilier, N. Abatzoglou, Quality control of multi-component, intact pharmaceutical tablets with three different near-infrared apparatuses. Pharmaceutical Development and Technology 13 (2008); 333-43.
[26] D.Q.M. Craig, P.G. Royall, V.L. Kett, M.L. Hopton, The relevance of the amorphous state to pharmaceutical dosage forms: glassy drugs and freeze dried systems. International Journal of Pharmaceutics 179 (1999); 179-207.
[27] B.M. Cullum, T. Vo-Dinh, Sample collection and preparation of liquid and solids. in: G. Gauglitz, T. Vo-Dinh, editors. Handbook of spectroscopy.Wiley-VCH, Weinheim, 2003.
[28] T.D. Davis, G.E. Peck, J.G. Stowell, K.R. Morris, S.R. Byrn, Modeling and monitoring of polymorphic transformations during the drying phase of wet granulation. Pharmaceutical Research 21 (2004); 860-6.
[29] T. De Beer, A. Burggraeve, M. Fonteyne, L. Saerens, J. Remon, C. Vervaet, Near infrared and Raman spectroscopy for the in-process monitoring of pharmaceutical production processes. International Journal of Pharmaceutics 417 (2011); 32-47.
[30] M. del Olmo, C. Diez, A. Molina, I. de Orbe, J.L. Vilchez, Resolution of phenol, o-cresol, m-cresol and p-cresol mixtures by excitation fluorescence using partial least-squares (PLS) multivariate calibration. Analytica Chimica Acta 335 (1996); 23-33.
[31] J.E. Dickens, Fluorescent sensing and process analytical applications. in: K.A. Bakeev, editor. Process Analytical Technology: Spectroscopic tools and implementation strategies for the chemical and pharmaceutical industries. John Wiley & Sons, Inc., Chippenham, Wiltshire, 2010.
[32] J.E. Dickens, Overview of process analysis and PAT. in: K.A. Bakeev, editor. Process Analytical Technology: Spectroscopic tools and implementation strategies for the chemical and pharmaceutical industries. John Wiley & Sons, Inc., Chippenham, Wiltshire, 2010.
[33] R. Domike, S. Ngai, C.L. Cooney, Light induced fluorescence for predicting API content in tablets: Sampling and error. International Journal of Pharmaceutics 391 (2010); 13-20.
[34] T.D. Dorney, R.G. Baraniuk, D.M. Mittleman, Material parameter estimation with terahertz time-domain spectroscopy. JOSA A 18 (2001); 1562-71.
[35] E. Dreassi, G. Ceramelli, P. Corti, S. Lornardi, P.L. Perruccio, Near-infrared reflectance spectrometry in the determination of the physical state of primary materials in pharmaceutical production. Analyst 120 (1995); 1005-8.
[36] M. Dyrby, S.B. Engelsen, L. Nørgaard, M. Bruhn, L. Lundsberg-Nielsen, Chemometric quantitation of the active substance (containing C N) in a pharmaceutical tablet using near-infrared (NIR) transmittance and NIR FT-Raman spectra. Applied Spectroscopy 56 (2002); 579-85.
[37] K.H. Esbensen, H.H. Friis-Petersen, L. Petersen, J.B. Holm-Nielsen, P.P. Mortensen, Representative process sampling - in practice: Variographic analysis and estimation of total sampling errors (TSE). Chemometrics and Intelligent Laboratory Systems 88 (2007); 41-59.
[38] K.H. Esbensen, D. Guyot, F. Westad, L.P. Houmøller, Multivariate data analysis, in practice, an introduction to multivariate data analysis and experimental design. Camo, Oslo, 2002.
[39] K.H. Esbensen, P. Paasch-Mortensen, Process sampling: Theory of sampling - The missing link in Process Analytical Technologies (PAT). in: K.A. Bakeev, editor. Process Analytical Technology: Spectroscopic tools and implementation strategies for the chemical and pharmaceutical industries. John Wiley & Sons, Inc., Chippenham, Wiltshire, 2010.
[40] J.C.G. Esteves da Silva, J.M.M. Leitão, F.S. Costa, J.L.A. Ribeiro, Detection of verapamil drug by fluorescence and trilinear decomposition techniques. Analytica Chimica Acta 453 (2002); 105-15.
[41] FDA, Pharmaceutical CGMPs for the 21st Century - A risk-based approach. 2004.
[42] FDA, A strategic plan: Advancing regulatory science at FDA. August 2011, http://www.fda.gov/downloads/ScienceResearch/SpecialTopics/RegulatoryScience/UCM268225 (accessed 10.05.13). 2011.
[43] FDA, PAT guidance for industry - a framework for innovative pharmaceutical development, manufacturing and quality assurance. 2004.
[44] B. Ferguson, X.C. Zhang, Materials for terahertz science and technology. Nature Materials 1 (2002); 26-33.
[45] I. Fix, K.J. Steffens, Quantifying low amorphous or crystalline amounts of alpha-lactose-monohydrate using X-ray powder diffraction, near-infrared spectroscopy, and differential scanning calorimetry. Drug Development and Industrial Pharmacy 30 (2004); 513-23.
[46] P. Frake, D. Greenhalgh, S.M. Grierson, J.M. Hempenstall, D.R. Rudd, Process control and end-point determination of a fluid bed granulation by application of near infra-red spectroscopy. International Journal of Pharmaceutics 151 (1997); 75-80.

[47] J.R. Freeman, H.E. Beere, Ritchie H.E., Generation and detection of terahertz radiation. in: K.E. Peiponen, A. Zeitler, M. Kuwata-Gonokami, editors. Terahertz spectroscopy and imaging. Springer, Heidelberg, 2013.
[48] T.P. Garcia, S.J. Wilkinson, J.F. Scott, The development of a blend-sampling technique to assess the uniformity of a powder mixture. Drug Development and Industrial Pharmacy 27 (2001); 297-307.
[49] P. Geladi, D. Macdougall, H. Martens, Linearization and scatter-correction for near-infrared reflectance spectra of meat. Applied Spectroscopy 39 (1985); 491-500.
[50] E.C. Gil, I. Caraballo, B. Bataille, Tablet design. in: S.C. Gad, editor. Pharmaceutical manufacturing handbook: production and processes. John Wiley & Sons, Inc., Hoboken, New Jersey, 2008.
[51] Á. Gombás, I. Antal, P. Szabó-Révész, S. Marton, I. Erõs, Quantitative determination of crystallinity of alpha-lactose monohydrate by Near Infrared Spectroscopy (NIRS). International Journal of Pharmaceutics 256 (2003); 25-32.
[52] J. Gottfries, H. Depui, M. Fransson, M. Jongeneelen, M. Josefson, F.W. Langkilde, D.T. Witte, Vibrational spectrometry for the assessment of active substance in metoprolol tablets: A comparison between transmission and diffuse reflectance near-infrared spectrometry. Journal of Pharmaceutical and Biomedical Analysis 14 (1996); 1495-503.
[53] J. Green, Optical spectroscopy. in: G. Gauglitz, T. Vo-Dinh, editors. Handbook of spectroscopy.Wiley-VCH, Weinheim, 2003.
[54] R.L. Green, G. Thurau, N.C. Pixley, A. Mateos, R.A. Reed, J.P. Higgins, In-line monitoring of moisture content in fluid bed dryers using near-IR spectroscopy with consideration of sampling effects on method accuracy. Analytical Chemistry 77 (2005); 4515-22.
[55] A. Grunenberg, J.O. Henck, H.W. Siesler, Theoretical derivation and practical application of energy temperature diagrams as an instrument in preformulation studies of polymorphic drug substances. International Journal of Pharmaceutics 129 (1996); 147-58.
[56] R. Guenard, G. Thurau, Implementation of Process Analytical Technologies. in: K.A. Bakeev, editor. Process Analytical Technology: Spectroscopic tools and implementation strategies for the chemical and pharmaceutical industries. John Wiley & Sons, Inc., Chippenham, Wiltshire, 2010.
[57] P. Gy, Sampling of discrete materials - a new introduction to the theory of sampling - I. Qualitative approach. Chemometrics and Intelligent Laboratory Systems 74 (2004); 7-24.
[58] P. Gy, Sampling of discrete materials - II. Quantitative approach-sampling of zero-dimensional objects. Chemometrics and Intelligent Laboratory Systems 74 (2004); 25-38.
[59] P. Gy, Sampling of discrete materials - III. Quantitative approach-sampling of one-dimensional objects. Chemometrics and Intelligent Laboratory Systems 74 (2004); 39-47.
[60] P. Gy, Sampling for analytical purposes, John Wiley & Sons, Inc., Chichester, West Sussex, 1998.
[61] M. Haaser, K.C. Gordon, C.J. Strachan, T. Rades, Terahertz pulsed imaging as an advanced characterisation tool for film coatings - A review. International Journal of Pharmaceutics (2013).
[62] S. Hammond, PAT to support QbD, continuous quality verification and RtR. Presentation, Sentronic User Meeting, 2013.
[63] P.Y. Han, M. Tani, M. Usami, S. Kono, R. Kersting, X.C. Zhang, A direct comparison between terahertz time-domain spectroscopy and far-infrared Fourier transform spectroscopy. Journal of Applied Physics 89 (2001); 2357-9.
[64] S.M. Han, P.G. Faulkner, Determination of SB 216469-S during tablet production using near-infrared reflectance spectroscopy. Pharmaceutical Research (New York) 12 (1995); S15.
[65] B.C. Hancock, G. Zograf, Characteristics and significance of the amorphous state in pharmaceutical systems. Journal of Pharmaceutical Sciences 86 (1997); 1-12.
[66] B.C. Hancock, M. Parks, What is the true solubility advantage for amorphous pharmaceuticals? Pharmaceutical Research 17 (2000); 397-404.
[67] C.L. Hansen, F. van den Berg, M.A. Rasmussen, S.B. Engelsen, S. Holroyd, Detecting variation in ultrafiltrated milk permeates - Infrared spectroscopy signatures and external factor orthogonalization. Chemometrics and Intelligent Laboratory Systems 104 (2010); 243-8.
[68] S. Hansen, S. Pedersen-Bjergaard, K. Rasmussen, Introduction to pharmaceutical chemical analysis, John Wiley & Sons, Inc., West Sussex, 2012.
[69] D.C. Harris, Quantitative chemical analysis.WH Freeman and Co., New York, 2007.
[70] J. Hisazumi, T. Suzuki, H. Nakagami, K. Terada, Quantification of pharmaceutical polymorphs and prediction of dissolution rate using theophylline tablet by terahertz spectroscopy. Chemical and Pharmaceutical Bulletin 59 (2011); 442-6.
[71] J. Hisazumi, T. Watanabe, T. Suzuki, N. Wakiyama, K. Terada, Using terahertz reflectance spectroscopy to quantify drug substance in tablets. Chemical and Pharmaceutical Bulletin 60 (2012); 1487-93.

[72] L. Ho, R. Mueller, K.C. Gordon, P. Kleinebudde, M. Pepper, T. Rades, Y. Shen, P. Taday, J.A. Zeitler, Monitoring the film coating unit operation and predicting drug dissolution using Terahertz Pulsed Imaging. Journal of Pharmaceutical Sciences 98 (2009); 4866-76.
[73] M. Hof, Basics of optical spectroscopy. in: G. Gauglitz, T. Vo-Dinh, editors. Handbook of spectroscopy.Wiley-VCH, Weinheim, 2003.
[74] I.C.H., Guideline. Quality risk management Q9. 2005.
[75] I.C.H., Guideline. Validation of analytical procedures: text and methodology Q2 (R1). 2005.
[76] I.C.H., Guideline. Pharmaceutical quality system Q10. 2008.
[77] I.C.H., Guideline Pharmaceutical development Q8 (R2). 2009.
[78] I.C.H., Guidance for Industry. Development and manufacturing of drug substances Q11. 2012.
[79] IBM Business Conculting Services, The metamorphosis of manufacturing - from art to science. http://www-935.ibm.com/services/us/imc/pdf/ge510-4034-metamorphosis-of-manufacturing.pdf (accessed July 30th 2013), 2005.
[80] Y. Ikeda, Y. Ishihara, T. Moriwaki, E. Kato, K. Terada, A novel analytical method for pharmaceutical polymorphs by terahertz spectroscopy and the optimization of crystal form at the discovery stage. Chemical & Pharmaceutical Bulletin 58 (2010); 76-81.
[81] J.D. Ingle Jr, S.R. Crouch, Spectrochemical analysis, Prentice Hall College Book Division, Old Tappan, New Jersey, 1988.
[82] M. Ito, T. Suzuki, S. Yada, A. Kusai, H. Nakagami, E. Yonemochi, K. Terada, Development of a method for the determination of caffeine anhydrate in various designed intact tables by near-infrared spectroscopy: A comparison between reflectance and transmittance technique. Journal of Pharmaceutical and Biomedical Analysis 47 (2008); 819-27.
[83] P.U. Jepsen, D.G. Cooke, M. Koch, Terahertz spectroscopy and imaging - Modern techniques and applications. Laser & Photonics Reviews 5 (2011); 124-66.
[84] P.U. Jepsen, B.M. Fischer, Dynamic range in terahertz time-domain transmission and reflection spectroscopy. Optics Letters 30 (2005); 29-31.
[85] M. Juuti, H. Tuononen, T. Prykari, V. Kontturi, M. Kuosmanen, E. Alarousu, J. Ketolainen, R. Myllyla, K.E. Peiponen, Optical and terahertz measurement techniques for flat-faced pharmaceutical tablets: a case study of gloss, surface roughness and bulk properties of starch acetate tablets. Measurement Science & Technology 20 (2009).
[86] M.M. Karim, C.W. Jeon, H.S. Lee, S.M. Alam, S.H. Lee, J.H. Choi, S.O. Jin, A.K. Das, Simultaneous determination of acetylsalicylic acid and caffeine in pharmaceutical formulation by first derivative synchronous fluorimetric method. Journal of Fluorescence 16 (2006); 713-21.
[87] M. Kawase, T. Saito, M. Ogawa, H. Uejima, Y. Hatsuda, S. Kawanishi, Y. Hirotani, M. Myotoku, K. Ikeda, H. Konishi, I. Iga, J. Yamakawa, S. Nishizawa, K. Yamamoto, M. Tani, Application of terahertz absorption spectroscopy to evaluation of aging variation of medicine. Analytical Sciences 27 (2011); 209-12.
[88] M.D. King, W.D. Buchanan, T.M. Korter, Identification and quantification of polymorphism in the pharmaceutical compound diclofenac acid by terahertz spectroscopy and solid-state density functional theory. Analytical Chemistry 83 (2011); 3786-92.
[89] H.G. Kristensen, Almen farmaci, Institut for Farmaci, Farmaceutisk Fakultet, University of Copenhagen, Copenhagen, 2008.
[90] M. Laasonen, T. Harmia-Pulkkinen, C. Simard, M. Rasanen, H. Vuorela, Development and validation of a near-infrared method for the quantitation of caffeine in intact single tablets. Analytical Chemistry 75 (2003); 754-60.
[91] C.K. Lai, C.C. Cooney, Application of a fluorescence sensor for miniscale on-line monitoring of powder mixing kinetics. Journal of Pharmaceutical Sciences 93 (2004); 60-70.
[92] C.K. Lai, D. Holt, J.C. Leung, C.L. Cooney, G.K. Raju, P. Hansen, Real time and noninvasive monitoring of dry powder blend homogeneity. Aiche Journal 47 (2001); 2618-22.
[93] C.K. Lai, A. Zahari, B. Miller, W.E. Katstra, M.J. Cima, C.L. Cooney, Nondestructive and on-line monitoring of tablets using light-induced fluorescence technology. Aaps Pharmscitech 5 (2004); E3.
[94] J.R. Lakowicz, Principles of fluorescence spectroscopy, Springer, New York, 2006.
[95] R. Leardi, L. Nørgaard, Sequential application of backward interval partial least squares and genetic of relevant spectral regions. Journal of Chemometrics 18 (2004); 486-97.
[96] Lee Beom-Jin, Pharmaceutical preformulation: Physicochemical properties of excipients and powers and tablet characterization. in: S.C. Gad, editor. Pharmaceutical manufacturing handbook: production and processes. John Wiley & Sons, Inc., Hoboken, New Jersey, 2008.

[97] J.M.M. Leitão, J.C. Esteves da Silva, A.J. Girón, A.M. de la Peña, Optimization of Verapamil Drug Analysis by Excitation-Emission Fluorescence in Combination with Second-order Multivariate Calibration. Journal of Fluorescence 18 (2008); 1065-76.
[98] R.A. Lionberger, S.L. Lee, L. Lee, A. Raw, X.Y. Lawrence, Quality by design: concepts for ANDAs. The AAPS journal 10 (2008); 268-76.
[99] H.B. Liu, Y. Chen, X. Zhang, Characterization of anhydrous and hydrated pharmaceutical materials with THz time-domain spectroscopy. Journal of Pharmaceutical Sciences 96 (2007); 927-34.
[100] P.E. Luner, S. Majuru, J.J. Seyer, M.S. Kemper, Quantifying crystalline form composition in binary powder mixtures using near-infrared reflectance spectroscopy. Pharmaceutical Development and Technology 5 (2000); 231-46.
[101] J. Luypaert, D.L. Massart, Y.V. Heyden, Near-infrared spectroscopy applications in pharmaceutical analysis. Talanta 72 (2007); 865-83.
[102] Y.H. Ma, Q. Wang, L.Y. Li, PLS model investigation of thiabendazole based on THz spectrum. Journal of Quantitative Spectroscopy & Radiative Transfer 117 (2013); 7-14.
[103] L. Maurer, H. Leuenberger, Terahertz pulsed imaging and near infrared imaging to monitor the coating process of pharmaceutical tablets. International Journal of Pharmaceutics 370 (2009); 8-16.
[104] V. McCurdy, Quality by design. in: I. Houson, editor. Process understanding: For scale-up and manufacture of active ingredients.Wiley - Verlag GmbH & Co. KGaA, Weinheim, 2011.
[105] A.I. McIntosh, B. Yang, S.M. Goldup, M. Watkinson, R.S. Donnan, Crystallization of amorphous lactose at high humidity studied by terahertz time domain spectroscopy. Chemical Physics Letters 558 (2013); 104-8.
[106] B. Mehta, Understanding ICH Q11- FDA's Guidance on the development and manufacture of drug substances. Pharmaceutical Technology 37 (2013); 64-8.
[107] P. Merckle, K.A. Kovar, Assay of effervescent tablets by near-infrared spectroscopy in transmittance and reflectance mode: acetylsalicylic acid in mono and combination formulations. Journal of Pharmaceutical and Biomedical Analysis 17 (1998); 365-74.
[108] J.N. Miller, J.C. Miller, Statistics and chemometrics for analytical chemistry. Pearson Prentice Hall, Harlow, Essex, 2005.
[109] A.B. Moreira, I.L.T. Dias, G.O. Neto, E.A.G. Zagatto, M.M.C. Ferreira, L.T. Kubota, Solid-phase spectrofluorimetric determination of acetylsalicylic acid and caffeine in pharmaceutical preparations using partial least-squares multivariate calibration. Talanta 67 (2005); 65-9.
[110] A.B. Moreira, I.L.T. Dias, G.O. Neto, E.A.G. Zagatto, L.T. Kubota, Solid-phase fluorescence spectroscopy for the determination of acetylsalicylic acid in powdered pharmaceutical samples. Analytica Chimica Acta 523 (2004); 49-52.
[111] A.B. Moreira, I.L.T. Dias, G.O. Neto, E.A.G. Zagatto, L.T. Kubota, Simultaneous spectrofluorimetric determination of paracetamol and caffeine in pharmaceutical preparations in solid-phase using partial least squares multivariate calibration. Analytical Letters 39 (2006); 349-60.
[112] A.B. Moreira, H.P.M. Oliveira, T.D.Z. Atvars, I.L.T. Dias, G.O. Neto, E.A.G. Zagatto, L.T. Kubota, Direct determination of paracetamol in powdered pharmaceutical samples by fluorescence spectroscopy. Analytica Chimica Acta 539 (2005); 257-61.
[113] L. Munck, L. Nørgaard, S.B. Engelsen, R. Bro, C.A. Andersson, Chemometrics in food science - a demonstration of the feasibility of a highly exploratory, inductive evaluation strategy of fundamental scientific significance. Chemometrics and Intelligent Laboratory Systems 44 (1998); 31-60.
[114] F.J. Muzzio, P. Robinson, C. Wightman, D. Brone, Sampling practices in powder blending. International Journal of Pharmaceutics 155 (1997); 153-78.
[115] T. Næs, T. Isaksson, T. Fearn, T. Davies, A user-friendly guide to multivariate calibration and classification, NIR publications, Chichester, 2002.
[116] M. Nakach, J.R. Authelin, A. Chamayou, J. Dodds, Comparison of various milling technologies for grinding pharmaceutical powders. International Journal of Mineral Processing 74 (2004); S173-S181.
[117] A. Navalon, R. Blanc, M. del Olmo, J.L. Vilchez, Simultaneous determination of naproxen, salicylic acid and acetylsalicylic acid by spectrofluorimetry using partial least-squares (PLS) multivariate calibration. Talanta 48 (1999); 469-75.
[118] D.A. Newnham, P.F. Taday, Pulsed terahertz attenuated total reflection spectroscopy. Applied Spectroscopy 62 (2008); 394-8.
[119] R. Nishikiori, M. Yamaguchi, K. Takano, T. Enatsu, M. Tani, U.C. de Silva, N. Kawashita, T. Taragi, S. Morimoto, M. Hangyo, M. Kawase, Application of partial least square on quantitative analysis of L-, D-, and DL-tartaric acid by terahertz absorption spectra. Chemical & Pharmaceutical Bulletin 56 (2008); 305-7.
[120] C.C. Nitchie, Quantitive analysis with the spectrograph. Industrial & Engineering Chemistry Analytical Edition 1 (1929); 1-7.

[121] L. Nørgaard, M.T. Hahn, L.B. Knudsen, I.A. Farhatc, S.B. Engelsen, Multivariate near-infrared and Raman spectroscopic quantifications of the crystallinity of lactose in whey permeate powder. International Dairy Journal 15 (2005); 1261-70.
[122] L. Nørgaard, A. Saudland, J. Wagner, J.P. Nielsen, L. Munck, S.B. Engelsen, Interval partial least-squares regression (iPLS): A comparative chemometric study with an example from near-infrared spectroscopy. Applied Spectroscopy 54 (2000); 413-9.
[123] M. Otsuka, J.i. Nishizawa, N. Fukura, T. Sasaki, Characterization of poly-amorphous indomethacin by terahertz spectroscopy. Journal of Infrared Millimeter and Terahertz Waves 33 (2012); 953-62.
[124] M. Otsuka, J.i. Nishizawa, J. Shibata, M. Ito, Quantitative evaluation of mefenamic acid polymorphs by terahertz-chemometrics. Journal of Pharmaceutical Sciences 99 (2010); 4048-53.
[125] E.P. Parrott, J. Zeitler, L.F. Gladden, Accurate determination of optical coefficients from chemical samples using terahertz time-domain spectroscopy and effective medium theory. Optics Letters 34 (2009); 3722-4.
[126] K.E. Peiponen, E. Gornov, Complex refractive index of media in the THz spectral range. in: K.E. Peiponen, J.A. Zeitler, M. Kuwata-Gonokami, editors. Terahertz spectroscopy and imaging. Springer, Heidelberg, 2013.
[127] O.P. Perumal, S.K. Podaralla, Role of preformulation in development of solid dosage forms. in: S.C. Gad, editor. Pharmaceutical manufacturing handbook: production and processes. John Wiley & Sons, Inc., Hoboken, New Jersey, 2008.
[128] L. Petersen, C.K. Dahl, K.H. Esbensen, Representative mass reduction in sampling - a critical survey of techniques and hardware. Chemometrics and Intelligent Laboratory Systems 74 (2004); 95-114.
[129] L. Petersen, K.H. Esbensen, Representative process sampling for reliable data analysis - A tutorial. Journal of Chemometrics 19 (2005); 625-47.
[130] L. Petersen, P. Minkkinen, K.H. Esbensen, Representative sampling for reliable data analysis: Theory of sampling. Chemometrics and Intelligent Laboratory Systems 77 (2005); 261-77.
[131] K.M. Picker-Freyer, Tablet production systems. in: S.C. Gad, editor. Pharmaceutical manufacturing handbook: production and processes.Wiley & Sons Inc., Hoboken, New Jersey, 2008.
[132] E. Pickwell, V.P. Wallace, Biomedical applications of terahertz technology. Journal of Physics D-Applied Physics 39 (2006); R301-R310.
[133] S. Pieters, W. Saeys, T. Van den Kerkhof, M. Goodarzi, M. Hellings, T. De Beer, H.Y. Vander, Robust calibrations on reduced sample sets for API content prediction in tablets: Definition of a cost-effective NIR model development strategy. Analytica Chimica Acta 761 (2013); 62-70.
[134] F.F. Pitard, The gouping and segregation error. Pierre Gy's sampling theory and sampling practice: heterogeneity, sampling correctness, and statistical process control. CRC Press, Boca Raton, Florida, 1993.
[135] A.L. Pomerantsev, O.Y. Rodionova, Process analytical technology: a critical view of the chemometricians. Journal of Chemometrics 26 (2012); 299-310.
[136] J. Rantanen, S. Lehtola, P. Ramet, J.P. Mannermaa, J. Yliruusi, On-line monitoring of moisture content in an instrumented fluidized bed granulator with a multi-channel NIR moisture sensor. Powder Technology 99 (1998); 163-70.
[137] Å. Rinnan, F. van den Berg, S.B. Engelsen, Review of the most common pre-processing techniques for near-infrared spectra. Trac-Trends in Analytical Chemistry 28 (2009); 1201-22.
[138] O. Rodionova, A. Pomerantsev, NIR-based approach to counterfeit-drug detection. Trac-Trends in Analytical Chemistry 29 (2010); 795-803.
[139] O. Rodionova, Y. Sokovikov, V, A. Pomerantsev, Quality control of packed raw materials in pharmaceutical industry. Analytica Chimica Acta 642 (2009); 222-7.
[140] M.B. Romía, M.A. Bernárdez, NIR spectroscopy in pharmaceutical analysis: Off-line and at-line PAT applications. in: K.A. Bakeev, editor. Process Analytical Technology: Spectroscopic tools and implementation strategies for the chemical and pharmaceutical industries. John Wiley & Sons, Inc., Chippenham, Wiltshire 2010.
[141] R.C. Rowe, P.J. Sheskey, M.E. Quinn, Handbook of pharmaceutical excipients, PhP Pharmaceutical Press, London, 2009.
[142] V. Sablinskas, G. Steiner, M. Hof, Applications. in: G. Gauglitz, T. Vo-Dinh, editors. Handbook of spectroscopy.Wiley-VCH, Weinheim 2003.
[143] V.A. Saharan, V. Kukkar, M. Kataria, V. Kharb, P. Choudhury, Ordered mixing: mechanism, process and applications in pharmaceutical formulations. Asian J Pharm Sci 3 (2008); 240-59.
[144] T. Schæfer, Lægemiddelteknik, Institut for Farmaci, Danmarks Farmaceutiske Universitet, Copenhagen, 2004.
[145] E.A. Schmitt, D. Law, G.G.Z. Zhang, Nucleation and crystallization kinetics of hydrated amorphous lactose above the glass transition temperature. Journal of Pharmaceutical Sciences 88 (1999); 291-6.

[146] S.S. Sekulic, J. Wakeman, P. Doherty, P.A. Hailey, Automated system for the on-line monitoring of powder blending processes using near-infrared spectroscopy - Part II. Qualitative approaches to blend evaluation. Journal of Pharmaceutical and Biomedical Analysis 17 (1998); 1285-309.
[147] Y. Shen, P. Taday, M. Pepper, Elimination of scattering effects in spectral measurement of granulated materials using terahertz pulsed spectroscopy. Applied Physics Letters 92 (2008).
[148] Y.C. Shen, Terahertz pulsed spectroscopy and imaging for pharmaceutical applications: A review. International Journal of Pharmaceutics 417 (2011); 48-60.
[149] H.W. Siesler, Introduction. in: H.W. Siesler, Y. Ozaki, S. Kawata, H.M. Heise, editors. Near-Infrared Spectroscopy. Principles, Instruments, Applications.Wiley-VCH, Weinheim, 2002.
[150] E. Skibsted, S.B. Engelsen, Spectroscopy for process analytical technology (PAT). Encyclopedia of Spectroscopy and Spectrometry (2010); 2651-61.
[151] D.A. Skoog, F.J. Holler, S.R. Crouch, Principles of instrumental analysis, Thomson Brooks/Cole, Belmont, California, 2007.
[152] P.L. Smith, A primer for sampling solids, liquids, and gases: based on the seven sampling errors of Pierre Gy.Siam, 2001.
[153] B. Smith-Goettler, On-line PAT applications of spectroscopy in the pharmaceutical industry. in: K.A. Bakeev, editor. Process Analytical Technology: Spectroscopic tools and implementation strategies for the chemical and pharmaceutical industries. John Wiley & Sons, Inc., Chippenham, Wiltshire, 2010.
[154] G. Steiner, Measuring techniques. in: G. Gauglitz, T. Vo-Dinh, editors. Handbook of spectroscopy.Wiley-VCH, Weinheim, 2003.
[155] C.J. Strachan, T. Rades, D.A. Newnham, K.C. Gordon, M. Pepper, P.F. Taday, Using terahertz pulsed spectroscopy to study crystallinity of pharmaceutical materials. Chemical Physics Letters 390 (2004); 20-4.
[156] C.J. Strachan, P.F. Taday, D.A. Newnham, K.C. Gordon, J.A. Zeitler, M. Pepper, T. Rades, Using terahertz pulsed spectroscopy to quantify pharmaceutical polymorphism and crystallinity. Journal of Pharmaceutical Sciences 94 (2005); 837-46.
[157] Sura, Electromagnetic Spectrum, http://www.sura.org/commercialization/docs/SURA_EMS_chart_full.jpg, (accessed 16/5-2013), 2013.
[158] H. Swierenga, F. Wulfert, O.E. de Noord, A.P. de Weijer, A.K. Smilde, L.M.C. Buydens, Development of robust calibration models in near infra-red spectrometric applications. Analytica Chimica Acta 411 (2000); 121-35.
[159] P.F. Taday, Applications of terahertz spectroscopy to pharmaceutical sciences. Philosophical Transactions of the Royal Society of London Series A-Mathematical Physical and Engineering Sciences 362 (2004); 351-63.
[160] P.F. Taday, I.V. Bradley, D.D. Arnone, M. Pepper, Using terahertz pulse spectroscopy to study the crystalline structure of a drug: A case study of the polymorphs of ranitidine hydrochloride. Journal of Pharmaceutical Sciences 92 (2003); 831-8.
[161] P.F. Taday, M. Evans, J.A. Zeitler, Y. Shen, D. Dey, Terahertz technology: Moving from the laboratory into the process world. Spectroscopy 25 (2010); 32-9.
[162] I. Takeuchi, K. Tomoda, T. Nakajima, H. Terada, H. Kuroda, K. Makino, Estimation of crystallinity of trehalose dihydrate microspheres by usage of terahertz time-domain spectroscopy. Journal of Pharmaceutical Sciences 101 (2012); 3465-72.
[163] S. Thiele, R. Salzer, Optical Spectroscopy. in: G. Gauglitz, T. Vo-Dinh, editors. Handbook of spectroscopy.Wiley-VCH, Weinheim, 2003.
[164] G. Thomas, Medicinal chemistry: an introduction, John Wiley & Sons, Inc., West Sussex, 2008.
[165] S.S. Thosar, R.A. Forbess, N.K. Ebube, Y.X. Chen, R.L. Rubinovitz, M.S. Kemper, G.E. Reiner, T.A. Wheatley, A.J. Shukla, A comparison of reflectance and transmittance near-infrared spectroscopic techniques in determining drug content in intact tablets. Pharmaceutical Development and Technology 6 (2001); 19-29.
[166] H.J. Venables, J.I. Wells, Powder mixing. Drug Development and Industrial Pharmacy 27 (2001); 599-612.
[167] M. Walther, B.M. Fischer, P.U. Jepsen, Noncovalent intermolecular forces in polycrystalline and amorphous saccharides in the far infrared. Chemical Physics 288 (2003); 261-8.
[168] B. Wang, J.J. Gagne, N.K. Choudhry, The epidemiology of drug recalls in the United States. Archives of internal medicine 172 (2012); 1110-1.
[169] H. Wu, E.J. Heilweil, A.S. Hussain, M.A. Khan, Process analytical technology (PAT): Quantification approaches in Terahertz spectroscopy for pharmaceutical application. Journal of Pharmaceutical Sciences 97 (2008); 970-84.
[170] H. Wu, E.J. Heilweil, A.S. Hussain, M.A. Khan, Process analytical technology (PAT): Effects of instrumental and compositional variables on terahertz spectral data quality to characterize pharmaceutical materials and tablets. International Journal of Pharmaceutics 343 (2007); 148-58.

[171] H. Wu, M. Khan, THz spectroscopy: An emerging technology for pharmaceutical development and pharmaceutical Process Analytical Technology (PAT) applications. Journal of Molecular Structure 1020 (2012); 112-20.
[172] D. Xiang, J. Berry, S. Buntz, P. Gargiulo, J. Cheney, Y. Joshi, B. Wabuyele, H.Q. Wu, M. Hamed, A.S. Hussain, M.A. Khan, Robust calibration design in the pharmaceutical quantitative measurements with Near-Infrared (NIR) spectroscopy: Avoiding the chemometric pitfalls. Journal of Pharmaceutical Sciences 98 (2009); 1155-66.
[173] S. Yamamura, H. Gotoh, Y. Sakamoto, Y. Momose, Physicochemical properties of amorphous precipitates of cimetidine-indomethacin binary system. European Journal of Pharmaceutics and Biopharmaceutics 49 (2000); 259-65.
[174] L.X. Yu, Pharmaceutical quality by design: product and process development, understanding, and control. Pharmaceutical Research 25 (2008); 781-91.
[175] L. Yu, Amorphous pharmaceutical solids: preparation, characterization and stabilization. Advanced Drug Delivery Reviews 48 (2001); 27-42.
[176] M. Zeaiter, J.M. Roger, V. Bellon-Maurel, Robustness of models developed by multivariate calibration. Part II: The influence of pre-processing methods. Trac-Trends in Analytical Chemistry 24 (2005); 437-45.
[177] M. Zeaiter, J.M. Roger, V. Bellon-Maurel, D.N. Rutledge, Robustness of models developed by multivariate calibration. Part I: The assessment of robustness. Trac-Trends in Analytical Chemistry 23 (2004); 157-70.
[178] J.A. Zeitler, K. Kogermann, J. Rantanen, T. Rades, P.F. Taday, M. Pepper, J. Aaltonen, C.J. Strachan, Drug hydrate systems and dehydration processes studied by terahertz pulsed spectroscopy. International Journal of Pharmaceutics 334 (2007); 78-84.
[179] J.A. Zeitler, D.A. Newnham, P.F. Taday, C.J. Strachan, M. Pepper, K.C. Gordon, T. Rades, Temperature dependent terahertz pulsed spectroscopy of carbamazepine. Thermochimica Acta 436 (2005); 71-7.
[180] J.A. Zeitler, D.A. Newnham, P.F. Taday, T.L. Threlfall, R.W. Lancaster, R.W. Berg, C.J. Strachan, M. Pepper, K.C. Gordon, T. Rades, Characterization of temperature-induced phase transitions in five polymorphic forms of sulfathiazole by terahertz pulsed spectroscopy and differential scanning calorimetry. Journal of Pharmaceutical Sciences 95 (2006); 2486-98.
[181] J.A. Zeitler, P.F. Taday, K.C. Gordon, M. Pepper, T. Rades, Solid-state transition mechanism in carbamazepine polymorphs by time-resolved terahertz spectroscopy. Chemphyschem 8 (2007); 1924-7.
[182] J.A. Zeitler, P.F. Taday, M. Pepper, T. Rades, Relaxation and crystallization of amorphous carbamazepine studied by terahertz pulsed spectroscopy. Journal of Pharmaceutical Sciences 96 (2007); 2703-9.
[183] J.A. Zeitler, P.F. Taday, D.A. Newnham, M. Pepper, K.C. Gordon, T. Rades, Terahertz pulsed spectroscopy and imaging in the pharmaceutical setting - a review. Journal of pharmacy and pharmacology 59 (2007); 209-23.
[184] X.C. Zhang, J. Xu, Introduction to THz wave photonics, Springer, New York, 2010.

Paper I

Measurement of Active Content in Escitalopram Tablets by a Near-Infrared Transmission Spectroscopy Model that Encompasses Batch Variability

Measurement of Active Content in Escitalopram Tablets by a Near-Infrared Transmission Spectroscopy Model that Encompasses Batch Variability

SOLVEIG WARNECKE,[1] ÅSMUND RINNAN,[1] MORTEN ALLESØ,[2] SØREN BALLING ENGELSEN[1]

[1]Department of Food Science, Faculty of Science, University of Copenhagen, Frederiksberg C DK-1958, Denmark

[2]Biologics and Pharmaceutical Science, H. Lundbeck A/S, Valby DK-2500, Denmark

Received 30 August 2012; revised 17 December 2012; accepted 9 January 2013

Published online 4 February 2013 in Wiley Online Library (wileyonlinelibrary.com). DOI 10.1002/jps.23461

ABSTRACT: Near-infrared transmission (NIT) spectroscopy, with high-performance liquid chromatography as reference method, was used to study the variation of the active pharmaceutical ingredient (API), escitalopram, in five tablet batches (4%–12%, w/w) manufactured by direct compression. This study investigates the influence of sample orientation, powder segregation, and compression force on the NIT spectra. For this purpose, tablet samples were taken at six different production time points, at three different compression forces, and presented to the spectrometer in four different orientations and in three spectroscopic replicates. A total set of 2160 NIT spectra was recorded. The variances between the spectra at each level of API content were thoroughly investigated by partial least squares regression using theory of sampling. The results show that a minimum of 18 tablets from each level of API content is required to establish a robust NIT calibration. The identified number of spectra is required for covering small differences in the spatial heterogeneity of the API as well as minor variations in optical properties, due to variations in the tablet compression force. NIT spectroscopy is demonstrated to be a powerful technique not only for measuring the API content in escitalopram tablets but also for routine content uniformity analysis. © 2013 Wiley Periodicals, Inc. and the American Pharmacists Association J Pharm Sci 102:1268–1280, 2013

Keywords: near-infrared spectroscopy; HPLC; content uniformity; partial least squares regression; multivariate analysis; theory of sampling; active pharmaceutical ingredient; sampling error

INTRODUCTION

The amount of active pharmaceutical ingredient (API) in tablets is a critical quality attribute in pharmaceutical tablet manufacturing. It is thus desirable to analyze this property noninvasively, preferably online, during production with, for example, near-infrared (NIR) spectroscopy. In contrast to current practice, wherein tablet content uniformity is assessed on the basis of random sampling from the finished batch, online nondestructive measurements allow for real-time analysis of much larger parts of the batch approaching 100% quality control (QC). This will improve the assurance of product quality, reduce the number of laborious off-line analyses, and allow faster product release to market. Besides being attractive from a drug manufacture point of view, the online approach is in full compliance with principles from US Food and Drug Administration's recommendations on how to innovate pharmaceutical development and manufacturing.[1]

Direct compression is the simplest tableting principle, but it requires that the major components of the blend have adequate density, flow, and compaction properties. In contrast to wet granulation technologies such as fluid-bed and high-shear granulation, direct compression offers reduced complexity, risk, and cost of processing. For direct compression processes, however, powder segregation upon discharging from hoppers is a known risk that may affect the content uniformity of the final tablet.[2]

Additional Supporting Information may be found in the online version of this article. Supporting Information

Correspondence to: Solveig Warnecke (Telephone: +45-35333257; Fax: +45-35333245; E-mail: warnecke@life.ku.dk)

Journal of Pharmaceutical Sciences, Vol. 102, 1268–1280 (2013)

According to European Pharmacopoeia (Ph. Eur; 2.9.6),[3] the normal procedure for testing content uniformity is to analyze 10 tablets. If one individual tablet is outside the limits (85%–115% of average content, but not exceeding 75%–125%), another 20 tablets, randomly selected, are tested. Out of a typical production batch of 1,000,000–4,000,000 tablets, 10 tablets provide a testing rate in the range from 0.001% to 0.00025%. With the use of noninvasive spectroscopic online testing, it is possible to increase this testing rate dramatically without sacrificing tablets, and thus provide a higher degree of process and QC and reduced risk of failure in the production. This is why the most recent guidance from Ph. Eur. (2.9.47)[4] recommends to use at least 100 samples when testing tablets in production with spectroscopic online testing.

The interest in using NIR spectroscopy for pharmaceutical applications has increased during the last decades.[5] Many pharmaceutical applications use diffuse NIR reflectance because of strong absorbance of the compact tablet. However, the development of more sensitive detectors and more powerful light sources has made the application of near-infrared transmission (NIT) of pharmaceutical tablets feasible.[6] Using transmittance, the sampling volume (SV) is increased and the tablet interior is measured and consequently, the probability of discarding tablets batches because of sampling-related heterogeneity will be reduced.[7] This is in accordance with the findings of Thosar et al.,[8] who showed that calibrations obtained using transmission data gave better prediction models of the actual API concentration (1%–40%, w/w) compared with calibrations using reflection data. Gottfries et al.[7] showed that despite the fact that smaller parts of the spectrum ($\lambda = 800$–1350 vs. 800–2500 nm) were usable for calibrations for transmission measurements compared with reflectance, transmission resulted in better calibrations. Root-mean-square-error of prediction (RMSEP) was 1.06 mg/tablet for transmission mode and 2.83 mg/tablet in reflectance mode for tablets with average content of 47.5 mg/tablet.

For nondestructive spectroscopic methods with random sampling orientation, it is important to know what difference it makes if the tablet is facing up or down when presented to the spectrometer. Laasonen et al.[9] found that in reflectance the two faces of a tablet gave different spectral information when analyzing the data with hierarchical cluster analysis. The difference was due to higher compression force in the upper punch than the lower punch, leading to a variation in tablet density and in turn a spectral difference. Even after pretreating the spectra with Savitzky–Golay second derivative, a considerable spectral difference remained and therefore an average of spectra from both faces of the tablet was used.

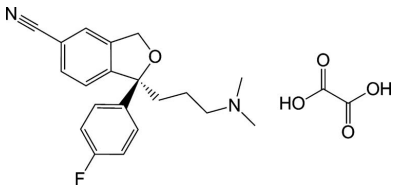

Figure 1. Structure of escitalopram oxalate.

According to Gy,[10–12] all natural systems or samples are to some degree spatially unevenly distributed. This fact is even more prevalent when dealing with direct compression due to differences in particle size and physical properties of the ingredients. An analogy to tablet measurements can be made from single wheat seed measurements. Using theory of sampling (TOS) on a NIT-based calibration, Tønning et al.[13] investigated the effect of different wheat kernel seed orientations in the spectrometer on the variation of protein concentration. They found that pointing the crease away from the light source resulted in the best calibration [root-mean-square error of cross-validation (RMSECV = 0.48% DM protein)] and averaging over three spectral replicates improved the model (RMSECV = 0.36% DM protein), but averaging over several orientations did not improve the models. The RMSECV from partial least squares (PLS) regression[14] was also used to determine the variance of the total analytical error (TAE) when using different sampling strategies. Many studies demonstrate the development of quantitative API models using NIR and NIT,[7–9,15–21] and some also measure using NIR in different points of tablet production.[22] Blanco et al.[23] found that because of production variability at least three production samples are required in a laboratory calibration sample set to obtain a good prediction of subsequent production samples. However, to the best of our knowledge, TOS has not been applied to evaluate the criteria of acceptance for a robust method.

In this study, the variation in tablet API concentration over the batch production time and with different compression forces is investigated as part of a comprehensive analytical approach including sampling parameters such as orientations of the tablets and multiple replicates. The API used as model in this sampling study is escitalopram oxalate at a tablet strength of 10 mg (8%, w/w; free base) (see Figure 1). Escitalopram tablets are manufactured by direct compression in laboratory scale. The aim is to establish the basic information needed to develop a NIT method for at-line prediction of the API concentration in the tablet. High-performance liquid chromatography (HPLC) is used as a reference method.

MATERIAL AND METHODS

Tablet Production

Escitalopram tablets containing 10 mg API (8%, w/w) are shaped as ellipsoids ($5.5 \times 8.0\,mm^2$). The tablets have a score and letters "E" and "L" embossing on one face of the tablet.

The five blends contained different amounts of API (4%, 6%, 8%, 10%, and 12%; w/w) corresponding to 50%–150% of the target concentration of 10 mg (free base). The change in API concentration was compensated for by changing the amount of filler, silicified microcrystalline cellulose (SMCC; Prosolv; JRS Pharma, Rosenberg, Germany) accordingly. Batch size was 2000 g.

A Bohle LM40 blender (L.B. Bohle, Ennigerloh, Germany) was used for mixing the API with filler and disintegrant and for subsequent lubrication. Blending time was 8 min followed by 3 min lubrication with magnesium stearate, both steps performed at 22–24 rpm.

Escitalopram tablets (total weight of 125 mg) were manufactured on a Kilian Pressima, 12-punch rotary tablet press (I.M.A Kilian GmbH & Company KG, Cologne, Germany) at a compression speed of 20,000 tablets/h. During the production, the compression force was varied to achieve tablets at three different tablet hardness levels: H_{medium}, H_{low}, and H_{high}; approximately 85, 70, and 100 N, respectively (corresponding to average compaction pressures of 72, 58, and 93 MPa).

This scheme leads to the following sampling strategy. For each target API (4%, 6%, 8%, 10%, and 12%, w/w), six sample sets were collected as described below:

Sample set 1: 25 tablets collected after the production of approximately 500 tablets, hardness H_{medium};

Sample set 2: 25 tablets collected after the production of approximately 2800 tablets, hardness H_{medium};

Sample set 3: 25 tablets collected after the production of approximately 4600 tablets, hardness H_{low};

Sample set 4: 25 tablets collected after the production of approximately 6600 tablets, hardness H_{high};

Sample set 5: 25 tablets collected after the production of approximately 10,000 tablets, hardness H_{medium};

Sample set 6: 25 tablets collected after the production of approximately 13,000 tablets, hardness H_{medium}.

Six tablets for spectroscopic analysis were randomly selected from the 25 tablets in the six sample sets.

Samples at hardness H_{medium} were collected at various time points throughout tableting to assess the impact of drift in the process (e.g., in-process segregation).

During the production, an adjustment of compression force was performed by measuring mass variation and hardness. In addition, tablet thickness was measured at the end of tableting.

NIR Analysis

Near-infrared transmission spectra were acquired in the region 4000–14,000 cm^{-1} (700–2500 nm) with a resolution of 8 cm^{-1} and using 64 scans per sample. The instrument used was an ABB Bomem FT-NIR MB-160 (ABB Bomem Inc., Montreal, Canada) equipped with a tablet Sampl*ir* (carousel) and a custom-made tray for 125 mg escitalopram tablets. The light source was situated below the sample with the detector on the upper side. Reference spectra were recorded using the internal ceramic standard (Spectralon 99%, Lapsphere Inc., North Sutton, New Hampshire) and used to convert the tablet spectra into absorbance units. Six tablets from each sample withdrawal were measured. Three spectra were recorded from the center of the tablet with four rotations of the tablet (lower part of Figure 2). Measurements of tablets in positions 1 and 2 had the score facing upward, and for positions 3 and 4, the score was facing downward. The samples were presented randomly to the autosampler. After the spectroscopic measurements, all the tablets were analyzed by HPLC using an in-house method. HPLC-determined content was corrected for tablet mass and reported in percentage (w/w) units.

DATA TREATMENT

All data processing was performed in Matlab 7.7.0 (Mathworks™, Natick, Massachusetts) using PLS toolbox (Eigenvector, Wenatchee, Washington). All NIT spectra were preprocessed with the standard normal variate (SNV)[24] to minimize effects of scatter caused by the density changes and to minimize artifacts from small changes in path length caused by small changes in the thickness of the tablets.

Principal component analysis (PCA)[25] was applied to explore the spectral data using the score plot and loading plot to find the largest variations within the dataset.

Calculation of Total Volume SV with NIT

For the calculation of the total volume of the tablet, the following equation was used:

$$V_{tablet}(mn^2) = \pi ABt$$

where, A is the radius of the one side, B is the radius of the other, and t is the thickness of the tablet.

 DOI 10.1002/jps

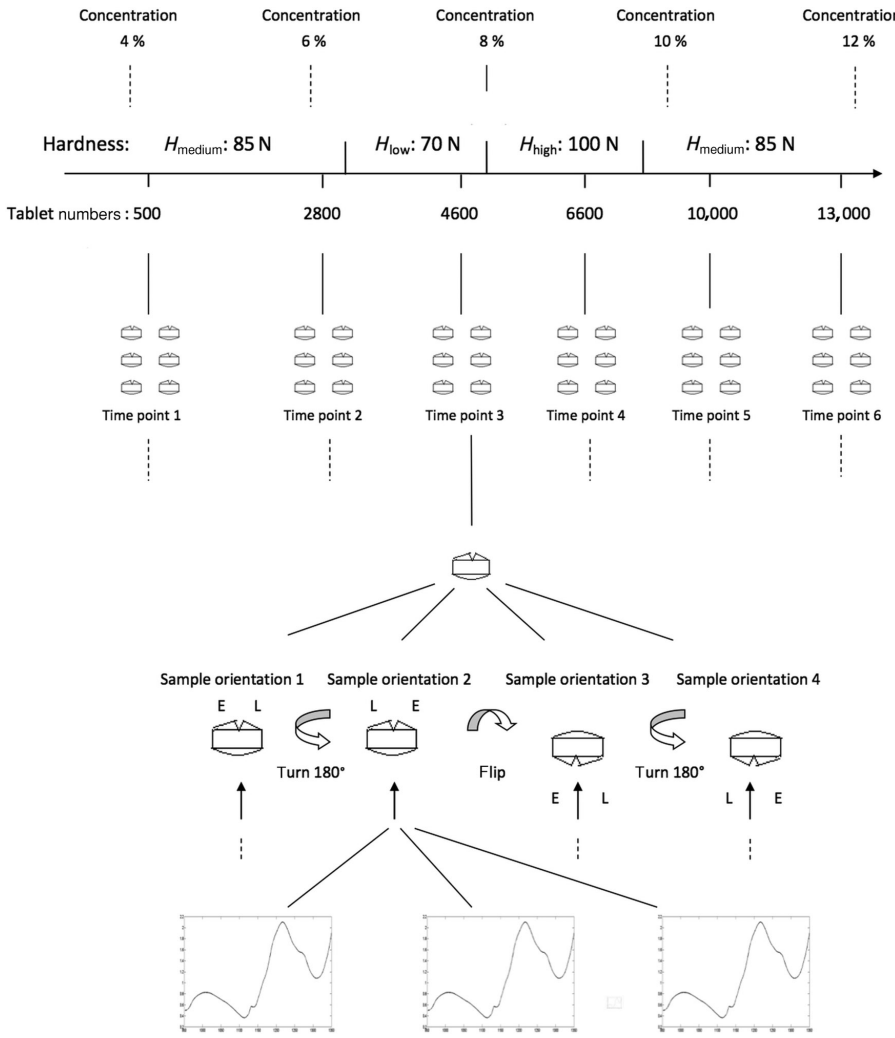

Figure 2. Experimental design. From the top: API concentration levels, tablet hardness levels, batch withdrawels, sample orientation, and NIT analysis. The experimental design includes five batches, six production time points, six tablets (taken out of the 25 from each sample collection), each tablets is presented to the spectrometer in four orientations, and each face of the tablet is presented in the spectrometer three times after one turn in the tablet carousel. This design gives a total of (5·6·6·4·3) 2160 NIT spectra. Each individual tablet was subsequently measured by HPLC (5·6·6) giving a total of 180 HPLC measurements..

The equation is an approximation, as it does not take into account the curving and the score of the tablet. The SV will be dependent on the thickness of the tablet, which varies in the design according to hardness/porosity. The NIR light enters the tablet through a 1.5-mm-diameter hole and exits the tablet (to the detector) through a hole with a diameter of 2.2 mm. Hence, the SV is (roughly) shaped as a truncated cone. Assuming an average thickness of t mm, the SV is estimated as:

$$\mathrm{SV}(\mathrm{mm}^3) = \pi t(1.1^2 + 0.75^2 + 1.1 \times 0.75)/3$$

This volume is an approximation, which only considers geometry and not how the light actually travels inside the tablet before reaching the detector.

Calculation of Variance

The variances of the NIT spectra for the spectral replicates [S(spectral replicates)], direction up/down [S(down)/S(up)], the four orientations [S(orientation)], the tablet replicates [S(tablet replicate)], tablets from only H_{medium} [$S(H_{\text{medium}})$], all the time points [S(processing time)], and from the different API [S(API)] were calculated from the SNV-corrected spectra.

The averaged variances across spectra are calculated as follows:

$$S^2_{\text{Rep}} = \frac{\sum_{j=1}^{j} \frac{\sum_{i=1}^{R} (x_{r,j} - \bar{x}j)}{R-1}}{J} \quad (1)$$

where $x_{r,j}$ is the rth replicate at wavelength j. R is the total amount of replicates, J is the total number of wavelengths measured, and S^2_{Rep} is the variance across spectra (and replicates). The average variance across several samples is thus:

$$\bar{S}^2_{\text{Rep}} = \frac{S^2_{\text{Rep}}}{N} \quad (2)$$

where N is the total numbers of samples averaged across. This is also used for calculations of the HPLC variances.

There is a certain hierarchy to be expected in the spectral variances. The variance between batches (API concentrations) should be larger than the variance between the processing time points. The variance between the processing time points should be comparable to the variance from only the medium hardness (H_{medium}) assuming that the compression force differences do not significantly affect the variance. These in turn should be larger than the tablet replicates, which in turn should be larger than the orientation replicates. The variances of the orientation replicates should be larger than the variances for tablets facing up or down, which should be larger than the spectral replicates (one turn in the tablet carousel):

$$\begin{aligned} S(\text{API}) \gg S(\text{processing time}) &\approx S(\text{tablet}\, H_{\text{medium}}) \\ &> S(\text{tablet replicates}) \\ &> S(\text{tablet orientation}) \\ &> S(\text{down})/S(\text{up}) \\ &> S(\text{spectral replicates}) \end{aligned}$$

Calibrations to HPLC Data

Partial least squares regression[14] was performed on the NIT spectra using the API concentration determined by HPLC as response variable. The models were optimized through variable selection using interval partial least-squares regression, iPLS (i.e., spectral region selection).[26]

The complexity of each model was estimated by finding the minimum or breakpoint in the RMSECV curve. For the cross validation, one time point will be left out sequentially (30 segments), so one of 30 of the spectra is left out at the time. To be able to better compare the different scenarios, the 2160 originally measured spectra were subsequently predicted using each of these prediction models. A RMSEP was calculated based on these predictions. It should be noted that the obtained RMSEP was not a real estimate of a future prediction, as the samples from the calibration set was part of the total 2160 spectra. It will, however, give a good indication of how production samples will be predicted. Therefore, it is marked "RMSEP" whenever prediction was carried out on samples included in the calibration set. RMSECV and "RMSEP" are calculated as follows:

$$\text{RMSE} = \sqrt{\frac{\sum_{i=1}^{N} (y_i - \hat{y}_i)^2}{N}} \quad (3)$$

where y_i is the true API value (here HPLC), $\hat{y}_i$ is the predicted value (from iPLS on NIT), and N is the total number of samples.

If the target is to develop a robust model for NIT prediction of API content of single tablets, the following questions should be investigated without making averages:

(1) Are spectral replicates important for the API prediction model?
(2) Is tablet orientation important for the API prediction model?
(3) Are tablet replicates important for the API prediction model?
(4) Do systematic changes in the tablet compression force improve the model?
(5) Do variations in processing time improve the model?

This was carried out as follows: Develop a PLS model for all spectra (2160 in total) and compare it with:

(1) PLS models for spectra from first, second, or third replicate (720 spectra in each).
(2) PLS models of each of the four orientations (180 spectra). Second, compare it with a PLS model with mixed directions, that is, up and down (180 spectra).
(3) PLS model of one-tablet replicate (30 spectra), two-tablet replicates (60 spectra), three-tablet replicates (90 spectra), four-tablet replicates (120 spectra), five-tablet replicates (150

spectra), and six-tablet replicates (180 spectra) using only one spectral replicate and one fixed orientation.

(4) PLS model for the four H_{medium} time points (1440 spectra). Furthermore, PLS models excluding either time point 3 (H_{low}) or time point 4 (H_{high}) using one spectral replicates, one fixed orientation, and all tablet replicates.

(5) PLS models for one (30 spectra), two (60 spectra), three (90 spectra), or four (120 spectra) time points from H_{medium} with one spectral replicate, one fixed orientation, and all the tablet replicates.

All models are cross validated by leaving one time point out at the time, and the RMSECV values are reported. All cases are compared with "RMSEP" found from predicting all the spectra (2160 spectra) and where it makes sense all the spectra from H_{medium} (1440 spectra). Furthermore, calibrations made on H_{medium} will be tested on samples from H_{low} and H_{high}, to investigate the performance with a slightly deviating process. The RMSEP values for H_{low} and H_{high} are true RMSEP values, as none of the spectra predicted are present in the calibration set.

Calculation of TOS Terms

As described by Tønning et al.,[13] the standard deviation of the TAE (S_{TAE}) can be calculated as follows:

$$S^2_{TAE} = \frac{RMSEP^2}{a_L^2 N} \quad (4)$$

where RMSEP is the root mean square error of prediction of a PLS calibration, a_L is the reference value of the concentration (from HPLC), and N is the number of samples.

The RMSEP values here are true RMSEP values, as the models are based on five time points and predicted on the last time point. The models are based on the recommended number of samples found in the previous section.

To assess the significance of the RMSEP values, a two-way analysis of variance (ANOVA) is performed. Because of large interaction effect, two one-way ANOVA are performed with the multicompare function to distinguish the variances within the time points and concentration. The six time points and five concentrations are divided into categories according to their internal significance (95% significance level). The multicompare function uses Tukey's honestly method of multiple comparison, and is based on the Studentized range distribution[27].

RESULTS

Sampled and Tablet Volume

Given the known heterogeneity problem of tablets produced by direct compression, the characteristics of the sampled volume are taken into account. From the average tablet thickness of 3.76 mm, the estimated NIT SV is 10 mm^3 and the total tablet volume, V_{tablet}, is 130 mm^3. This provides a sampling efficiency of 8% per tablet, which will be compared with the HPLC results that will analyze the whole tablet.

Spectral Interpretation and Exploratory Analysis

Only the short-wavelength part of the NIR spectrum (952–1350 nm) is used, as the absorption level becomes too large in the long-wavelength region. This is in line with the findings of Dyrby et al.[6] Figure 3a shows the raw NIT data in the interval from 952 to 1350 nm. Figure 3b shows the reflectance spectra of escitalopram oxalate and the main excipient, SMCC. Figure 3c displays the average NIT spectra of tablets at the five API levels after SNV correction. As indicated by Figure 3c, the absorbance at 1132 nm is linearly correlated to the API concentration in the tablet. The SNV pretreatment clearly reduces the total variance of the spectral data set while enhancing the API-specific peak at 1132 nm, corresponding to the second overtone of aromatic C—H stretching.[6]

Figure 4a shows the PCA score plot of PC1 and PC2 on the SNV and mean-centered spectral data and colored according to API concentration. The score plot reveals that the API gradient spreads out along PC2, whereas the variance along the first PC is related to uptake of water because of the hygroscopic character of celluloses (see loading plot below).[28] Figure 4b shows the corresponding loading plot for PC1 and PC2. PC2 has a large peak in the spectral area around 1132 nm characteristic of the API. For PC1, a large part of the spectral information is found in the area from 950 to 1100 nm corresponding to the second overtone of the O—H stretching of water, demonstrating that water adsorption is significant. This is consistent with the findings of Gottfries et al.,[7] who found that tablets analyzed before and after storage were distributed along PC1 according to their water content. The broad band in PC1 at 1150–1300 nm is probably due to microcrystalline cellulose and increasing water content, as Luukkonen et al.[29] found an upward displacement of absorbance spectra baseline in this area for SMCC. The fact that the spectral variation caused by the API is only the second largest is related to the fact that it is a minor component in the tablet (microcrystalline cellulose being the largest).

Analysis of Spectral V*ariances*

The differences between the NIT spectra are presented as the variance between spectra in the area

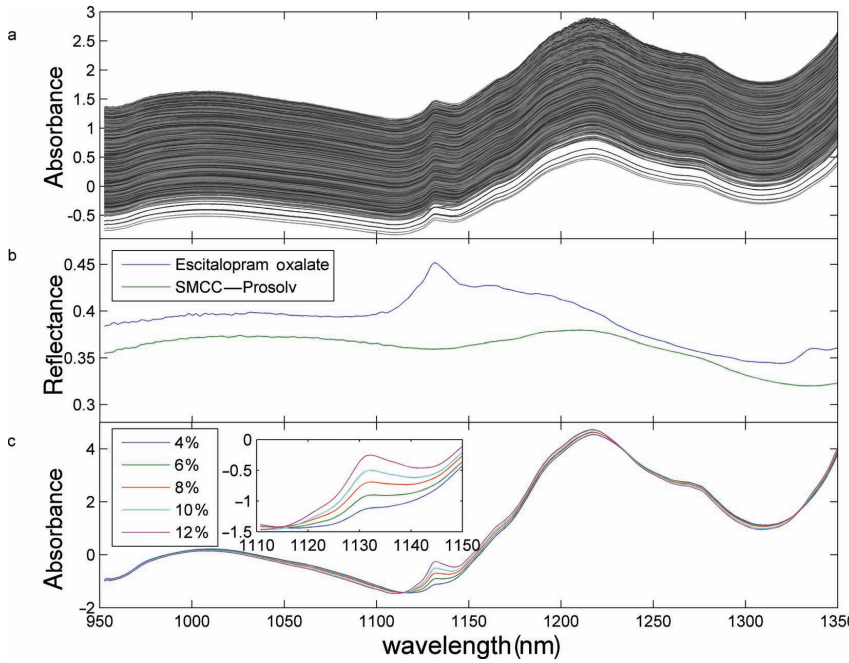

Figure 3. (a) Raw NIT spectra of all samples from 952 to 1350 nm. (b) Reflectance NIR spectra of pure constituents, escitalopram oxalate, and silicified microcrystalline cellulose (SMCC—Prosolv) 952–1350 nm. The peak at 1132 nm is assigned to second overtone C—H stretch of the escitalopram oxalate molecule. (c) SNV-corrected NIT spectra from tablets of five loads of API from 952–1350 nm. The insert shows a magnified wavelength region specific to the API.

from 952 to 1350 nm after SNV correction. Figure 5 shows the variances of the tablet replicates, upward facing, all four tablet orientations, downward facing, tablet replicates, and tablet replicates including only tablets of H_{medium}. As evident from Figure 5, the variance between the spectral replicates [S(spectral replicates) = 0.0010] is low compared with all the other spectral variances. This is expected and shows that there will be a larger difference between spectra as soon as the sample has been moved in the tablet sampler.

When investigating the spectral variance from tablets with all four orientations (Figure 5b), the variance becomes slightly higher [S(tablet orientation) = 0.0023]. The additional variance is introduced by repositioning of the tablet in the tablet carousel and by a lower transmittance and higher light scattering when the score is presented toward the light source compared with the score presented away from the light source. The fact that there are large variations between spectra of the same tablet measured at different sample orientations could also be due to heterogeneity, which is a known issue for direct compression tablet formulations.

From Figure 5, it is also observed that the spectral variance between the tablet replicates [S(tablet replicates) = 0.0032] is of the same magnitude as the spectral variance between the processing time points only including H_{medium} [S(H_{medium}) = 0.0030] and processing time [S(processing time) = 0.0034, (result not shown—only five bars)]. This indicates that the added variation between processing points is almost hidden in the spectral variation by the tablet replicates, and that the differences in compression forces are only adding a little to the spectral variance. Finally, the spectral variation between the API batches was found to be S(API) = 0.054, which is a great deal larger than the other variations and should be sufficient for robust calibrations.

Analysis of HPLC Replicate Variance

In Figure 6, the variances calculated from the HPLC results is shown. The first histogram (Figure 6a) shows the dilution replicates, which basically is triple injection on HPLC performed on 15 out of the 180 tablets. This is very low [S(dilution) = 0.0002], as expected. The second and third histograms (Figs. 6b and 6c) both show the variances between the tablet

 DOI 10.1002/jps

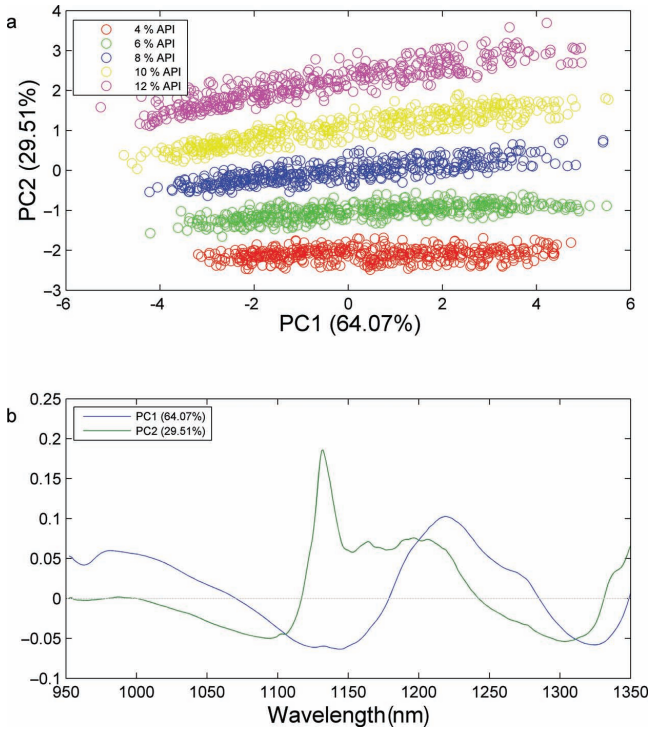

Figure 4. PCA on the SNV and mean centered NIT data. a) Scoreplot of PC1 versus PC2 colored by API loads. b) Loading plot for PC1 and PC2.

replicates but colored by time points and batches, respectively. The variance for the tablet replicates [S(tablet replicates) = 0.014] is larger, as in this analysis, each represent individual tablets. When observing the time points, no one stands out to be lower or higher than the other, which means that there are no signs of segregation. Regarding the batches, batch 2 (6%, w/w) shows lower variances than the remaining batches. For the overall variances from each batch (0.028, 0.009, 0.015, 0.038, and 0.027) it is also seen that batches 2 and 3 vary the least and batches 1, 4, and 5 vary the most. This suggests that it is more difficult to produce the batches with higher API concentration than the target value (8%, w/w) or the fact that the HPLC method was developed for the target value.

PLS Regression Analysis

In order to investigate the requirements for building a robust quantitative NIT model, PLS regressions were performed using the five scenarios mentioned in the *Material and Methods* section. After an initial set of PLS models, it was decided to refine all models by applying variable selection using iPLS. The spectra were divided into 46 intervals and the iPLS algorithm was run with forward selection, that is, until no further model improvement could be seen. The selected intervals (1126–1132 and 1287–1295 nm) were used for all scenarios. The first interval covers the information of the API, whereas the second interval includes information from the tablet matrix. Models only including signal from the API were also tried, but they were found to be inferior to the selected model. In addition to spectral region selection, several preprocessing treatments were evaluated[30] and SNV (performed on whole spectra, 952–1350 nm) was chosen as the most suitable preprocessing based on cross-validated results. SNV reduces the effects from spectral differences due to varying tablet porosity and thickness and thus spectroscopic path length as a consequence of the different applied compression forces. Furthermore, the models were tested for outliers, but none were found. The models are cross validated in selections, so one time point is taken out at the time. In this article, only the most important results are highlighted, but all the models can be found in *Supporting Information* (*SI*).

Each individual PLS model is evaluated by predicting API content (%, w/w) using all the spectra (2160) as well as spectra only from H_{medium} (1440). In

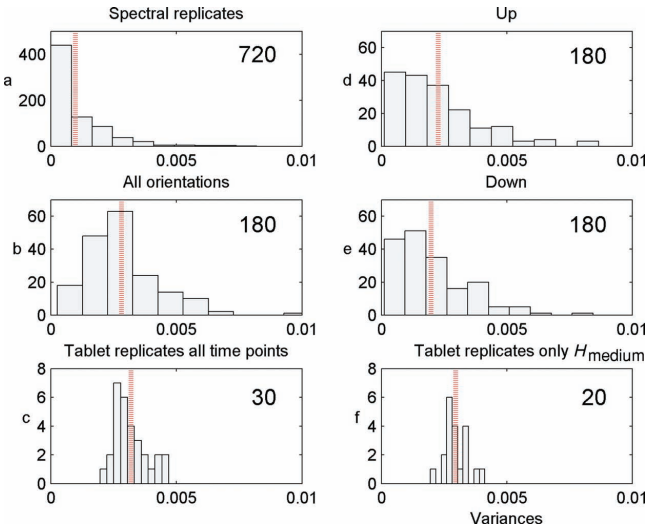

Figure 5. Histograms of variances between SNV corrected spectra. Red lines mark the average variation. Histogram of spectral variance between a) spectral replicates (3·720), average is 0.0010. b) tablet orientations (3·4·180), average is 0.0028. c) tablet replicates (3·4·6·30), average is 0.0032. d) tablet orientations with face up (3·2·180), average is 0.0023. e) tablet orientations with face down (3·2·180), average is 0.0020. f) tablet replicates from H_{medium} (3·4·6·20), average is 0.0030.

general, all the RMSE values are in the range from 0.25% to 0.30% (w/w), which are in good agreement with the findings of Dyrby et al.[6] on the same API. "RMSEP" values are generally lower for predictions made on tablets of H_{medium} compared with predictions using all spectra. This suggests better prediction, when tablet hardness is kept fixed.

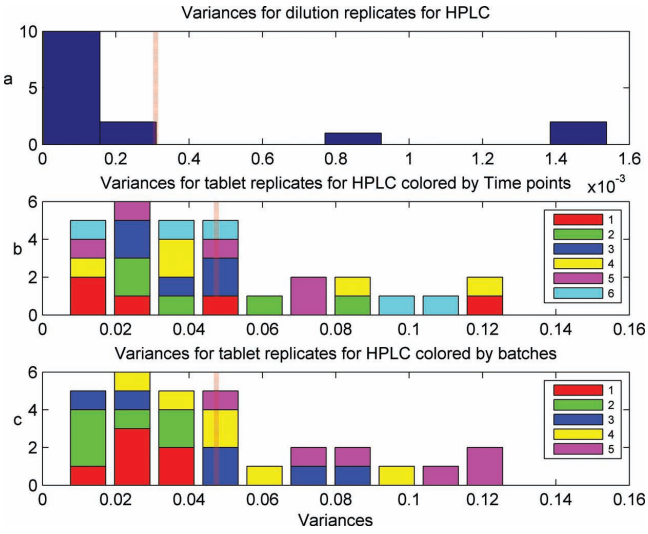

Figure 6. Variances from HPLC from (a) dilution replicates (15 out of 180 tablets, average is 0.0002), (b) tablet replicates colored by time points (average is 0.014), and (c) tablet replicates colored by batches.

The all-spectra-model is giving RMSECV of 0.251% (w/w). When comparing with the model only including spectra from H_{medium} (RMSECV = 0.247%, w/w), there is not much difference. This means that including spectra from different hardness does not degrade the overall model. The H_{medium} calibration is also evaluated on the deviating hardness H_{low} and H_{high}. This is performed to simulate how calibration will perform on a slightly deviating process (still within specifications), when calibration is only made of tablets of H_{medium}. The performance of the H_{medium} model on the spectra from H_{low} (RMSEP = 0.267% w/w) is worse than all the spectra and spectra from H_{high} (RMSEP = 0.246%, w/w).

The sensitivity of a NIR model toward hardness variations is a direct cause of different tablet porosities, which in turn give different levels of scatter. Porosity, that is, percentage of interparticulate voids, affects light scatter and total path length in the sample that is observed as apparently increased absorbance levels that sometimes cannot be 100% compensated for by spectral preprocessing.[31] In our case, the following average porosities (oil intrusion, in-house method) were found for H_{low}, H_{medium}, and H_{high} tablets: 23%, 19%, and 17%, respectively. Hence, the porosity difference between H_{low} and H_{medium} tablets (4%) is larger than the corresponding H_{medium} to H_{high} tablets (2%). This variation in porosity explains the slightly inferior predictions on H_{low} tablets when using the H_{medium} tablets for calibration.

Models made only of first, second, or third replicates are compared with the total model (shown in *SI*, calibration number 3–5), and as it does not improve the models to add more replicates, only one replicate (second replicate) is used for further investigation.

The next step was to compare models from tablets placed up or down in the autosampler. The models for the tablets facing upward have lower RMSECV (RMSECV = 0.238% and 0.240%, w/w) than the models facing downward (RMSECV = 0.279% and 0.291%, w/w)—the score facing toward the light source. Predictions of all the spectra with models only based on one direction (up/down) give "RMSEP" between 0.259% and 0.261% (w/w). Models wherein both up- and down-facing spectra are included (mix models, calibration numbers 10–14 in *SI*) will give RMSECV in between the RMSECV seen for the "upward" and "downward" models (RMSECV = 0.249%–0.257%, w/w). The prediction of all the spectra ("RMSEP" = 0.250%–0.258%, w/w) seems to be improved by including spectra from both directions (up and down), which makes sense, as both directions are included in the total amount of spectra. This can be of relevance, if it is not possible to fix the position of the tablets in the production, for example, in online measurements. Then, the best performance for future predictions will be obtained including both directions in the calibration set. In the study, although we are interested in finding the best performance; therefore, only spectra from upward-facing tablets (position 1) are chosen for further investigation.

Next, an investigation of how many tablet replicates from each withdrawal are necessary was performed. Six tablets from each withdrawal were analyzed, and RMSECV and "RMSEP" values are increasing as the fewer spectra are included in the calibrations. As there are more possibilities for choosing one-to-five-tablet replicates out of six-tablet replicates, it is also necessary to examine the range of the results. This will give an idea of the worst and best scenarios. The range for RMSECV is also increasing with the fewer amounts of tablet replicates. Going from three-tablet replicates, equal to 90 spectra, (RMSECV = 0.212%–0.264%, w/w) to two-tablet replicates, equal to 60 spectra (RMSECV = 0.205%–0.286%, w/w), the range for RMSECV is increasing markedly. Therefore, it seems like that at least three tablets are needed from each withdrawal or 90 spectra in total. Using fewer than 90 spectra (18 from each API level) caused the performance of the models to vary too much, which yields inconsistence results, and the outcome is random as to whether or not a robust calibration is achieved.

Testing a model made only of spectra from H_{medium}, using all six tablet replicates (only second spectral replicate and first orientation), has a lower RMSECV (RMSECV = 0.227%, w/w). Although predictions of spectra from tablets with H_{low} (RMSEP = 0.266%, w/w) and H_{high} (RMSEP = 0.258% w/w) are, as shown earlier, not performing as well.

Considering whether it is important to withdraw tablets at different time points, models from four, three, two, and one time points (all H_{medium}) were evaluated (calibrations 48–63 in *SI*). The performance of the models vary significantly when two time points or 60 spectra were used (RMSECV = 0.198%–0.284%, w/w) compared with three time points or 90 spectra (RMSECV = 0.212%–0.254%, w/w). This is more likely caused by too few spectra than the fact that the tablets are collected at different time points. Furthermore, models with 120 spectra from each time point [first and second spectral replicate, first and second orientation (up), and six-tablet replicates] are tested, and show only minor differences in the predictions errors (results not shown).

The recommendations for building a calibration from this part, is to only analyze tablets with the score facing away from the light source, unless both orientations will be present in on-line measurements. The minimum requirement with regard to number of spectra is 90 spectra (18 spectra per batch/API concentration level). Furthermore, as certain variation in hardness will naturally occur during production, it is recommended to include tablets with a wide range

of hardness in the calibration set to make the model robust to such possible changes in future samples.

To investigate any changes in performance of the models during process time, RMSEP values for batches (API concentrations) and time points 1–6 are calculated (Table 1). Furthermore, the S_{TAE}, which takes the drug concentration into account, are shown in *SI*. For each of the models, 100 spectra are used [four tablet replicates from five out of six time points and five API concentration levels, only using the second spectral replicate and the first orientation (up)]. The four-tablet replicates from each time point are randomly chosen (out of six tablet replicates) 20 times, so the RMSEP values used are the averages. The last time point is used for validation using all six tablet replicates. The classes from the ANOVA test (multicomparison) for the API level and the time points are reported in Table 1.

In general, the average RMSEP for the batches seem to be hyperbolic shapes with 8% (w/w), the target level of the API, being the vertex. Batch 5 with 12% API is significantly higher than the other batches. This is also in line with the findings from the HPLC analysis, where batches 1, 4, and 5 were higher than the target level. When comparing the RMSEP values for the time points, it becomes obvious that the calibration generally performs poorest for tablets of H_{low} (time point 3; 70 N), as seen from the highest RMSEP, but it is not significantly higher than time point 2 (hardness 85 N). Time point 6 is having the lowest RMSEP, but it is not significantly lower than time point 1. As the RMSEP does not seem to increase over time (time pointes 5 and 6 versus 1 and 2), there are no signs of systematic segregation in the process.

Regarding the S_{TAE} (shown in *SI*), time point 4 (hardness 100 N, $S_{TAE} = 9.72$) for the batch with 4% (w/w) API has a high S_{TAE} compared with the other batches. As the S_{TAE} is found by dividing the squared RMSEP by the squared API concentration ($a_L{}^2$), it is expected to be larger at smaller API concentrations. However, there seems to be a large difference between 4% (w/w; $S_{TAE} = 7.85$) and 6% (w/w; $S_{TAE} = 4.28$) and the remaining batches ($S_{TAE} \sim 3$). This means that even though the RMSEP is at the same level for all batches, the relative error is much larger for 4% (w/w) than the other batches, which is probably because of the fact that squared small API concentration has a high impact on S_{TAE}.

CONCLUSIONS

In order to establish a robust NIT calibration for determining the API concentration (%, w/w) in single tablets, at least 18 tablets from each API concentration are required (for five levels, this corresponds to 90 spectra). Furthermore, if it is desired that the created model should be able to predict tablets within a wide

Table 1. RMSEP values at given API concentration and time.[a] Classes from one-way ANOVA multicompare are also shown.

API (%, w/w)	Time Point 1, 85 N	Time Point 2, 85 N	Time Point 3, 70 N	Time Point 4, 100 N	Time Point 5, 85 N	Time Point 6, 85 N	Average of Time Points	Group From Multicompare One-Sided ANOVA Analysis
4	0.334	0.289	0.337	0.394	0.319	0.235	0.318	d
6	0.224	0.418	0.317	0.229	0.213	0.169	0.262	ab
8	0.212	0.165	0.325	0.231	0.254	0.255	0.240	a
10	0.202	0.455	0.364	0.213	0.355	0.232	0.303	cd
12	0.485	0.282	0.367	0.439	0.347	0.399	0.387	e
Average over batches	0.291	0.322	0.342	0.301	0.298	0.258		
Group from multicompare one-sided ANOVA analysis	ab	cd	d	bc	bc	a		

[a]RMSEP values are calculated using four tablet replicates randomly chosen from five time points and evaluated with the last time point (all six tablet replicates). Only second spectral replicate and first orientation (up) are used. The calculations are performed 20 times and the RMSEP values are averages of these. The spectral areas 1126-1132 and 1287-1295 nm and three latent variables are used for creating the models.

DOI 10.1002/jps

range of compression forces, such tablets should be included in the calibration set for the improvement of the prediction model for the production samples. Concerning the orientation of the tablet presentation to the spectrometer, it was shown that the spectra from tablets with the score facing upward gave better calibrations than those from tablets facing downward. This may be important if a random tablet orientation setup is required.

However, the largest fraction of the variation between spectra was found when displacing the tablet in the tablet sampler. The S_{TAE} and the RMSEP for different number of spectra included in the calibrations are useful approaches to evaluate the construction of robust quantitative NIR calibrations. This study confirmed that NIT is a very powerful measurement technique for tablet QC and it is only the sampling efficiency that sets the limits of the method for approaching 100% QC. In the presented case, the optimal calibration model for predicting the API concentration had an "RMSEP" of 0.24% (w/w) in the range of 4%–12% (w/w).

ACKNOWLEDGMENTS

The authors wish to thank the Danish Ministry of Science, Technology and Innovation for financial support of a Ph.D. stipendium to Solveig Warnecke through the QbD consortium (www.qbd.dk).

REFERENCES

1. Bush L. 2004. FDA publishes final PAT guidance. Pharm Technol 28:16.
2. Tang P, Puri VM. 2004. Methods for minimizing segregation: A review. Particulate Sci Technol 22:321–337.
3. Council of Europe. 2010. Chaptor 2.9.6. Uniformity of content of single-dose preparations. European Pharmacopoeia 7.0Strasbourg, France: Council of Europe, p.– 266.
4. Council of Europe. 2012. General chapter 2.9.40. Uniformity of dosage units. European Pharmacopoeia 7.4. Strasbourg, France: Council of Europe.
5. Luypaert J, Massart DL, Heyden YV. 2007. Near-infrared spectroscopy applications in pharmaceutical analysis. Talanta 72:865–883.
6. Dyrby M, Engelsen SB, Nørgaard L, Bruhn M, Lundsberg-Nielsen L. 2002. Chemometric quantitation of the active substance (containing C N) in a pharmaceutical tablet using near-infrared (NIR) transmittance and NIR FT-Raman spectra. Appl Spectrosc 56:579–585.
7. Gottfries J, Depui H, Fransson M, Jongeneelen M, Josefson M, Langkilde FW, Witte DT. 1996. Vibrational spectrometry for the assessment of active substance in metoprolol tablets: A comparison between transmission and diffuse reflectance near-infrared spectrometry. J Pharm Biomed Anal 14:1495–1503.
8. Thosar SS, Forbess RA, Ebube NK, Chen YX, Rubinovitz RL, Kemper MS, Reier GE, Wheatley TA, Shukla AJ. 2001. A comparison of reflectance and transmittance near-infrared spectroscopic techniques in determining drug content in intact tablets. Pharm Dev Technol 6:19–29.
9. Laasonen M, Harmia-Pulkkinen T, Simard C, Rasanen M, Vuorela H. 2003. Development and validation of a near-infrared method for the quantitation of caffeine in intact single tablets. Anal Chem 75:754–760.
10. Gy P. 2004. Sampling of discrete materials—A new introduction to the theory of sampling—I. Qualitative approach. Chemometrics Intell Lab Syst 74:7–24.
11. Gy P. 2004. Sampling of discrete materials—II. Quantitative approach-sampling of zero-dimensional objects. Chemometrics Intell Lab Syst 74:25–38.
12. Gy P. 2004. Sampling of discrete materials—III. Quantitative approach-sampling of one-dimensional objects. Chemometrics Intell Lab Syst 74:39–47.
13. Tønning E, Nørgaard L, Engelsen SB, Pedersen L, Esbensen KH. 2006. Protein heterogeneity in wheat lots using single-seed NIT—A theory of sampling (TOS) breakdown of all sampling and analytical errors. Chemometrics Intell Lab Syst 84:142–152.
14. Wold S, Martens H, Wold H. 1983. The multivariate calibration-problem in chemistry solved by the PLS method. Lect Notes Math 973:286–293.
15. Xiang D, Berry J, Buntz S, Gargiulo P, Cheney J, Joshi Y, Wabuyele B, Wu HQ, Hamed M, Hussain AS, Khan MA. 2009. Robust calibration design in the pharmaceutical quantitative measurements with near-infrared (NIR) spectroscopy: Avoiding the chemometric pitfalls. J Pharm Sci 98:1155–1166.
16. Blanco M, Alcala M. 2006. Content uniformity and tablet hardness testing of intact pharmaceutical tablets by near infrared spectroscopy—A contribution to process analytical technologies. Anal Chim Acta 557:353–359.
17. Saeed M, Saner S, Oelichmann J, Keller H, Betz G. 2009. Assessment of diffuse transmission mode in near-infrared quantification—part I: The press effect on low-dose pharmaceutical tablets. J Pharm Sci 98:4877–4886.
18. Shah RB, Tawakkul MA, Khan MA. 2007. Process analytical technology: Chemometric analysis of Raman and near infrared spectroscopic data for predicting physical properties of extended release matrix tablets. J Pharm Sci 96:1356–1365.
19. Cogdill RP, Anderson CA, Drennen JK. 2004. Using NIR spectroscopy as an integrated PAT tool. Spectroscopy 19:104–109.
20. Blanco M, Coello J, Iturriaga H, Maspoch S, Pou N. 2000. Development and validation of a near infrared method for the analytical control of a pharmaceutical preparation in three steps of the manufacturing process. Fresenius J Anal Chem 368:534–539.
21. Rosa SS, Barata PA, Martins JM, Menezes JC. 2008. Near-infrared reflectance spectroscopy as a process analytical technology tool in *Ginkgo biloba* extract qualification. J Pharm Biomed Anal 47:320–327.
22. Han SM, Faulkner PG. 1995. Determination of SB 216469-S during tablet production using near-infrared reflectance spectroscopy. Pharm Res (New York) 12:S15.
23. Blanco M, Coello J, Iturriaga H, Maspoch S, delaPezuela C. 1996. Quantitation of the active compound and major excipients in a pharmaceutical formulation by near infrared diffuse reflectance spectroscopy with fibre optical probe. Anal Chim Acta 333:147–156.
24. Dhanoa MS, Lister SJ, Sanderson R, Barnes RJ. 1994. The link between multiplicative scatter correction (MSC) and standard normal variate (SNV) transformations of NIR spectra. J Near Infrared Spectrosc 2:43–47.
25. Esbensen KH, Guyot D, Westad F, Houmøller LP. 2002. Multivariate data analysis, in practice, an introduction to multivariate data analysis and experimental design. 5th ed. p 19–74. Oslo, Norway, CamoPress AS
26. Nørgaard L, Saudland A, Wagner J, Nielsen JP, Munck L, Engelsen SB. 2000. Interval partial least-squares regression (iPLS): A comparative chemometric study with an

example from near-infrared spectroscopy. Appl Spectrosc 54:413–419.
27. Hochberg YA, Tamhane C. 1987. Multiple comparison procedures. Hoboken, New Jersey: John Wiley & Sons.
28. Rowe RC, Sheskey PJ, Quinn ME. 2009. Handbook of pharmaceutical excipients. 6th ed. London: PhP Pharmaceutical Press.
29. Luukkonen P, Rantanen J, Makela K, Rasanen E, Tenhunen J, Yliruusi J. 2001. Characterization of wet massing behavior of silicified microcrystalline cellulose and alpha-lactose monohydrate using near-infrared spectroscopy. Pharm Dev Technol 6:1–9.
30. Rinnan A, van den Berg F, Engelsen SB. 2009. Review of the most common pre-processing techniques for near-infrared spectra. TrAC Trends Anal Chem 28:1201–1222.
31. Martens H, Nielsen JP, Engelsen SB. 2003. Light scattering and light absorbance separated by extended multiplicative signal correction. Application to near-infrared transmission analysis of powder mixtures. Anal Chem 75:394–404.

Table S1: Overview of PLS models for the different selection of spectra evaluated against all the spectra (RMSEP all) and all the spectra from hardness H_{medium} (RMSEP H_{medium}). Spectra are preprocessed with SNV and mean centered prior to selection of spectral areas 1126-1132 and 1295-1287 nm. Three latent variables (LV) are used for all models. Recommendations for orientation and minimum number of spectra are marked in grey.

Calibration no	Description	No of spectra	RMSECV % w/w	RMSEP all % w/w	RMSEP H_{medium} % w/w	RMSEP H_{low} % w/w	RMSEP H_{high} % w/w
1	All spectra	2160	0.251		0.242		
2	All spectra from time point 1,2,5,6	1440	0.247	0.247		0.267	0.246
3	Only 1st replicate	720	0.251	0.251	0.248		
4	Only 2nd replicate	720	0.251	0.248	0.244		
5	Only 3rd replicate	720	0.261	0.253	0.245		
6	2nd rep, 1st orientation (up)	180	0.238	0.259	0.250		
7	2nd rep, 2nd orientation (up)	180	0.240	0.267	0.256		
8	2nd rep, 3rd orientation (down)	180	0.279	0.262	0.251		
9	2nd rep, 4th orientation (down)	180	0.291	0.261	0.254		
10-14	Mix directions (up and down) average of 4 calculations	180	0.253 0.249-0.257	0.254 0.250-0.258	0.249 0.247-0.252		
15-20	2nd rep, 1st orientation, 5 tablet replicates, average of 6 calculations	150	0.238 0.222-0.251	0.260 0.253-0.271	0.251 0.247-0.258		
21-26	2nd rep, 1st orientation, 4 tablet replicates, average of 6 calculations	120	0.239 0.208-0.256	0.263 0.250-0.290	0.254 0.244-0.272		
27-32	2nd rep, 1st orientation, 3 tablet replicates, average of 6 calculations	90	0.238 0.212-0.264	0.266 0.251-0.293	0.256 0.248-0.275		
33-38	2nd rep, 1st orientation, 2 tablet replicates, average of 6 calculations	60	0.243 0.205-0.286	0.279 0.255-0.301	0.267 0.249-0.287		
39-44	2nd rep, 1st orientation, 1 tablet replicate, average of 6 calculations	30	0.253 0.163-0.321	0.297 0.260-0.311	0.284 0.250-0.303		
45	2nd rep, 1st	150	0.236	0.264	0.253		

	orientation, 6 tab rep, time point 1,2,3,5,6						
46	2nd rep, 1st orientation, 6 tab rep, time point 1,2,4,5,6	150	0.230	0.261	0.252		
47	2nd rep, 1st orientation, 6 tab rep, time point 1,2,5,6	120	0.227	0.266	0.256	0.266	0.258
48-51	2nd rep, 1st orientation, 3 time points, average of 4 calculations	90	0.245 0.212-0.254	0.270 0.255-0.287	0.258 0.249-0.270		
52-57	2nd rep, 1st orientation, 2 time points, average of 6 calculations	60	0.244 0.198-0.284	0.277 0.255-0.319	0.264 0.247-0.267		
58	2nd rep, 1st orientation, 6 tab rep, time point 1	30	0.284	0.338	0.306		
59	2nd rep, 1st orientation, 6 tab rep, time point 2	30	0.272	0.313	0.291		
60	2nd rep, 1st orientation, 6 tab rep, time point 3	30	0.245	0.306	0.293		
61	2nd rep, 1st orientation, 6 tab rep, time point 4	30	0.256	0.279	0.271		
62	2nd rep, 1st orientation, 6 tab rep, time point 5	30	0.307	0.277	0.264		
63	2nd rep, 1st orientation, 6 tab rep, time point 6	30	0.187	0.259	0.252		

Table S2: Standard deviation of the total analytical error s_{TAE} at a given API concentration and time points ($\sqrt{RMSEP}/a_L^2 \cdot N$) times 10^3.[1]

API (% w/w)	Time point 1 85 N	Time point 2 85 N	Time point 3 70 N	Time point 4 100 N	Time point 5 85 N	Time point 6 85 N	Average of time points
4	8.25	7.12	8.31	9.72	7.88	5.80	7.85
6	3.65	6.84	5.18	3.75	3.48	2.76	4.28
8	2.63	2.05	4.03	2.87	3.16	3.17	2.99
10	2.01	4.54	3.64	2.13	3.54	2.32	3.03
12	4.03	2.34	3.05	3.64	2.88	3.31	3.21
Average over batches	4.11	4.58	4.84	4.42	4.19	3.47	

[1] a_L is the average of 36 samples from HPLC for each batch. RMSEP is calculated using four randomly chosen tablet replicates from five time points and evaluated with the last time point (all six tablet replicates). Only second spectral replicates and first orientation (up) is used. The calculations are preformed 20 times and the RMSEP is average of this. The spectral areas 1126-1132 and 1295-1287 nm and three latent variables are used for creating the models. N is 100 samples.

[1] a_L is the average of 36 samples from HPLC for each batch. RMSEP is calculated using four randomly chosen tablet replicates from five time points and evaluated with the last time point (all six tablet replicates). Only second spectral replicates and first orientation (up) is used. The calculations are preformed 20 times and the RMSEP is average of this. The spectral areas 1126-1132 and 1295-1287 nm and three latent variables are used for creating the models. N is 100 samples.

Paper II

Using interval-PLS to eliminate spectral moisture interference from a quantitative near infrared calibration model on pharmaceutical tablets

Using interval-PLS to eliminate spectral moisture interference from a quantitative near infrared calibration model on pharmaceutical tablets

Solveig Warnecke[a], *Åsmund Rinnan*[a]*, *Morten Allesø*[b], *Søren B. Engelsen*[a].

[a]Department of Food Science, Faculty of Science, University of Copenhagen, Rolighedsvej 30, DK-1958 Frederiksberg C, Denmark. *aar@food.ku.dk, +45 35333542;

[b]Biologics and Pharmaceutical Science, H. Lundbeck A/S, Ottiliavej 9, DK-2500 Valby, Denmark

Abstract

Near infrared spectroscopy is a technique commonly applied to pharmaceutical tablets to quantify the active pharmaceutical ingredient (API). During its life-time the tablet product may absorb water, which can result in poor performance of the initial calibration model. However, through variable subset reduction, it is possible to avoid the spectral interference from water uptake in the tablets. Calibration models based on samples with lower water uptake, were predicted on samples with higher water uptake. Reducing the wavelength range to only the range for which the API absorb resulted in a prediction error of 0.236 % (w/w) to be compared with the prediction error of 0.332 % (w/w) for the full spectral range.

Keywords: Near-infrared spectroscopy, content uniformity, moisture sorption, tablet, multivariate analysis, chemometrics

Introduction

Determination of the moisture content in pharmaceutical powders, granulates, and tablets are well established near infrared spectroscopy (NIR) applications. This is due to the strong NIR absorption of water which has specific bands centered around 1950 nm (OH stretching and HOH bending combination), 1450 nm (1st overtone OH stretching), 1200 nm (1st overtone OH stretching + 1st overtone HOH bending) and at 970 nm (2nd overtone OH stretching). Many studies have demonstrated the usefulness of NIR for determining the moisture content of a granulate for tablet manufacturing[1-5]. Likewise, numerous studies describe the development of NIR and near infrared transmission (NIT)[6-14] models for quantification of active pharmaceutical ingredient (API) in either intermediate or final product (e.g. tablets)[1]. In order to implicitly deal with water absorption, Gottfries et al.[6] added tablets that were stored under humid conditions to make the calibration more robust to variations in humidity.

In this study it is proposed to instead use variable subset selection in the form of interval partial least square (iPLS)[15] to reduce the spectral interference information. In this study the tablet API concentration were determined by NIT using high performance liquid

chromatography (HPLC) as a reference method. The measurements of the tablets were performed over 15 different days of analysis which covered a total period of two months. Due to the inclusion of hygroscopic microcrystalline cellulose in the formulation, this prolonged analysis time had a significant effect on the moisture uptake of the tablets. This short communication demonstrates how variable subset selection can eliminate the spectral interferences from water uptake and create a more parsimonious calibration model with improved predictive performance for API quantification.

Materials and methods

Tablet production

Escitalopram tablets containing 10 mg API (8% w/w) are shaped as ellipsoids (5.5 mm x 8.0 mm). The tablets have a score and letters "E" and "L" embossing on one face of the tablet.

The five blends contained different amounts of API (4, 6, 8, 10, and 12 % w/w) corresponding to 50-150 % of the target concentration of 10 mg (free base). The change in API concentration was compensated for by changing the amount of filler, silicified microcrystalline cellulose, SMCC (Prosolv, JRS Pharma, Germany) accordingly. For details of the tablet production see Warnecke et al.[16]. During the production the compression force was varied to achieve tablets at three different tablet hardness levels: H_{medium}, H_{low}, and H_{high}; approximately 85 N, 70 N and 100 N, respectively. Tablets were taken out a six different time points during production. From each time point six tablets were measured, which gave 36 tablets from each API concentration level (4, 6, 8, 10, and 12 % w/w), and 180 tablets in total.

Near Infrared analysis

NIT spectra were acquired in the spectral range from 4000 to 14,000 cm^{-1} (700-2500 nm), with a resolution of 8 cm^{-1} and by averaging over 64 scans per sample spectrum. The instrument used was an ABB Bomem FT-NIR MB-160 (ABB Bomem Inc., Canada) equipped with a Tablet Samplir (carousel) and a custom-made tray for 125 mg escitalopram tablets. The light source was situated below the sample with the detector on the upper side. Reference spectra were recorded using the internal ceramic standard (Spectralon 99 %) and used to convert the tablet spectra into absorbance units. Each tablet was measured in three spectral replicates recorded from the center of the tablet with four orientations of the tablet. Measurements of tablets in position 1 and 2 had the scored line facing upwards, and 3 and 4 the scored line was facing downwards. The samples were randomly presented to the autosampler, and all the measurements were performed on 15 days of analysis (over 60 days). A total of 2160 spectra were obtained. After the spectroscopic measurements, all the tablets were analyzed for API concentration by HPLC using an in-house method. The HPLC determined content was corrected for the tablet mass and reported in % w/w units.

Data treatment

All data processing was performed in Matlab 7.14.0 (Mathworks™, USA) using PLS-toolbox (Eigenvector, USA). All NIT spectra were pre-processed using the standard normal variate (SNV)[17] method in order to minimize effects of scatter caused by density changes and to minimize artifacts from small changes in path length caused by small changes in the thickness of the tablets.

Principal component analysis (PCA) was used to investigate the variation in the data. Interval partial least squares regression (iPLS[15]) was used for variable selection. iPLS is an extension to PLS that creates local PLS models on subintervals of the full-spectrum region, thereby focusing on important spectral regions while removing interferences from other regions. Local interval models are compared to the full-spectrum global model mainly by the root-mean-squared-error-of-cross-validation (RMSECV). The iPLS was employed in the simple forward stepwise selection mode, in which all intervals are tested individually and the one with the lowest error is chosen. Then the performance of all the remaining intervals are examined in combination with the selected interval, and intervals are added until the RMSECV increases by introduction of new intervals[15].

Result and discussion

Figure 1a shows the raw NIT spectra of all samples from 952 to 1350 nm, while Figure 1b shows the reflectance NIR spectra of pure constituents, escitalopram oxalate and silicified microcrystalline cellulose (SMCC – Prosolv). Figure 1c shows the SNV corrected NIT spectra from tablets of five API concentrations. The SNV pre-processing clearly reduces the total variance of the spectral data set while enhancing the API specific peak at 1132 nm, corresponding to the second overtone of aromatic C-H stretching[18]. Figure 1d shows the iPLS selection of wavelengths for a calibration on escitalopram. It is observed that the spectral region for the API specific peak is chosen as the one providing the lowest RMSECV in the iPLS.

Figure 2a shows the score plot from the PCA on NIT on escitalopram tablets colored according to the API concentration. The same score plot is shown in Figure 2b, but colored according to the day of analysis. The systematic trend in the scores reveal an uptake of water by the hygroscopic SMCC[19]. This interpretation fits well with the loading plot (Figure 2c) where the first loading (blue line) has a water absorption peak at 950-1100 nm, corresponding to the 2nd overtone of the O-H stretching of water, and a characteristic 1st overtone combination peak at around 1200 nm. The measurements were carried out over the course of two months (15 days of analysis), and the tablets were stored at room temperature in NIR vials.

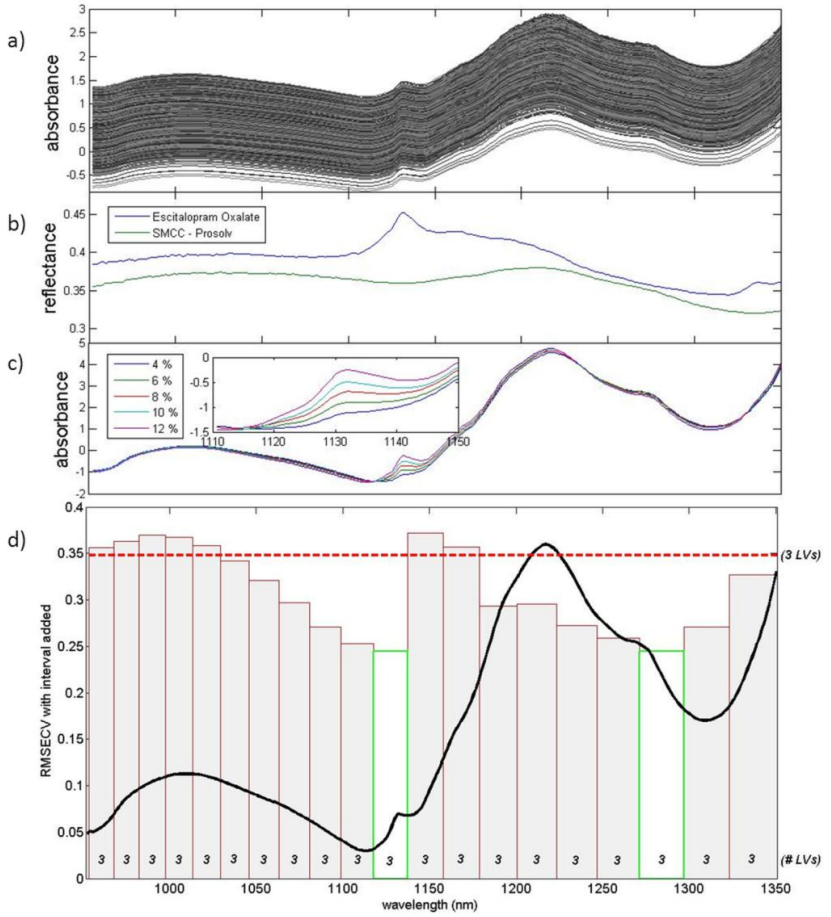

Figure 1: a) Raw NIT spectra of all samples from 952 to 1350 nm. b) Reflectance NIR spectra of pure constituents, escitalopram oxalate and silicified microcrystalline cellulose (SMCC – Prosolv) c) SNV corrected NIT spectra from tablets of five loads of API. The insert shows a magnified wavelength region specific to the API. d) : iPLS on NIT spectra correlated to escitalopram. The red line shows the RMSECV for the global model including all wavelengths. Each bar shows the RMSECV for the model only including the particular area. The two green bars (1118-1137 and 1272-1296 nm) are the variable areas chosen as they can create models with the lowest RMSECV.

In order to investigate how the water uptake will affect a calibration model, partial least squares regression (PLS) models of sample spectra from day 1-9 of analysis (taken within the first 50 days) were calculated and (test set) validated against the spectra from day 10-15 of analysis (taken within the last 10 days).

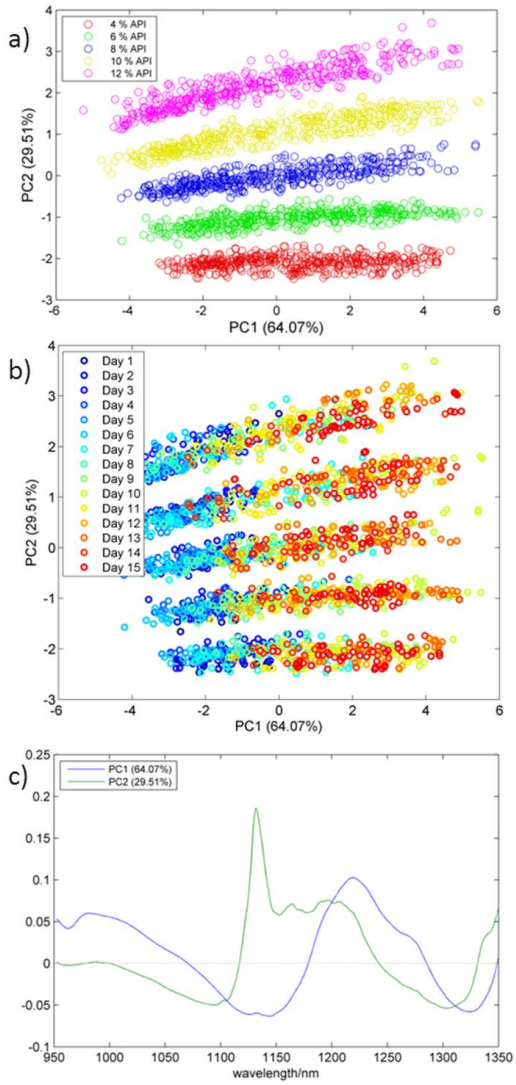

Figure 2: a) PCA score plot of NIT spectra of escitalopram colored according to API level b) PCA score plot of NIT spectra of escitalopram colored according to day of analysis. b) Corresponding PCA loading plot.

Figure 3a shows the PLS calibration model using three latent variables (LVs) of the full spectral range (952-1350 nm) model for the calibration set (day 1-9) and the test set (day 10-15). The resulting root mean square error of cross-validation (RMSECV) is 0.308 % (w/w) and the corresponding root mean squares error of prediction (RMSEP) is 0.332 % (w/w). Figure 3b shows a three LVs PLS model on the same calibration and test set, but on a reduced spectral range (1118-1137 and 1272-1296 nm). Using the optimal spectral range selected by iPLS, the RMSECV is reduced to 0.244 % (w/w) and the RMSEP to 0.236 % (w/w), which are close to the calibration result obtained when using all the spectra on a similar wavelength range (RMSECV 0.251 % (w/w))[16]. These results demonstrate that by

spectral subset reduction, the model for the API concentrations is not only improving, but it also becomes unaffected by the interfering water uptake.

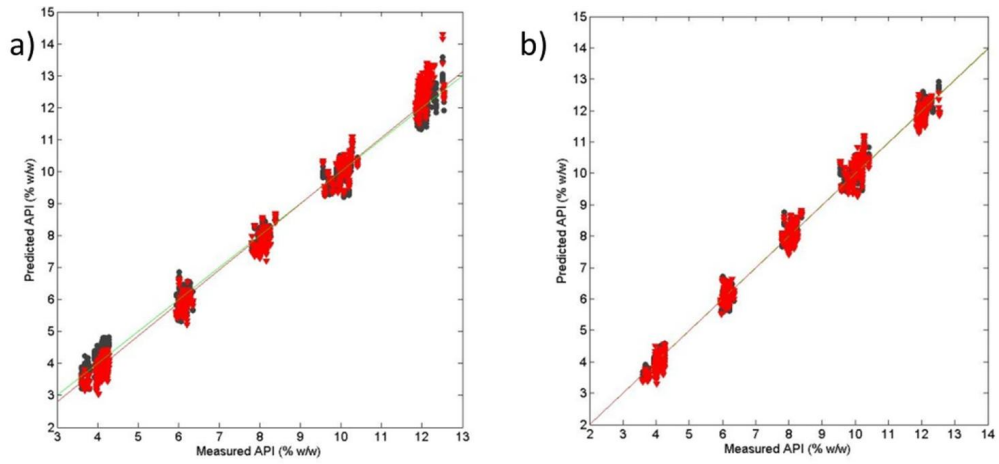

Figure 3: a) PLS calibrations on escitalopram tablets divided into calibration set (black), day 1-9 and validation set (red), day 10-15. a) Spectral range used from 952-1350 nm, RMSECV is 0.308 % (w/w) and RMSEP is 0.332 % (w/w). b) Calibration on spectral ranges 1118-1137and 1272-1296 nm, RMSECV is 0.244 % (w/w) and RMSEP is 0.236 % (w/w). There are used three latent variables and SNV and mean centering of the spectra.

Conclusion

Through variable subset reduction it is possible to avoid the spectral interference from water uptake in pharmaceutical tablets during storage. Calibrations based on samples with lower water uptake were predicted on samples with higher water uptake. By reducing the wavelength range to the spectral region that only include the API resulted in a RMSEP of 0.236 % (w/w) which have to be compared to a RMSEP of 0.332 % (w/w) for the full spectral range.

Acknowledgment

The authors wish to thank the Danish Ministry of Science, Technology and Innovation for financial support of a PhD stipendium to Solveig Warnecke through the QbD consortium (www.qbd.dk).

Reference List

1. Han SM, Faulkner PG 1995. Determination of SB 216469-S during tablet production using near-infrared reflectance spectroscopy. Pharmaceutical Research (New York) 12:S15.
2. Frake P, Greenhalgh D, Grierson SM, Hempenstall JM, Rudd DR 1997. Process control and end-point determination of a fluid bed granulation by application of near infra-red spectroscopy. International Journal of Pharmaceutics 151:75-80.
3. Rantanen J, Lehtola S, Ramet P, Mannermaa JP, Yliruusi J 1998. On-line monitoring of moisture content in an instrumented fluidized bed granulator with a multi-channel NIR moisture sensor. Powder Technology 99:163-170.
4. Green RL, Thurau G, Pixley NC, Mateos A, Reed RA, Higgins JP 2005. In-line monitoring of moisture content in fluid bed dryers using near-IR spectroscopy with consideration of sampling effects on method accuracy. Analytical Chemistry 77:4515-4522.
5. Burgbacher J, Wiss J 2008. Industrial applications of online monitoring of drying processes of drug substances using NIR. Organic Process Research & Development 12:235-242.
6. Gottfries J, Depui H, Fransson M, Jongeneelen M, Josefson M, Langkilde FW, Witte DT 1996. Vibrational spectrometry for the assessment of active substance in metoprolol tablets: A comparison between transmission and diffuse reflectance near-infrared spectrometry. Journal of Pharmaceutical and Biomedical Analysis 14:1495-1503.
7. Blanco M, Coello J, Iturriaga H, Maspoch S, Pou N 2000. Development and validation of a near infrared method for the analytical control of a pharmaceutical preparation in three steps of the manufacturing process. Fresenius Journal of Analytical Chemistry 368:534-539.
8. Thosar SS, Forbess RA, Ebube NK, Chen YX, Rubinovitz RL, Kemper MS, Reier GE, Wheatley TA, Shukla AJ 2001. A comparison of reflectance and transmittance near-infrared spectroscopic techniques in determining drug content in intact tablets. Pharmaceutical Development and Technology 6:19-29.
9. Laasonen M, Harmia-Pulkkinen T, Simard C, Rasanen M, Vuorela H 2003. Development and validation of a near-infrared method for the quantitation of caffeine in intact single tablets. Analytical Chemistry 75:754-760.
10. Cogdill RP, Anderson CA, Drennen JK 2004. Using NIR spectroscopy as an integrated PAT tool. Spectroscopy 19:104-109.
11. Blanco M, Alcala M 2006. Content uniformity and tablet hardness testing of intact pharmaceutical tablets by near infrared spectroscopy - A contribution to process analytical technologies. Analytica Chimica Acta 557:353-359.
12. Shah RB, Tawakkul MA, Khan MA 2007. Process analytical technology: Chemometric analysis of Raman and near infra-red spectroscopic data for predicting physical properties of extended release matrix tablets. Journal of Pharmaceutical Sciences 96:1356-1365.
13. Saeed M, Saner S, Oelichmann J, Keller H, Betz G 2009. Assessment of Diffuse Transmission Mode in Near-Infrared Quantification-Part I: The Press Effect on Low-Dose Pharmaceutical Tablets. Journal of Pharmaceutical Sciences 98:4877-4886.
14. Xiang D, Berry J, Buntz S, Gargiulo P, Cheney J, Joshi Y, Wabuyele B, Wu HQ, Hamed M, Hussain AS, Khan MA 2009. Robust Calibration Design in the Pharmaceutical Quantitative Measurements with Near-Infrared (NIR) Spectroscopy: Avoiding the Chemometric Pitfalls. Journal of Pharmaceutical Sciences 98:1155-1166.
15. Nørgaard L, Saudland A, Wagner J, Nielsen JP, Munck L, Engelsen SB 2000. Interval partial least-squares regression (iPLS): A comparative chemometric study with an example from near-infrared spectroscopy. Applied Spectroscopy 54:413-419.
16. Warnecke S, Rinnan Å, Allesø M, Engelsen SB 2013. Measurement of active content in escitalopram tablets by a near-infrared transmission spectroscopy model that encompasses batch variability. Journal of Pharmaceutical Sciences1268-1280.
17. Dhanoa MS, Lister SJ, Sanderson R, Barnes RJ 1994. The link between Multiplicative Scatter Correction (MSC) and Standard Normal Variate (SNV) transformations of NIR spectra. Journal of Near Infrared Spectroscopy 2:43-47.
18. Dyrby M, Engelsen SB, Norgaard L, Bruhn M, Lundsberg-Nielsen L 2002. Chemometric quantitation of the active substance (containing C N) in a pharmaceutical tablet using near-infrared (NIR) transmittance and NIR FT-Raman spectra. Applied Spectroscopy 56:579-585.
19. Rowe RC, Sheskey PJ, Quinn ME 2009. Handbook of pharmaceutical excipients , 6th ed. London : PhP Pharmaceutical Press .

Paper III

Quantifying crystalline α-lactose monohydrate in amorphous lactose using Terahertz Time Domain Spectroscopy and Near Infrared Spectroscop

Quantifying crystalline α-lactose monohydrate in amorphous lactose using Terahertz Time Domain Spectroscopy and Near Infrared Spectroscopy

Solveig Warnecke[a], Jian X. Wu[b], Åsmund Rinnan[a], Morten Allesø[c], Frans van den Berg[a], Peter Uhd Jepsen[d], Søren Balling Engelsen[a].*

[a]Department of Food Science, Faculty of Science, University of Copenhagen, Rolighedsvej 30, DK-1958 Frederiksberg C, Denmark

[b]Department of Pharmacy, Faculty of Health and Medical Sciences, University of Copenhagen, Universitetsparken 2, DK-2100 København Ø, Denmark

[c]Biologics and Pharmaceutical Science, H. Lundbeck A/S, Ottiliavej 9, DK-2500 Valby, Denmark

[d]DTU Fotonik, Department of Photonics Engineering, Technical University of Denmark, DK-2800 Kongens Lyngby, Denmark

*) corresponding author, aar@food.ku.dk, +45 35333542.

Abstract

Spray-dried lactose consists of an amorphous component (10-20%) as well as the crystalline monohydrate form [1]. It is commonly used as a diluent in direct compression, mainly because of its better flow characteristics compared to pure crystalline lactose. The amorphous form is metastable and can relative easily crystallize, which will affect the functionality of the pharmaceutical product. It is therefore of interest to establish methods for non-invasive and rapid assessment of the level of crystallinity in a pharmaceutical formulation. In this study, two spectroscopic methods, near infrared (NIR) spectroscopy and terahertz time domain spectroscopy (THz-TDS), are compared for their ability to determine low levels of crystalline lactose in a mixture. The aim was to find the limit of detection and limit of quantification for the two techniques. Partial least squares (PLS) regression models were developed and the root-mean-square-error-of-cross-validation (RMSECV) for the models with full concentration range were found to be 2.91 % (w/w) and 0.87 % (w/w) for THz-TDS and NIR, respectively. Calibrations developed on samples containing 0-10 % (w/w) crystalline material resulted in RMSECVs of 0.30 % (w/w) and 0.20 % (w/w) for THz-TDS and NIR, respectively, while the limits of detection were 0.80 % (w/w) and 0.43 % (w/w), respectively. Both instrumental techniques are thus able to quantify the content of crystalline lactose in a mixture. To select one method over the other in an industrial quality assurance setting, further includes other aspects - such as sample handling, sample size, outlier information, instrument stability, etc. In all these aspects, NIR spectroscopy currently performs better than THz-TDS.

Keywords: Terahertz time domain spectroscopy; near infrared spectroscopy; lactose; crystalline; amorphous; limit of detection

Abbreviations:
API: active pharmaceutical ingredient
iPLS: interval partial least squares regression
LOD: limit of detection
LOQ: limit of quantification
LV: latent variable
NIR: near-infrared spectroscopy
PC: principle component
PCA: principal component analysis
PE: polyethylene
PLS: partial least squares regression
QbD: quality by design
RMSECV: root-mean-square-error-of-cross-validation
SEM: scanning electron microscopy
SNV: standard normal variate
THz: terahertz
THz-TDS: terahertz time domain spectroscopy
XRPD: x-ray powder diffraction

1. Introduction

It has been shown that about 80 % of active pharmaceutical ingredients (APIs) have polymorphs [2]. The arrangement of the molecules in amorphous or different crystalline forms can impact the dissolution rate, solubility, bioavailability and manufacturability of pharmaceuticals [3]. An amorphous form may have short-range order, but unlike crystalline forms, the amorphous state has no long-range order of molecular packing [4]. Many APIs are poorly water soluble, which has increased the interest in formulating amorphous compounds and also amorphous binary mixtures [4; 5]. The amorphous form typically has a much higher apparent solubility and enhanced dissolution, due to the fact that it does not need to be released from a firm (typically) hydrogen-bonded crystal lattice before solubilization. Presence of smaller seeds of crystalline impurities and water can initiate and propagate a phase transition process, and over longer storage times change the form of the product which, in turn, will impact the stability, solubility, or other functionalities of the pharmaceutical product [6]. This highlights the need for analytical method development in order to detect and quantify the small amount of crystalline material.

Characterization of the amorphous and crystalline states can be accomplished via several different instrumental techniques that observe changes in physical properties such as density, viscosity, or heat capacity. The current gold standard to study long range molecular order is X-ray diffraction. In X-ray powder diffraction (XRPD) lack of long-range order will be observed as a halo compared to the sharp crystalline reflections observed for crystalline forms [7]. The limit of quantification for crystalline structure in XRPD is approximately 5 % [7; 8]. Fix and Steffens [9] developed an improved XRPD method which is able to quantify amor-

phous and crystalline lactose in binary mixtures with a limit of detection (LOD) at the 0.5 % (w/w) level. Variations in particle shape and sample presentation is known to affect the XRPD pattern through preferred orientation. This effect is seen as random changes in diffraction intensities which impairs its use for quantification [10], an effect that can be partially eliminated by spinning the sample. Another well-established method for characterization of amorphous powders is differential scanning calorimetry (DSC) [7], which measures the presence of a glass transition temperature (T_g). Fix and Steffens [9] found that DSC did not show linearity with the crystallinity of lactose in binary mixtures of amorphous and crystalline lactose, and concluded that DSC was not capable of detecting crystalline lactose below 10 %. Other studies have demonstrated that near infrared spectroscopy (NIR) and Raman spectroscopy are able to quantitatively differentiate between amorphous and crystalline pharmaceutical ingredients [8; 11-16].

Terahertz spectroscopy [17] has, since it is measuring the crystal lattice vibrations [18], earlier shown good results in detecting crystalline materials [19-24]. Zeitler et al. [24] found that terahertz spectroscopy could easily detect mixtures of the different sulfathiazole polymorphs, which was not possible with mid-IR or NIR spectroscopy. The electromagnetic radiation used in terahertz and NIR spectroscopy is orders of magnitude lower in energy and intensity as compared to Raman spectroscopy, which has demonstrated heating effects of the sample during measurement [25; 26]. As the photon energy of terahertz radiation is approximately a million times smaller than that of X-ray radiation, and a thousand times smaller than that of UV light, no photochemical effects are expected in the terahertz region at the power levels relevant for terahertz spectroscopic investigations [23]. The corresponding numbers for NIR spectroscopy are approximately 100,000 times lower that X-ray radiation and 10-100 times lower than UV light. This makes it a promising technique for fast screening and characterization of API solid forms during pharmaceutical development and potentially during commercial manufacturing as a quality control tool.

Only a few terahertz spectroscopy studies have discussed the LOD and limit of quantification (LOQ) of different polymorphic API forms in mixtures. Strachan et al. [21] investigated carbamazepine form I in 0-10 % (w/w) mixtures with form III, and found an LOD of 1.2 % (w/w) and LOQ of 3.7 % (w/w). For enalapril acetate form I in a 0-10 % mixture with form II they found an LOD of 0.69 % (w/w) and LOQ of 2.1 % (w/w). For quantification of 0-100 % (w/w) binary mixtures of crystalline and amorphous indomethacin, the same authors [21] found an LOD of 1.1 % (w/w) and LOQ of 3.2 % (w/w). For crystalline fenoprofen calcium 0-100 % (w/w) the LOD was 2.7 % (w/w) and LOQ was 8.2 % (w/w).

In terahertz transmission spectroscopic experiments, it is often desirable to keep the amount of sample material to a minimum in order to maximize the spectral bandwidth of the instrument, which, without dilution, results in a sample thickness down to 0.2 mm [27]. This can cause multiple reflections from the pellet-air interfaces, effectively causing the signal reverberation in the sample – the so-called etalon or Fabry-Perot effect. In the time domain, this is seen as echoes of the main peak [27-29], and the effect manifests itself as oscillations in the measured transmission spectra. For this reason, sample dilution is often required in order not to exceed the limits of the dynamic range of the instrument [27; 30]. High-density polyethylene (PE) fine powder is frequently added for this purpose in concentrations ranging from

25-96 % (w/w) of the total sample amount [19-21; 31; 32]. Ultrahigh molecular weight PE is a good binder and is virtually transparent and with a nearly frequency independent refraction index of 1.53 in the terahertz region [33]. When adding PE to the sample, the dynamic range of the spectrometer can be fully exploited, while thicker samples will result in a larger separation of the time domain of etalon echoes, which are then easy to remove by standard time window procedures [27; 28]. The drawback of adding PE is the need of sample preparation, making the analytical method less applicable for in-line process monitoring. Wu et al. [32] reported that when preparing a sample disk for analysis, drying time, composition, and particle size could influence the intensities and peak positions of the terahertz transmission spectra. Additionally, the authors found that the component concentration in the disks affected the terahertz spectra. For theophylline and lactose higher concentrations gave more intense peaks, but also a higher spectral baseline shift, which was probably due to increased scattering of the THz radiation because of the finite size of the particles. The concentration levels of the disk were 4-12 % (w/w), and the measurements were done on a modified FT-IR interferometer with a range of 50-700 cm^{-1} (1.5-21 THz), which is slightly higher than normally used in terahertz experiments and well into the infrared region.

In the present study, lactose monohydrate (the crystalline form of α-lactose) was selected as a model compound in binary amorphous-crystalline sample mixtures. Samples were purposely not diluted with PE in order to simulate the measurement performance in a production environment. The aim of this study was to estimate LOD and LOQ for terahertz time domain spectroscopy (THz-TDS) for crystalline lactose in a compact pellet. The omnipresent PAT spectroscopic technique NIR spectroscopy [34] is used for comparison.

2. Materials and methods

2.1 Sample preparation

α-Lactose monohydrate (Pharmatose 450M) was purchased from DFE pharma (Goch, Germany). Lactose monohydrate was dissolved in Milli-Q water ($0.20 g \cdot ml^{-1}$). The solution was spray dried using a Büchi B-290 spray dryer (Büchi Labortechnik AG, Postfach, Switzerland) using the following process parameters: atomization gas flow and drying air flow rate 667 $L \cdot h^{-1}$, inlet temperature 175°C, outlet temperature 85-92 °C and a feed rate of 5 $ml \cdot min^{-1}$. In order to minimize the recrystallization of the amorphous lactose, the samples were stored at 5 °C immediately after spray drying. Prior to spectroscopic measurements the samples were weighed and gently mixed with mortar and pestle using the geometric dilution principle. A total of 21 binary samples – 2.5 g of each - with the following % (w/w) lactose monohydrate were produced: 0, 0.5, 1, 2, 5, 7, 10, 20, 30, 40, 50, 60, 70, 80, 90, 93, 95, 97, 99, 99.5 and 100 % (w/w). The samples from 0.5-7 % (w/w) and 93-99.5 % (w/w) were produced in duplicates.

2.3 Terahertz spectroscopy

From each of the powder mixtures a compact pellet with 0.25 g total mass was prepared by compressing with 2 tons of force in a hydraulic press (Atlas, Specac Inc., Swedesboro, New Jersey) between two disks of Teflon (20 mm diameter). The pellet and the Teflon blocks were transferred to a sample holder and analyzed in transmission mode using the Terahertz instrument T-Ray^{TM} 4000 THz-TDS System (Picometrix, Ann Arbor, Michigan, USA) interfaced with the T-REX software (ver. 4.5). Each measurement was acquired as an average of 10.000 scans (total recording time of 100 seconds) and each sample was analyzed in triplicate. Reference waveforms were obtained with the sample holder including the Teflon blocks but no sample material. THz waveforms were smoothed before Fourier transformation. Subsequently, the ratio between the sample and the reference spectra was converted into absorbance units and used for further data analysis.

2.4 NIR spectroscopy

The powder mixtures were filled into a glass vial and NIR reflectance spectra were acquired using an ABB Bomem FT-NIR MB-160 (ABB Bomem Inc., Montreal, Canada, GRAMS Light software) with 8 cm^{-1} resolution. Each spectrum was recorded as the average of 64 scans in the range 4,000-10,000 cm^{-1} (1,000-2,500 nm, 121-303 THz). The spectra were measured in stationary reflectance mode through the bottom of the glass vials. The powder mixture inside the glass vials was gently mixed between measurements. Reference spectra were recorded using a standard material (Spectralon 99%, Lapsphere Inc., North Sutton, New Hampshire) and used to convert the tablet spectra into absorbance units.

2.5 X-Ray powder diffraction

X-ray powder diffraction measurements were carried out on a PANalytical X'Pert PRO MPD system (PW3040/60, Philips, The Netherlands) equipped with a PIXcel detector using Cu Kα radiation with $\lambda = 1.542$Å (45kV and 40mA) and automatic divergence slit. Samples were prepared on a zero background aluminum wafer and scanned from 5° to 40° 2θ with a step size of 0.026° and scanning speed of 0.067° per second.

2.6 Scanning electron microscopy

The particle morphology and size were analyzed by Scanning Electron Microscopy (SEM; XL30, FEI, Hillsboro, Oregon) and Helos Particle Size Analyzer (H0793, Sympatec, Clausthal, Germany) equipped with Aspiros and Vibri feeders and using Windox 5 software.

2.7 Data treatment

All data processing was performed in Matlab 7.14.0 (Mathworks^{TM}, Natick, Massachusetts) using the PLS_Toolbox 6.7.1 (Eigenvector, Wenatchee, Washington). All spectra were pre-processed with standard normal variate correction (SNV) [35] or when explicitly mentioned first or second derivatives (Savitzky-Golay) in order to minimize effects of scatter, minor differences in compact thickness and baseline drift [36].

Principal Component Analysis (PCA) [37] was applied to explore the main variations in both the NIR and terahertz spectral datasets. Partial Least Squares (PLS) regression [38] was performed on NIR and terahertz spectral datasets using the crystalline concentrations (% w/w) as reference. Variable selection through application of interval PLS (iPLS) [39] was used to identify the spectral ranges that contain the most information about the crystalline concentration. The complexity of each model was estimated by finding the minimum or breakpoint in the root-mean-square-error of cross validation (RMSECV) curve. For cross validation the samples were divided into three groups. The samples were ranked after concentration level and every third sample was taken out, so replicates were left out at the same time, except for the pure amorphous and pure crystalline samples. RMSECV are calculated as follows:

$$\mathrm{RMSECV} = \sqrt{\sum_{i=1}^{N}(y_i - \hat{y}_i)^2/N} \quad (1)$$

where yi is the crystallinity (here weight % w/w), $\hat{y}_i$ is the predicted value, and N is the total number of samples.

The LOD and LOQ were calculated as described in the guideline Q2 from the International Conference on Harmonization (ICH) [40]:

$$\mathrm{LOD} = 3.3\sigma \quad (2)$$

where σ is the standard deviation of the 100 % amorphous samples.

$$\mathrm{LOQ} = 10\,\sigma \quad (3)$$

3. Results and discussion

3.1 Particle size and morphology

Scanning electron micrographs of amorphous and crystalline lactose are presented in Figure 1, which illustrates that the amorphous lactose particle size is smaller compared to the crystalline. The average of three determinations of the median particle size, D50, ± standard deviation, was 5.7 ± 0.4 μm for amorphous lactose and 20.5 ± 0.3 μm for crystalline lactose. It can be observed that the spray drying created nearly spherical particles, and that some agglomerating of smaller particles is present in both samples.

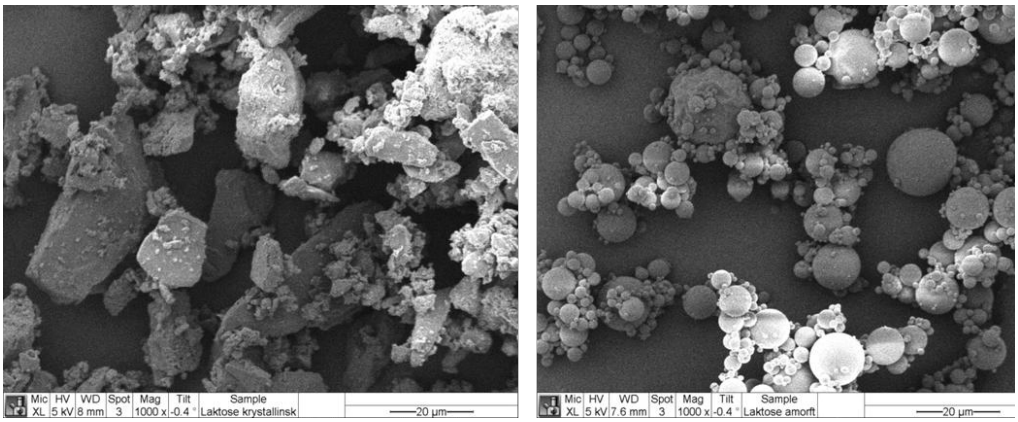

Figure 1: SEM of crystalline α-lactose monohydrate (left) and amorphous lactose (right).

3.2 Terahertz spectroscopy

Due to a large compact pellet thickness (approximately 1 mm) only the spectral range from 0.1-1.0 THz is useful for further analysis. Figure 2 presents the terahertz spectra of binary mixtures of amorphous and crystalline lactose with increasing level of crystallinity. By examining the concentration arranged spectra, the peak at 0.53 THz, due to an externally hindered rotational mode of the hydrogen-bonded crystalline lattice [31] becomes visible at approximately 10 % and increases with higher levels of crystallinity. Taday [41] found that crystalline lactose analyzed with terahertz spectroscopy has strong absorption lines at 0.58, 1.51, and 2.83 THz and McIntosh et al. [28] found the region between 0.3 and 0.8 THz to be the most informative for studying lactose due to larger scattering from the amorphous lactose above this frequency range. When the crystallization of amorphous lactose occurred, the peak at 0.53 THz increased in intensity and the elevated background at the higher frequencies decreased [28]. This matches well with the strong background seen at frequencies above 0.6 THz for low levels of crystallinity present in Figure 2 (low sample numbers).

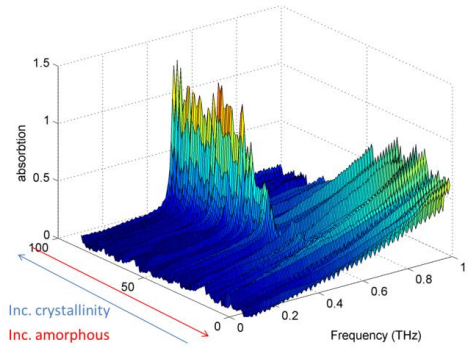

Figure 2: Terahertz spectra 0.1-1.0 THz of lactose samples with increasing level of crystallinity.

Although a selective peak for lactose monohydrate is present in the current data set, particulate scattering and other baseline effects make it more likely for a multivariate data analytical approach to yield a more robust model than a univariate/single-peak method [42]. Hence, in order to understand the main variations in the underlying data set, an exploratory PCA analysis of the mean centered terahertz spectra colored according to level of crystallinity is presented in Figure 3a. As can be seen in Figure 3a, the two main principal components, PC1 and PC2, explain 98 % of the total spectral variation and spreads out the samples from lowest to highest level of crystallinity. The corresponding loading plot for the PCA model is presented in Figure 3b. The loading plot of PC1 shows a positive baseline tilt (amorphous) and a negative peak (crystalline) which confirm that the two components are inversely correlated to each other in the calibration design. PC2 describe primarily the crystalline form and only to a small extent a little baseline tilt.

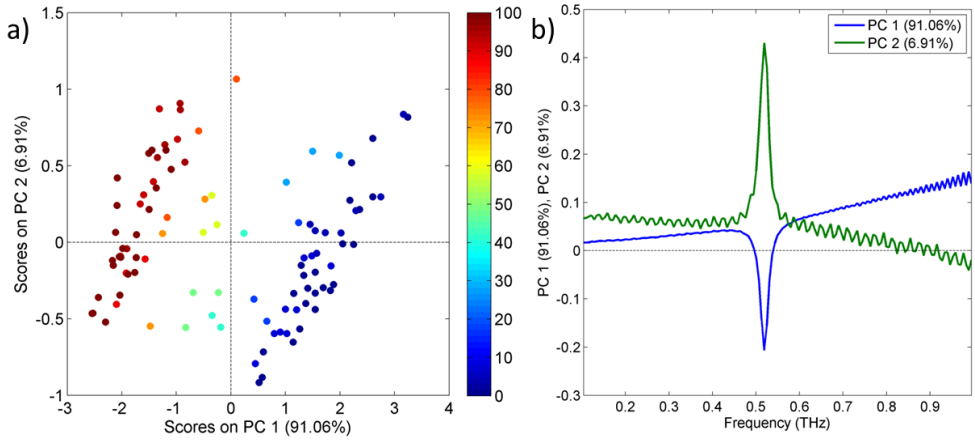

Figure 3: a) Score plot from PCA of mean centered terahertz spectra, colored by level of crystallinity from amorphous (blue) to 100 % (w/w) crystalline (red). b) Corresponding loading plot for 0.1-1.0 THz for PC1 and PC2.

The predicted versus measured plot from the two-component PLS model of terahertz spectra (SNV plus mean centered) is shown in Figure 4a. The pattern of the predicted data points seems to follow a weak sigmoidal shaped curve which indicates that some non-linearity is present. However, the lower concentrations (up to around 30 % w/w) seem to fit one line and the highest concentrations (from 60-70 % w/w and up) seem to follow another line. The concentrations in the middle of the calibration range are not very well explained by this model. This can be explained by the fact that the THz signals for the amorphous and crystalline components are measured by two different types of signals and that none of them are very sensitive to a low concentration. It is also possible that the distribution of the objects with many points at the extremes and only a sparse set in the middle of the concentration range, bias the model towards the extremes. The corresponding PLS loadings are shown in Figure

4b. From the figure it is obvious that the main information comes from the crystalline lactose peak at 0.53 THz and to a lesser extent from the 'elevated' background of the amorphous component in the range 0.6-1.0 THz.

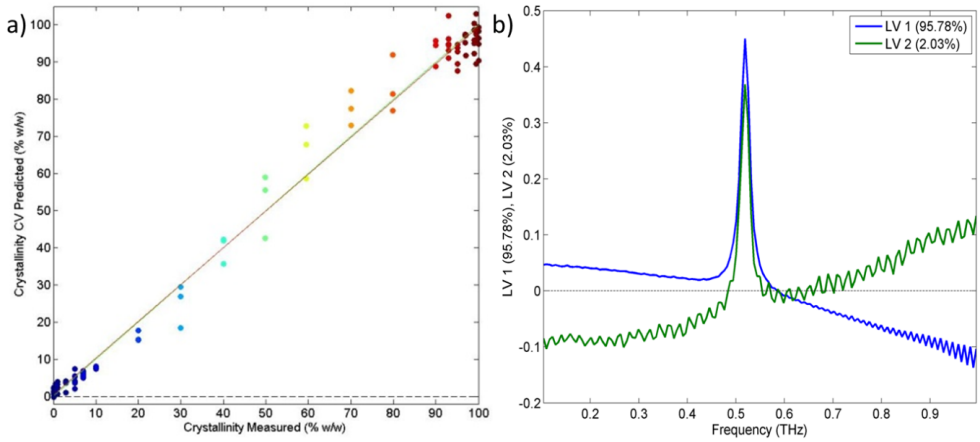

Figure 4: a) PLS model of crystallinity of the Terahertz spectra after SNV and mean centering. Two latent variables are used and the RMSECV is 2.91% (w/w). b) Corresponding loading plot from PLS model of Terahertz spectra from 0.1-1.0 THz.

As the main interest of this study is to estimate LOD and LOQ, regression models built on the reduced concentration range 0-10 % (w/w) crystalline lactose were calculated. The best result, using second derivative preprocessing, is shown in Figure 5.

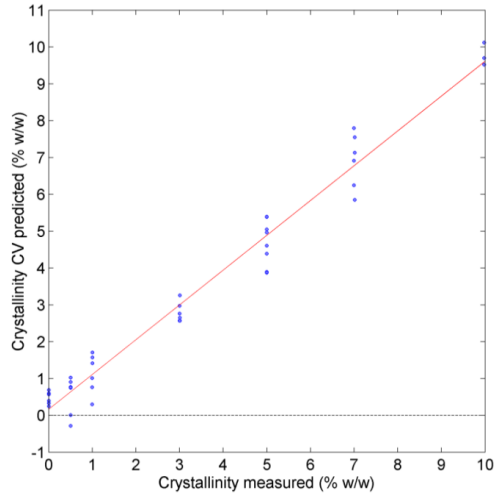

Figure 5: PLS model of crystallinity 0-10 % (w/w) from Terahertz spectra treated with SNV, second derivative and mean centering. Three latent variables are used and the RMSECV is 0.30 % (w/w).

3.3 NIR spectroscopy

Figure 6 displays the SNV treated NIR spectra colored by crystallinity. A shift in the 1st overtone for O-H bands from 1460 nm to 1540 nm is observed when the crystallinity increase. In a similar experimental set-up Gombás et al. [8] found that the shift in O-H band occurred from 1480 nm to 1550 nm. Other spectral differences between amorphous and crystalline lactose observed in Figure 6 are the combination bands at 1900-1980 nm (O-H stretch and O-H deformation of H_2O) [16], the combination bands at 2040-2100 nm (O-H stretch and O-H deformation of ROH lactose) [8; 16], and the combination bands at 2220-2280 nm (O-H stretch and O-H deformation of lactose) [16].

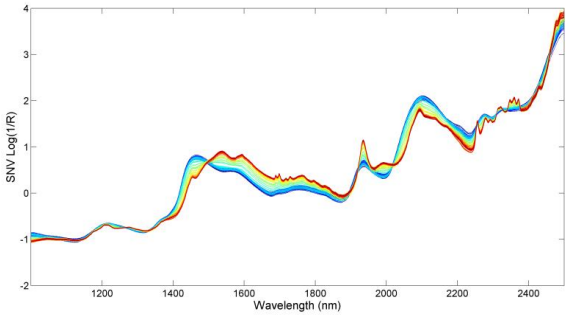

Figure 6: Plot of SNV treated NIR spectra colored by crystallinity where amorphous is blue, 50 % (w/w) crystalline is green and 100 % (w/w) crystalline is red.

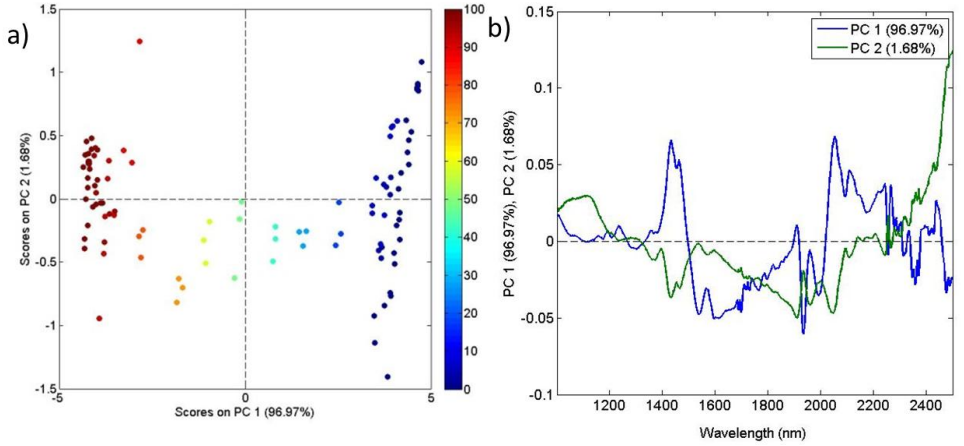

Figure 7: a) PCA score plot of NIR spectra after SNV and mean centering colored by crystallinity from amorphous (blue) to 100 % (w/w) crystalline (red). b) Corresponding loading plot for PC1 and PC2.

The PCA score plot based on the SNV and mean centered NIR spectra is presented in Figure 7a and the corresponding loading plot in Figure 7b. Most of the variation in the NIR spectra

(97 %) is explained by the first principal component that clearly explains the degree of crystallinity.

When developing PLS models for the crystallinity, the best model was found using the combination of SNV preprocessing, mean centering and variable selection using the iPLS algorithm. The model using the full concentration range (0-100 % w/w) is shown in Figure 8, and the selection of the spectral range found with iPLS is shown in Figure 9. The spectral range that gave the best calibration model for the full concentration range (0-100 % w/w), was 2015-2095 nm, which corresponds to the combination band of O-H for lactose (2040-2100 nm [16]).

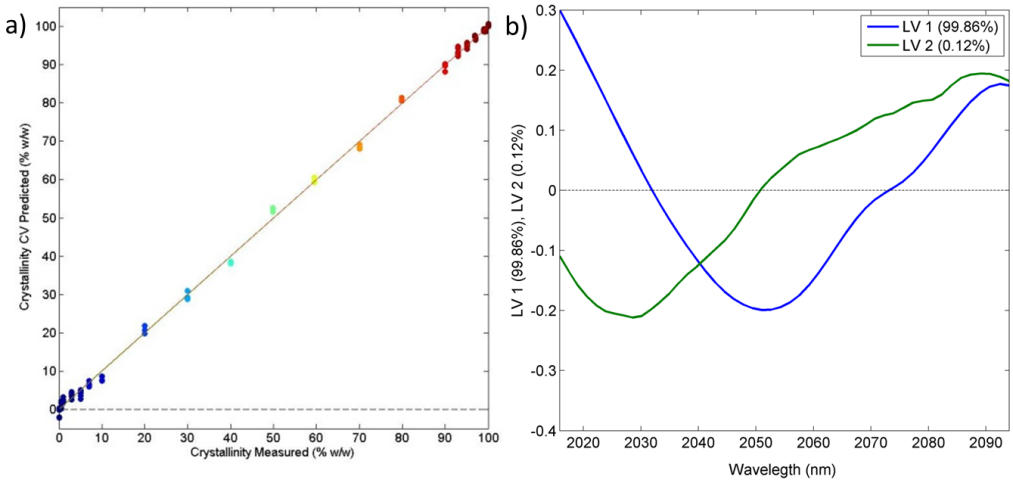

Figure 8: a) PLS calibration of 0-100 % (w/w) crystallinity for SNV, mean centered NIR spectra. The spectral area used is 2015-2095 nm. Two latent variables are used for the model and RMSECV is 0.87 % (w/w). b) Corresponding loading plot from 2015-2095 nm.

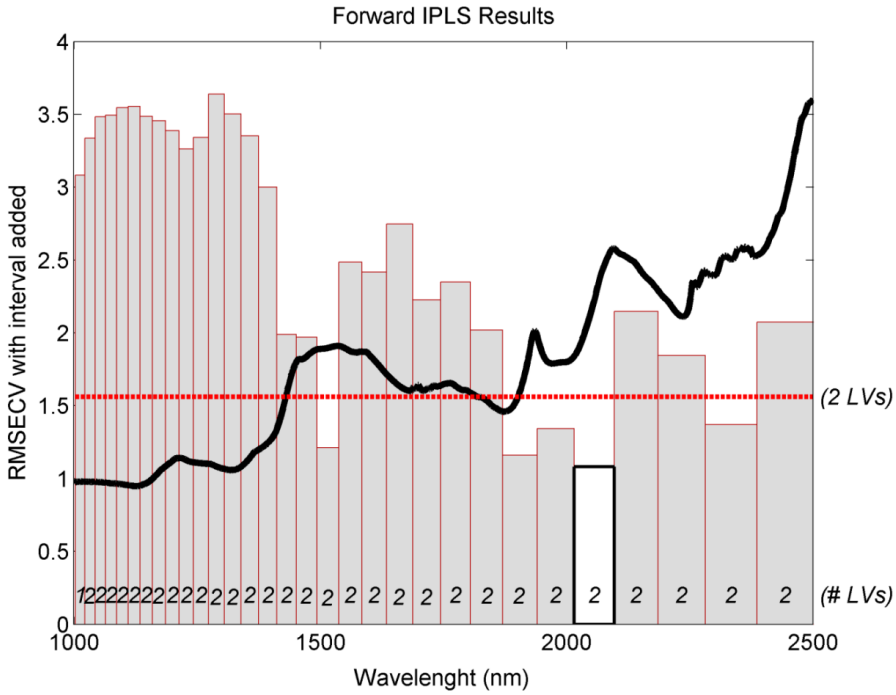

Figure 9: iPLS of crystallinity for SNV, mean centered NIR spectra. The red line is the RMSECV for global model using all wavelengths (1000-2500), where the individual bars are the RMSECV using each interval (based on 50 spectral variables). The white area (2015-2095 nm) is the one chosen for the full concentration range model. Local models are compared to the full-spectrum, global model by RMSECV. All intervals are tested individually and the one with the lowest error is chosen. Then the intervals are tried in combination with this selected interval, and intervals are added until the RMSECV increases by introduction of new intervals.

The best PLS models for NIR in the range of 0-10 % (w/w) crystalline lactose is shown in Figure 10a. The spectral areas that gave the best calibration, chosen by iPLS, are shown in the loading plot in Figure 10b. It is obvious that the main information used in the calibration is in the area 1870-2014 nm (O-H combination band, 1900-1980 nm [16]) and to a lesser extent 1537-1560 (O-H 1st overtone) and the area around 1200 nm, probably due to C-H 2nd overtone [8]. Obviously the spectral areas chosen for the two concentration ranges are different. This is possibly due the fact that for 0-10 % (w/w) crystallinity, only minor differences in the spectra of the two species are present, and therefore more diverse spectral areas are required to support a reliable calibration.

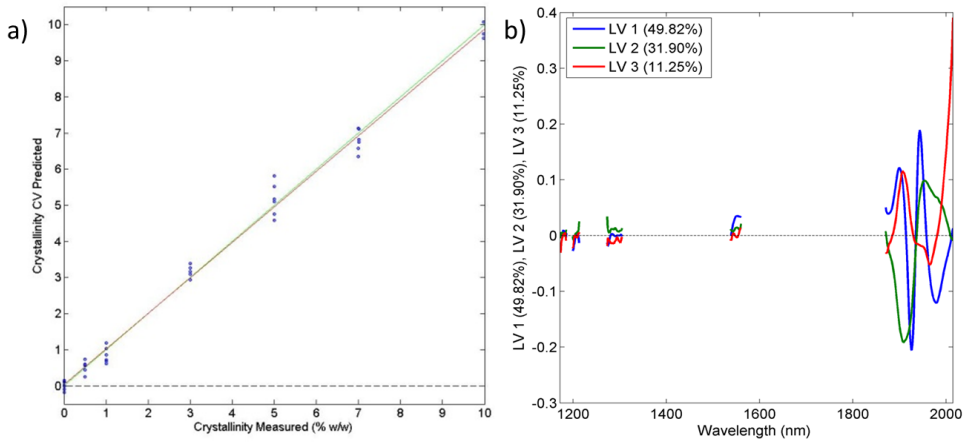

Figure 10: a) PLS model of 0-10 % (w/w) crystallinity from SNV, first derivative, and mean centered NIR spectra. The spectral areas used are 1172-1185, 1200-1213, 1273-1304, 1537-1560, 1870-2014 nm, found by iPLS. There are used three latent variables for the model and RMSECV 0.20% (w/w). b) Corresponding loading plot.

Table 1: Overview of best achieved calibrations for the crystallinity by terahertz (THz) and NIR spectroscopy for 0-100 % (w/w) and 0-10 % (w/w) crystallinity.

	THz 0-100 % (w/w)	**NIR 0-100 % (w/w)**	**THz 0-10 % (w/w)**	**NIR 0-10 % (w/w)**
Pre-processing	SNV, mean	SNV, mean, iPLS	SNV, 2nd derivative (2nd order, filter size 15), mean	SNV, 1st derivative (2nd order, filter size 15), mean, iPLS
Range	0.1-1.0 THz	2015-2095 nm	0.1-1.0 THz	1172-1185, 1200-1213, 1273-1304, 1537-1560, 1870-2014 nm
Latent variables	2	2	3	3
RMSECV (% w/w)	2.91	0.87	0.30	0.20
LOD (% w/w)	3.21	3.76	0.80	0.43
LOQ (% w/w)	9.91	11.04	2.42	1.31

Table 1 gives a comparison of the models for crystallinity using terahertz or NIR spectroscopy for the full concentration range (0-100 % w/w), and for the low concentration range (0-10 % w/w). The table reveals that NIR spectroscopy in general performs significantly better than terahertz spectroscopy to predict lactose crystallinity. However, in the models for the full concentration range, the LOD and LOQ are higher for the NIR measurements than for terahertz measurements, and much higher than for the low concentration calibrations. For NIR calibration of the full concentration range, the chosen spectral area may describe phenomena that are mainly present in the high concentration of crystalline lactose, e.g. the presence of water bound to the lactose molecule. Therefore, this model performs poorly in explaining the amorphous lactose (LOD, LOQ), despite the lower RMSECV. In the low concentration calibration model for NIR, the spectral areas included in the calibrations are better at explaining the amorphous samples compared to the full concentration calibration. The preprocessing

methods applied on the two calibrations are also different. In the low concentration models (0-10 % w/w crystallinity), both for NIR and terahertz data, derivatives are necessary to obtain good models. This makes sense for terahertz spectroscopy, where the amorphous lactose is seen as a broad background, and this is effectively removed by second derivatives [36]. Nørgaard et al. [16] quantified crystalline lactose in binary mixtures of amorphous and crystalline lactose (50-98 % w/w) with a RMSECV of 0.778 % (w/w), and mixtures of the same samples combined with whey permeate powder samples with a RMSECV of 0.627 %. For binary mixtures of amorphous and crystalline lactose in the range of 10-90 % (w/w), Fix and Steffens [9] found a calibration error RMSECV of 1.79 % (w/w). Calibration with 0-10 % (w/w) crystalline lactose gave an RMSECV of 0.54 % (w/w), and LOD and LOQ of 0.75 % (w/w) and 2.5 % (w/w), respectively [9]. In this study LOD and LOQ for NIR (0-10 % w/w) are lower than the value reported by Fix and Steffens [9] in a similar experiment.

NIR spectroscopy, in general, performs better than terahertz spectroscopy for determining crystalline impurities or conversion to the crystalline state in amorphous lactose. However, NIR spectroscopy is a mature method that has been refined over many years, whereas currently terahertz spectroscopy is still developing. Terahertz spectroscopy still faces the instrumental challenges but has the potential to become a valid method in quantifying crystallinity in pharmaceuticals.

4. Conclusion

Despite the fact that NIR spectroscopy measure only indirectly intermolecular interactions and terahertz spectroscopy directly probe lattice vibrations, this study has shown that NIR spectroscopy in general performs better than terahertz spectroscopy for determining crystalline impurities or conversion to the crystalline state in amorphous lactose. PLS regression models were developed and the RMSECV for the models with full concentration range were found to be 2.91 % (w/w) and 0.87 % (w/w) for THz-TDS and NIR, respectively. Calibrations created on samples containing 0-10 % (w/w) crystalline material gave RMSECVs of 0.30 % (w/w) and 0.20 % (w/w) for THz-TDS and NIR, respectively, while the limits of detection were 0.80 % (w/w) and 0.43 % (w/w), respectively.

5. Acknowledgment

The authors wish to thank the Danish Ministry of Science, Technology and Innovation for financial support of a PhD stipendium to Solveig Warnecke through the QbD consortium (www.qbd.dk). Jian X. Wu acknowledges The Danish Council for Technology and Innovation via the Innovation Consortium NanoMorph (952320/2009) for financial support of his PhD stipendium. The authors wish to thank Mogens Frost, H. Lundbeck A/S for performing SEM and laser diffraction measurements, Tianwu Wang, DTU Fotonik, for assistance with terahertz spectroscopy, and Mingshi Yang for support with spray drying.

6. Reference List

[1] R. C. Rowe, P. J. Sheskey, S. C. Owen, *Handbook of Pharmaceutical Excipients,* Pharmaceutical Press, 2005.
[2] A. Grunenberg, J. O. Henck, H. W. Siesler, *Int. J. Pharm.* **129,** (1996) 147-158.
[3] D. Q. M. Craig, P. G. Royall, V. L. Kett, M. L. Hopton, *Int. J. Pharm.* **179,** (1999) 179-207.
[4] L. Yu, *Adv. Drug Deliver. Rev.* **48,** (2001) 27-42.
[5] S. Yamamura, H. Gotoh, Y. Sakamoto, Y. Momose, *Eur. J. Pharm. Biopharm.* **49,** (2000) 259-265.
[6] E. A. Schmitt, D. Law, G. G. Z. Zhang, *J. Pharm. Sci.* **88,** (1999) 291-296.
[7] B. C. Hancock, G. Zograf, *J. Pharm. Sci.* **86,** (1997) 1-12.
[8] Á. Gombás, I. Antal, P. Szabó-Révész, S. Marton, I. Erõs, *Int. J. Pharm.* **256,** (2003) 25-32.
[9] I. Fix, K. J. Steffens, *Drug Dev. Ind. Pharm.* **30,** (2004) 513-523.
[10] J. Aaltonen, M. Alleso, S. Mirza, V. Koradia, K. C. Gordon, J. Rantanen, *Eur. J. Pharm. Biopharm.* **71,** (2009) 23-37.
[11] J. A. Zeitler, P. F. Taday, D. A. Newnham, M. Pepper, K. C. Gordon, T. Rades, *J. Pharm. Pharmacol.* **59,** (2010) 209-223.
[12] G. Buckton, E. Yonemochi, J. Hammond, A. Moffat, *Int. J. Pharm.* **168,** (1998) 231-241.
[13] M. Savolainen, A. Heinz, C. Strachan, K. C. Gordon, J. Yliruusi, T. Rades, N. Sandler, *Eur. J. Pharm. Sci.* **30,** (2007) 113-123.
[14] A. Heinz, M. Savolainen, T. Rades, C. J. Strachan, *Eur. J. Pharm. Sci.* **32,** (2007) 182-192.
[15] A. Heinz, C. J. Strachan, K. C. Gordon, T. Rades, *J. Pharm. Pharmacol.* **61,** (2009) 971-988.
[16] L. Nørgaard, M. T. Hahn, L. B. Knudsen, I. A. Farhatc, S. B. Engelsen, *Int. Dairy J.* **15,** (2005) 1261-1270.
[17] P. U. Jepsen, D. G. Cooke, M. Koch, *Laser Photonics Rev.* **5,** (2011) 124-166.
[18] P. U. Jepsen, S. J. Clark, *Chem. Phys. Lett.* **442,** (2007) 275-280.
[19] P. F. Taday, I. V. Bradley, D. D. Arnone, M. Pepper, *J. Pharm. Sci.* **92,** (2003) 831-838.
[20] C. J. Strachan, T. Rades, D. A. Newnham, K. C. Gordon, M. Pepper, P. F. Taday, *Chem. Phys. Lett.* **390,** (2004) 20-24.
[21] C. J. Strachan, P. F. Taday, D. A. Newnham, K. C. Gordon, J. A. Zeitler, M. Pepper, T. Rades, *J. Pharm. Sci.* **94,** (2005) 837-846.
[22] M. Otsuka, J. i. Nishizawa, J. Shibata, M. Ito, *J. Pharm. Sci.* **99,** (2010) 4048-4053.
[23] I. Takeuchi, K. Tomoda, T. Nakajima, H. Terada, H. Kuroda, K. Makino, *J. Pharm. Sci.* **101,** (2012) 3465-3472.
[24] J. Zeitler, D. A. Newnham, P. F. Taday, T. L. Threlfall, R. W. Lancaster, R. W. Berg, C. J. Strachan, M. Pepper, K. C. Gordon, T. Rades, *J. Pharm. Sci.* **95,** (2006) 2486-2498.
[25] Y. C. Shen, *Int. J. Pharm.* **417,** (2011) 48-60.
[26] S. Rehder, J. X. Wu, J. Laackmann, H. U. Moritz, J. Rantanen, T. Rades, C. S. Leopold, *Eur. J. Pharm. Sci.* **48,** (2013) 97-103.
[27] E. P. Parrott, J. Zeitler, L. F. Gladden, *Opt. Lett.* **34,** (2009) 3722-3724.
[28] A. I. McIntosh, B. Yang, S. M. Goldup, M. Watkinson, R. S. Donnan, *Chem. Phys. Lett.* **558,** (2013) 104-108.
[29] T. D. Dorney, R. G. Baraniuk, D. M. Mittleman, *J. Opt. Soc. Am. A* **18,** (2001) 1562-1571.
[30] P. U. Jepsen, B. M. Fischer, *Opt. Lett.* **30,** (2005) 29-31.
[31] D. Allis, A. Fedor, T. Korter, J. Bjarnason, E. Brown, *Chem. Phys. Lett.* **440,** (2007) 203-209.
[32] H. Wu, E. J. Heilweil, A. S. Hussain, M. A. Khan, *Int. J. Pharm.* **343,** (2007) 148-158.
[33] M. Walther, B. M. Fischer, P. U. Jepsen, *Chem. Phys.* **288,** (2003) 261-268.
[34] A. L. Pomerantsev, O. Y. Rodionova, *J. Chemometr.* **26,** (2012) 299-310.
[35] R. J. Barnes, M. S. Dhanoa, S. J. Lister, *Appl. Spectrosc.* **43,** (1989) 772-777.
[36] Å. Rinnan, F. van den Berg, S. B. Engelsen, *Trac-Trend. Anal. Chem.* **28,** (2009) 1201-1222.
[37] S. Wold, K. Esbensen, P. Geladi, *Chemometr. Intell. Lab.* **2,** (1987) 37-52.
[38] S. Wold, H. Martens, H. Wold, *Lect. Notes Math.* **973,** (1983) 286-293.
[39] L. Nørgaard, A. Saudland, J. Wagner, J. P. Nielsen, L. Munck, S. B. Engelsen, *Appl. Spectrosc.* **54,** (2000) 413-419.
[40] I. C. H. Guideline, *IFPMA: Geneva* (2005).
[41] P. F. Taday, *Philos. T. Roy. Soc. A.* **362,** (2004) 351-363.
[42] J. Rantanen, H. Wikström, F. E. Rhea, L. S. Taylor, *Appl. Spectrosc.* **59,** (2005) 942-951.

Paper IV

Quantification of two active pharmaecutical ingredients in a tablet formulation using fluorescence spectroscopy

Quantification of two active pharmaceutical ingredients in a tablet formulation using fluorescence spectroscopy

Solveig Warnecke[a], Åsmund Rinnan[a], Morten Allesø[b], Søren B. Engelsen[a].*

[a]Department of Food Science, Faculty of Science, University of Copenhagen, Rolighedsvej 30, DK-1958 Frederiksberg C, Denmark. *warnecke@life.ku.dk, +45 3533 3257;

[b]Biologics and Pharmaceutical Science, H. Lundbeck A/S, Ottiliavej 9, DK-2500 Valby, Denmark

Abstract

Many pharmaceuticals include highly potent active pharmaceutical ingredients (API), which only require a small dosage to obtain the desired therapeutic effect. This leads to a challenge for quantification of the API by process analytical technology (PAT), as the standard non-destructive measurement techniques do not have the capability to quantify below 1% (w/w) API content. In formulations that use more than one API, this challenge is further increased. The purpose of this study is to scrutinize the potential of fluorescence spectroscopy for the simultaneous quantification of two APIs; flupentixol (FLU) in low dosage (0.208-0.625 % w/w free base) and melitracen (MEL) (4.17-12.5 % w/w free base) in a tablet formulation. Despite internal quenching between the ingredients and the two APIs, this paper demonstrates that it is possible to establish calibrations using partial least square regression (PLS) on unfolded fluorescence landscapes with a root-mean-square-error-of-prediction (RMSEP) and relative error of 0.038 % (w/w) and 9.1 %, for FLU and 0.344 % (w/w) and 4.1 % for MEL, respectively.

Highlights

- Determination of two active pharmaceutical ingredients in tablets by fluorescence spectroscopy
- Low concentration determination
- Presence of quenching is dealt with by multivariate data analysis

Keywords: Fluorescence spectroscopy; API; flupentixol; melitracen; partial least square regression; quenching

Abbreviations:

API: active pharmaceutical ingredient
CQA: critical quality attribute
CU: content uniformity
EEM: excitation-emission matrices
FLU: flupentixol
iPLS: interval partial least square regression
LIF: laser-induced fluorescence
LOD: limit of detection
LOQ: limit of quantification
LV: latent variable
MEL: melitracen
NIR: near-infrared spectroscopy
PARAFAC: parallel factor analysis
PAT: process analytical technology
PC: principle component
PCA: principal component analysis
PLS: partial least squares regression
QbD: quality by design
RMSEP: root-mean-square-error of prediction
RMSECV: root-mean-square-error of cross-validation
RSD: relative standard deviation
TLD: trilinear decomposition
U-PCA: unfolded principle component analysis

1. Introduction

Content uniformity (CU) of tablets is a critical quality attribute (CQA) due to its link to therapeutic effect and thus patient safety. Traditionally, API content determination is done by HPLC analysis, but in a PAT (process analytical technology) context a more rapid and non-destructive method is required. This paper describes the development of a fluorescence method for determination of active content in Deanxit tablets. Deanxit is an anti-depressive drug, containing two active ingredients, flupentixol and melitracen. A combination of 0.5 mg flupentixol (FLU) and 10 mg of melitracen (MEL) is used in conditions of anxiety, depression and apathy [1].

The API content of both MEL [2] and FLU [3] is traditionally measured by HPLC, but also UV-VIS spectrophotometry has been used for FLU [4] and for FLU and MEL in combination[5]. Furthermore, LC/MS/MS and LC/ESI/MS methods have been reported for quantification of FLU and MEL in human plasma [6-8]. However, these techniques carry the disadvantages of being destructive, time-consuming, and laborious. It is therefore of interest to be able to quantify the API's in a non-destructive manner for direct PAT monitoring of the production process [9; 10]. Near-infrared spectroscopy (NIR), in particular, is often used to quantify API in tablet formulation. However, NIR has not shown good results below 1% (w/w) API content [11].

In contrast to the food area [12] fluorescence spectroscopy has so-far only found limited application in pharmaceutical PAT studies [13]. Recently, the measurement of excitation-emission matrices (EEM) was proposed together with chemometric methods for analysis of pharmaceutical formulations [14]. Active ingredients often consist of substituted aromatic and heterocyclics that may exhibit fluorescence at the right wavelength [15]. Approximately 60 % of the top two hundred API molecules are estimated to fluoresce while most excipients (lactose, starch, etc.) do only fluoresce to a less extend [16]. The high sensitivity of fluorescence spectroscopy therefore makes it a palpable alternative to the omnipotential NIR spectroscopy [13; 17].

Many studies have shown fluorescence properties of FLU after different chemical reactions with added solvents [18-21]. For instance FLU when oxidized with nitrous acid [20] exhibit fluorescence at 440 nm when excited at 370 nm. However, this fluorescence is most likely related to the reaction rather than the actual flupentixol molecule. Fluorescence in liquid and solid phase can act differently. Moreira et al. [22] reported that paracetamol does not fluoresce in liquid solutions, but has fluorescent properties in solid phase. Solid phase fluorescence is very attractive due to the reduced sample preparation and a minimum of consumption of reagents and low cost of analysis [14].

Moreira et al. [23] developed a fluorescence method for acetylsalicylic acid in tablet formulations in the range 50-170 mg/g with a relative standard deviation of 2.3 %, a detection limit of 2.2 mg/g and quantification limit of 7.3 mg/g. Subsequently, Moreira et al. [24] proved that they were able to simultaneously determine acetylsalicylic acid and caffeine in powder mixtures in the range of 50-170 mg/g and 5-20 mg/g using fluorescence and PLS with relative standard deviations of 3.1 % and 4.0 % respectively. Domike et al. [25] used

fluorescence for prediction of triamterene in tablets with RSDs of 1.8-12.3 % in the API load range 1.6-4.75 % (w/w) and caffeine with RSDs of 3.7-6.9 % in the range 5-20 % (w/w).

Problems with selectivity in fluorescence measurements can occur when analyzing a sample matrix with more than one component due to overlapping bands of structurally identical components. Furthermore, specificity can be a problem in the determination of fluorescent drugs [26]. In cases where univariate spectrofluorimetry is not sufficient, time consuming separation techniques can be avoided by applying multivariate PLS to the fluorescence data [26-28]. Moreira et al. [29] found that simultaneous determination of two actives in diluted powder mixtures was not possible with a univariate approach, due to overlapping spectral bands. The authors solved this issue with the application of PLS. A different method to overcome the problem with emission overlapping peaks is to use first derivate synchronous fluorescence, where the difference between excitation and emission is kept constant during measurement. Karim et al. [26] used first derivate synchronous fluorescence to simultaneously determine acetylsalicylic acid and caffeine. Another approach is to use the second-order advantage of the EEM. Esteves de Silva et al. [30] and Leitão et al. [31] used EEM and PARAFAC (parallel factor analysis) and TLD (trilinear decomposition) to detect verapamil in methanol solution. They also calculated different excitation and emission spectra with PARAFAC due to a changed background for verapamil from tablets compared to a pure verapamil standard. Furthermore, down weighing spectral regions with scatter band (1^{st} and 2^{nd} order scatter) gave better results in the PARAFAC models. Alves and Poppi [14] simultaneously determined acetylsalicylic acid (337-463 mg/g), paracetamol (59-101 mg/g), and caffeine (226-404 mg/g) with errors in the range from 0.2-13 % and relative standard deviations RSD of 0.5-4.8 % using PARAFAC. García-Reiriz et al. [32] used unfolded principal component analysis combined with different artificial neural network techniques to determine different solvent systems using second-order advantage.

So far, only a few studies have been conducted using fluorescence spectroscopy for on-line measurements in the pharmaceutical industry, but the possibilities are promising [14-17; 25]. Lai et al. [17] developed a laser-induced fluorescence (LIF) sensor for on-line monitoring of powder blend homogeneity for triamterene down to 0.1 % (w/w) in lactose matrix with less than 5 % RSD. Later, Lai and Cooney [15] found a limit of detection below 0.02 % (w/w) on a similar setup. In 2004, Lai et al. [16] simulated a production line and applied a LIF sensor with a measurement rate of up to 3000 tablets per minute.

In the production of pharmaceutical tablets, it is desirable to analyze the API content, non-invasively and preferably online. The aim of this study is to evaluate the potential of using a fluorescence sensor for the simultaneous and non-destructive quantification of two APIs in a tablet formulation: flupentixol (FLU) in low dosage and melitracen (MEL).

2. Experimental section

2.1. Apparatus

Samples were analyzed on LS55 Perkin Elmer Fluorescence Spectrometer (Waltham, Massachusetts) at 280-365 nm excitation and 300-500 nm emission, with a 5 nm and 0.5 nm

resolutions, respectively. Excitation slit was set to 11 nm, emission slit was 2.5 nm, and scan speed was 1200 nm/min. Samples were analyzed front-face in a 40 mm round sample cup with a custom made inner sample holder of 8 mm.

2.2. Samples

Tablet cores (total weight of 120 mg) were manufactured according to an in-house batch formula. The final blend, subject to tablet compression, is a mixture of two granulates, I and II, containing FLU and MEL, respectively, and an extra-granular phase. An overview of excipients used is given in Table 1.

Table 1 Solid ingredients for production of tablets listed in descending order (of the target formulation).* indicates ingredients that are interchanged with FLU or MEL, to provide a given granule concentration.

Granulate I	**Granulate II**	**Extra granulate excipients**
Corn starch	Corn starch*	Microcrystalline cellulose, PH102
Betadex, Kleptose	Melitracen hydrochloride	Hydroxypropylcellulose, Klucel
Lactose monohydrate*	Lactose monohydrate*	Croscarmellose sodium, Ac-Di-Sol
Hydroxypropylcellulose, Klucel	Hydroxypropylcellulose, Klucel	Hydrogenated vegetable oil, Lubritab
Flupentixol-dihydrochloride		Magnesium Stearate
		Talc

Six granulations per API were carried out, each sub-batch providing different concentration of active content. Concentration levels were 0 (placebo), 50, 75, 100, 125 and, 150 % of the nominal content in the intragranular phase. Wet granulations were performed in a high shear mixer (Diosna P25, Dierks & Söhne GmbH, Osnabrück, Germany) using water as binder liquid. As stated in Table 1, FLU was interchanged with lactose to provide a given concentration, while MEL was interchanged with corn starch and lactose, the latter two excipients kept at a constant ratio.

A total of 36 tablet batches were manufactured by combining the six concentrations of granulate I with the six concentrations of granulate II (Figure 1). In this manner, all combinations of granulate I and II were utilized. Due to the different concentrations of the intragranular phases, it was possible to maintain identical amounts of intra- and extragranular phases for all 36 batches, thereby providing tablets of similar mechanical strength. A Bohle LM40 blender (L.B. Bohle, Ennigerloh, Germany) was used for mixing granulates with the extragranular excipients. Blending time was 8 min followed by 3 min lubrication with magnesium stearate, both steps performed at 22-24 rpm.

Tablets with a total weight of 120 mg were manufactured on a Kilian Pressima, 12 punch rotary tablet press (I.M.A Kilian GmbH & Co. KG, Cologne, Germany) at a compression speed of 20,000 tablets/hour. Batch size was approximately 2000 g.

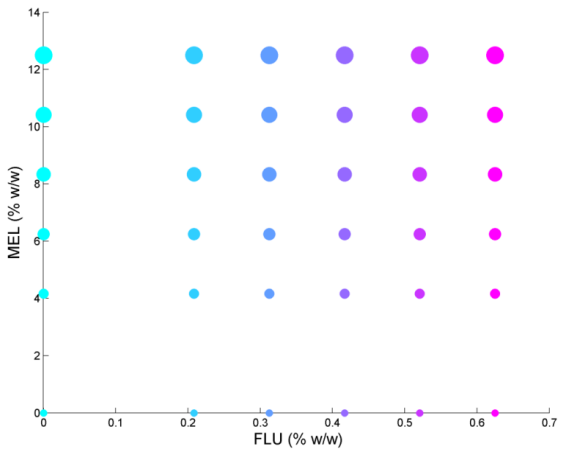

Figure 1. Experimental design of the 36 tablet batches containing 0-0.625 % (w/w) FLU and 0-12.5 % (w/w) MEL. The nominal (100%) content of FLU and MEL is 0.417 and 8.33 % w/w free base, respectively.

2.3. Procedure

Each sample was ground and transferred to the sample cup. Three samples from each batch (3 × 36 samples) were analyzed. Furthermore, 24 samples from 8 independent batches were used for testing the models. The test samples were a mixture of production- and lab-scale batches. As the main interest was to verify the predictions at the target values, only samples at the target values were chosen together with a placebo batch for the test set.

HPLC values were determined as an assay of five tablets using an in-house procedure with an analytical RSD of 0.4 % for FLU and 0.6 % for MEL.

2.4. Data analysis

Data analysis was performed in MATLAB version 7.14.0 (Mathworks™, Natick, Massachusetts) using PLS toolbox 6.7.1 (Eigenvector, Wenatchee, Washington).

The data analysis was done on unfolded data with first order Rayleigh scatter removed (any emission wavelength ≤ excitation wavelength + 20 nm) [33]. The data was unfolded in the excitation mode, i.e. the new dimensionality of the data is samples × (emission spectra at excitation 1 + emission spectra at excitation 2, etc.). Unfolding of the three-way matrix is illustrated in Figure 2 [34].

Principal Component Analysis (PCA) [35] was applied to explore the unfolded excitation-emission matrix (EEM), creating an unfolded PCA.

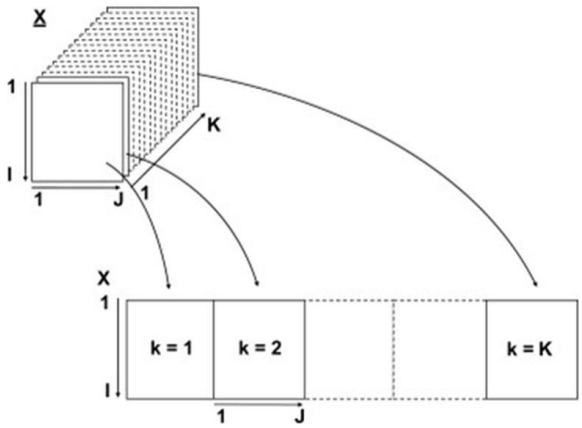

Figure 2. Unfolding of the three-way fluorescence data matrix, X (samples x emission wavelength x excitation wavelength), into a two-dimensional matrix, X (samples x emission wavelength (excitation wavelength 1; excitation wavelength 2; …; excitation wavelength k) [34]**.**

Partial Least Square Regression (PLS) [36] was performed on the unfolded data using the API concentrations (% w/w) determined by HPLC as response. Furthermore, variable selection through application of interval PLS (iPLS) [37], was used to identify the spectral ranges best describing the API concentration. The complexity of each model was estimated by finding the minimum or breakpoint in the RMSECV (root-mean-square-error of cross-validation) curve. For the cross validation all three samples from each batch was left out sequentially (36 segments), so 1/36 of the data was left out at a time. A root-mean-square-error of prediction (RMSEP) was calculated based on the independent test samples.
RMSECV and RMSEP are calculated as follows:

$$RMSE = \sqrt{\sum_{i=1}^{N}(y_i - \hat{y}_i)^2/N} \quad (1)$$

where y_i is the true API value (here HPLC), $\hat{y}_i$ is the predicted value (from EEM), and N is the total number of samples.

$$SEP = \sqrt{\sum_{i=1}^{n}(\hat{y}_i - y_i - Bias)^2/N - 1} \quad (2)$$

where,

$$Bias = \sum_{i=1}^{n}(\hat{y}_i - y_i)/N \quad (3)$$

Repeatability is calculated as the average standard deviation

$$\overline{SDev} = \sqrt{1/n \times (J-1) \times \sum_{i=1}^{n}\sum_{j=1}^{J}(y_{ij} - \overline{y}_i)^2} \quad (4)$$

where n is the number of samples, and J is the number of replicate measurements on one sample [38].

Domike et al. [25] found that for caffeine, logarithmic transformation of the emission intensities gave a better calibration. Therefore, logarithmic functions of the Y matrix as well as logarithmic function of the EEM (X matrix) were examined.

The limit of detection (LOD) and limit of Quantification (LOQ) were calculated as described in the ICH Q2 [39] guideline:

$$LOD = 3.3\sigma \quad (5)$$

where σ is the mean value of the standard deviation of the two batches of placebo tablets (each three samples), one from the calibration set and one from test set.

$$LOQ = 10\,\sigma \quad (6)$$

To simulate the performance of a system only analyzing at single wavelengths, the correlation to the maxima of FLU (excitation 350 nm, and emission 380 nm) and MEL (excitation 310 nm and emission 350 nm) were calculated.

Furthermore, PARAFAC [40] with standard settings (non-negativity) was examined, but did not improve the results, and is therefore not reported here.

3. Results and discussion

The fluorescence landscapes of pure FLU and MEL of excitation wavelength 280-365 nm and emission 300-450 nm is shown in Figure 3.

The fluorescence excitation-emission landscapes of nine out of the 36 batches used for calibration are shown in Figure 4. The top left batch, which is the placebo, shows very little fluorescence. The top middle and right batches which only include FLU at increasing concentrations display increasing fluorescence at excitation 280-350 nm and emission around 400 nm. The left middle and bottom batches which only include MEL at increasing concentrations, show weak but increasing fluorescence at excitation 310 nm and emission 350 nm. When both APIs are present (four remaining batches in Figure 4), the fluorescence from MEL is not visible and part of the fluorescence from FLU (excitation 280-300 nm, emission 400 nm) seems to disappear due to quenching [41] between the two molecules or their excipients. In the formulation MEL is used as melitracen hydrochloride, and chloride ions are like other halogens known to be a quencher [42]. Together with each flupentixol molecule are also added two hydrochloride molecules, but melitracen is added in approximately 20 times the concentration of flupentixol. It is therefore possible that the chloride from the MEL addition is quenching the FLU signal. It is also possible that energy transfer, or Förster quenching [42] is occurring as FLU excites light in the range of MEL's emission around 350 nm. Moreira et al. [22; 23] found that different excipients; magnesium stearate, talc, corn starch, stearic acid, polyvonylpyrrolidone and lactose, gave different effects on acetylsalicylic acid fluorescence probably due to specific interaction between the fluorophore and the ingredients. This underlines the importance of including all excipients when producing samples for calibration purposes.

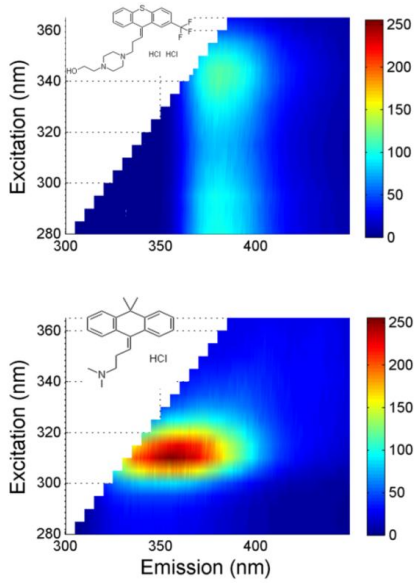

Figure 3. Excitation and emission landscapes of pure MEL (melitracen hydrochloride) and FLU (flupentixol dihydrochloride). To correct for Rayleigh scatter, any emission wavelength ≤ excitation wavelength + 20 nm have been removed.

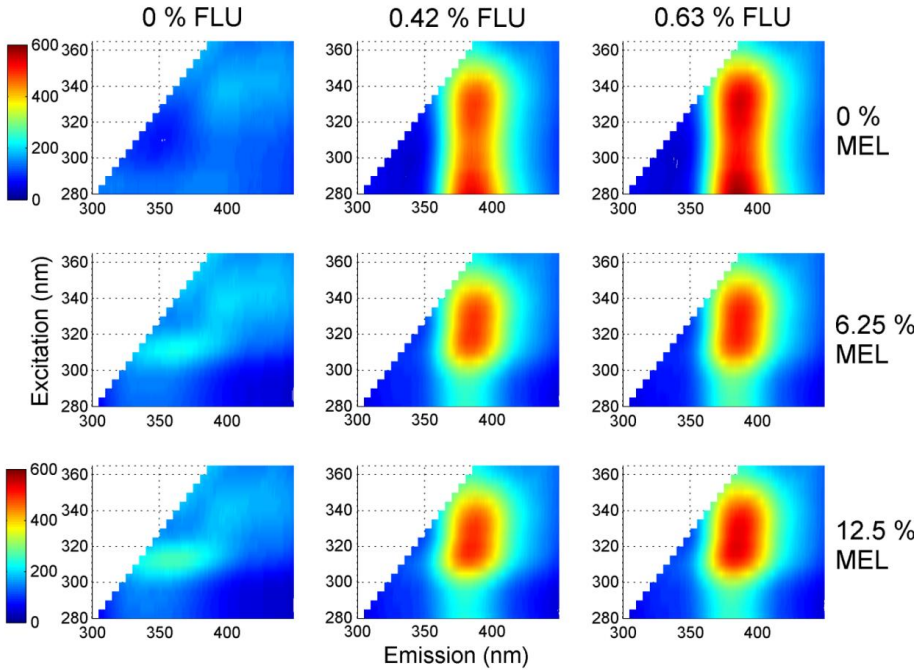

Figure 4. Fluorescence landscapes of 9 batches (average of 3 tablets) with the two APIs, FLU and MEL. First batch is placebo, FLU (0-0.625 % w/w) increases in the horizontal direction and MEL (0-12.5 % w/w) in the vertical direction. To correct for Rayleigh scatter, any emission wavelength ≤ excitation wavelength + 20 nm have been removed.

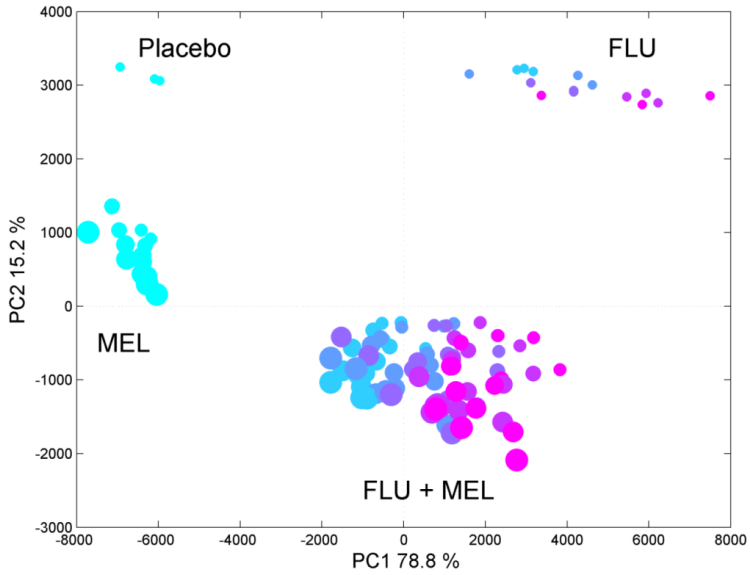

Figure 5. Scoreplot from unfolded PCA colored by the FLU concentration (turquoise indicate low values, blue indicate medium values and pink indicate high values). The sizes indicate the concentrations of MEL (see Figure 1 for the color indications).

The PCA score plot from the unfolded PCA (U-PCA) is shown in Figure 5. The score plot divides the samples in four groups. The upper left group consists of the three placebo samples; the lower left group consists of the tablet samples containing only MEL. The upper right group consists of tablet samples containing only FLU, and the lower right group consists of the remaining samples including both FLU and MEL. The score plot shows that the largest variation in the data, spanning PC1, is the FLU fluorescence, which is also the strongest signal in the EEM landscapes (Figure 4). The second largest variation, described by PC2, is the MEL fluorescence, which is also notable in the EEM landscapes. Curiously, FLU is the strongest fluorophore in this matrix, despite the fact that its concentration is approx. 20 times lower than the concentration of MEL. Perhaps this is the reason why it is beneficial for the calibrations of MEL to only use parts of the landscape, where FLU is not so dominating. Figure 6 shows the selected parts of the unfolded landscape by regional variable selection by iPLS. From the iPLS plot is it observed that the RMSECV is decreased when only four out of the 18 excitation wavelength are selected (280, 300, 315, and 320 nm).

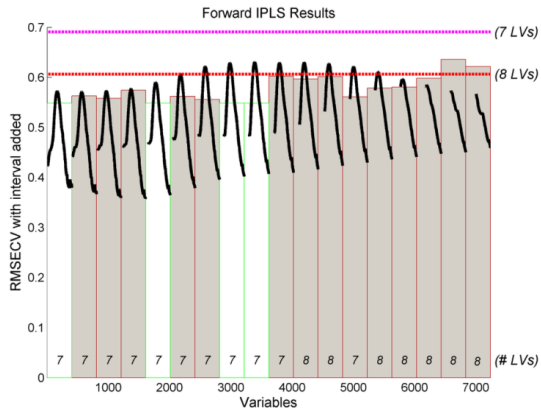

Figure 6. iPLS plot of the selected areas by interval PLS (iPLS) for MEL on logarithmically treated EEM from excitation 280-365 nm and emission 300-500 nm. For each interval consisting of one excitation wavelength (18 in total) a local model is found. These are compared to the global (all interval) models RMSECV for 7 LVs (pink line) and 8 LVs (red line). Only the intervals that will contribute to a lower RMSECV will be included in the final model (white intervals).

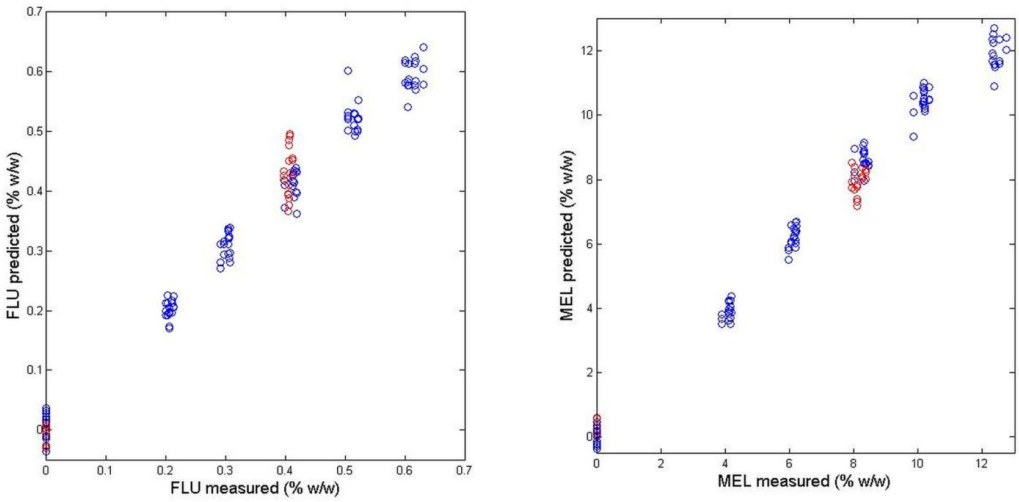

Figure 7. Predicted versus measured for the PLS models a) FLU using 7 Latent Variables b) MEL using 7 Latent Variables. Blue samples are from calibration set, red samples are test samples.

The performance of selected regression models is shown in Figure 7. The figure shows the calibration models for FLU and MEL calibrations performed on unfolded data and Table 2 shows the statistics of the corresponding models. For FLU the calibration model was based on the logarithmic function to Y+1 in order to handle the 0 % placebo. The resulting prediction error (RMSEP) was 0.038 % (w/w) for FLU corresponding to 9.1 % relative to the nominal concentration. From the predictions of earlier lab scale samples and recent real

production batches (Table 3), it appears that the prediction is better for the production batches, than for the lab scale productions. The reason for this may be lot-to-lot variation between batches of excipients that is not included in the calibration. For the MEL calibration only four excitation wavelengths were used and the calibration was based on the logarithmic function to EEM. The resulting RMSEP for MEL was found to be 0.344 % (w/w) corresponding to 4.1 % of the nominal content, see Table 2. The number of latent variables used for the models are relatively high (7 latent variables), compared to other studies. Moreira et al. [29] used 4 latent variables for prediction of paracetamol and caffeine. We ascribe the high number of latent variables to be due to the complexity of the matrix in our application. This is in agreement with Esteves de Silva et al. [30] who found two additional factors necessary to model the verapamil matrix.

For flupentixol, despite the low active content, the highest concentration point (0.625 % w/w) appear to be on the edge of the linear range. This is, however, overcomed by using the logarithmic function, which is in line with the findings of Domike et al. [25]. They found that for higher concentrations of caffeine (5-20 % w/w) the best curve fit was a locarithmic function, due to partial saturation of the detector. Lai et al. [16] solved the problems with inner filter effects due to high fluorescence from triamterene by using longer excitation wavelengths (weaker emission) for samples containing > 1 % triamterene. Moreira et al. [22] describe different possibilities for dealing with a fluorescence signal of too high intensity by modifying the distance between the optical fiber and the sample and changing the excitation slit, thereby reducing the intensity of the radiation source.

Table 2. Calibration overview for FLU and MEL for calibration and test set.

API	No of samples	Nominal conc. (% w/w)	LV	RMSECV	RMSEP	Relative error	Repeatability	SEP	LOD	LOQ
Flupentixol (FLU)										
Calibration	108	0.417	7	0.015		3.6 %	0.020	0.015	0.057	0.171
Test	24	0,417			0.038	9.1 %	0.016			
Melitracen (MEL)										
Calibration	107	8.33	7	0.345		4.1 %	0.310	0.461	0.897	2.717
Test	24	8.33			0.344	4.1 %	0.233			

Table 3. Recovery for FLU and MEL for test samples compared to HPLC analysis.

Sample	FLU recovery ± relative standard deviation[a]	MEL recovery ± relative standard deviation [a]
Lab samples 12b	115.9 % ± 4.4 %	
Lab samples 13b		98.7 % ± 2.1 %
Lab samples 15b	116.1 % ± 9.2 %	100.5 % ± 4.5 %
Lab samples 16a		97.9 % ± 1.9 %
Lab samples 17a	107.8 % ± 3.7 %	
Production batch 2167520	96.3 % ± 4.1 %	94.4 % ± 2.9 %
Production batch 2167521	107.3 % ± 1.8 %	101.5 % ± 5.1 %
Production batch 2167521	95.4 % ± 4.0 %	91.8 % ± 4.3 %

[a)] Only samples at nominal concentration are included

The values for repeatability for FLU and MEL of 0.02 and 0.31 % (w/w) respectively, are relatively high which is assumed to be due to the fact that the fluorescence primarily occurs from the surface of the powder. Therefore, the result depend not only on wavelength but also on the surface topology (particle size and packing density) [15]. In contrast to HPLC analysis in which five tablets are dissolved and analyzed, fluorescence spectroscopy only measures a small part of the sample which is hit by the beam. This sampling inconsistency can be a challenge, especially for low concentrations of API, and one way to solve the problem is to increase the amount of calibration samples. Another way of improving the predictions and the repeatability is to increase the spot size or sampling area (assuming the spot size is bigger than the current sample size) or to measure more tablets from the same batch.

In the production of pharmaceutical tablets, it is desirable to analyze the API content, non-invasively and preferably online. For this purpose, filter fluorescence system would be a possible solution [16]. However, a spectrofluorometer with only one filter cannot compensate for minor changes in the fluorescence from the excipients and it cannot deal with quenching. Due to the complex nature of the FLU/MEL formulation, online measurements is a major challenge as the single point approach did not show good results in the current study. The results obtained by only using the excitation/emission maxima for calibrations are: FLU: RMSEP 0.10 % (w/w), 23.9 % relative deviation, LOD 0.059 %, LOQ 0.180 %. MEL: RMSEP 11.55 % (w/w), 138.6 % relative deviation, LOD 1.12 %, LOQ 3.39 %. In particular, the prediction of the test set seems to be poor for MEL. This may imply that there is more information in the fluorescence landscape, not covered by the chosen excitation wavelength that contains valuable information for especially new batches. The FLU/MEL application is therefore not expected to be suitable for a LIF sensor with only one or few excitation wavelengths. It should, however, be mentioned that the single point approaches have similar LOD and LOQ for both FLU and MEL compared to the model based on landscape data.

In this study, each sample measurement took 7-8 minutes, but it is possible to speed up the process with fewer excitation wavelengths and much fewer emission wavelengths (lower resolution). Simulations of the minimum number of wavelengths required, showed that 12 excitation wavelengths out of 18, and every fourth emission wavelength (2 nm resolution) gave similar results (not shown) as the calibrations listed in Table 2. This could reduce the analysis time down to 1.5 minute per sample. Moreover, it would be of interest to measure fully non-invasively, i.e. directly on the tablet instead of on the ground sample. This optimization should be possible, as a limited number of the tablets were analyzed directly in a Varian Cary Eclipse that uses a different sample holder (result not shown). In this study, a complex dataset with 36 tablet batches based on 12 granulate batches (one for each API level) was investigated. Each granulate consists, of API and several excipients. In many studies, pure standard of the API is added to spread the range of the calibration. This does not take the variation of the excipients from the granulation into account. In this study, the calibrations are based on real batches (lab-scale), and the ratios between the added granulations are varied.

While this feasibility study can serve as a proof of concept, future studies will require many more samples to be included in order to study the different sources of variation [43].

Furthermore, it would be beneficial to investigate the quenching more in detail in order to understand more fully why and how the quenching occurs.

Despite interference from quenching, this study demonstrates that it is possible to achieve relative errors between 3-9 % for both APIs by multivariate data analysis of the unfolded fluorescence landscapes.

4. Conclusion

A total of 36 tablet batches were analyzed with fluorescence spectroscopy using excitation wavelengths from 280-365 nm and emission wavelengths from 300-500 nm. The study demonstrates that single point calibrations are not sufficiently accurate and that a multivariate approach is required. Principal Component Analysis of the unfolded fluorescence data nicely recovers the experimental setup. Partial Least Square regression with variable selection (iPLS) allows for simultaneous quantification of both actives, with an RMSEP of 0.038 % (w/w) and a relative error of 9.1 % for flupentixol (0.417 % w/w), and respective values of 0.344 % (w/w) and 4.1 % for melitracen (8.33 % w/w).

5. Acknowledgment

The authors wish to thank the Danish Ministry of Science, Technology and Innovation for financial support of a PhD stipendium to Solveig Warnecke through the QbD consortium (www.qbd.dk).

6. Reference List

[1] J. Hashash, H. Abdul-Baki, C. Azar, I. I. Elhajj, L. El Zahabi, H. Chaar, A. I. Sharara, Clinical trial: a randomized controlled cross-over study of flupenthixol plus melitracen in functional dyspepsia, *Aliment. Pharm. Therap.* **27,** (2008) 1148-1155.

[2] L. Wedy, G. Bohn, G. Blaschke, Bestimmung tricyclischer Antidepressiva in Körperflüssigkeiten und Organmaterial mittels HPLC, *Fresen. J. of Anal. Chem.* **332,** (1988) 266-269.

[3] A. M. A. Verweij, M. L. Hordijk, P. J. L. Lipman, Liquid chromatographic thermospray tandem mass spectrometric quantitative analysis of some drugs with hypnotic, sedative and tranquillising properties in whole blood, *J. Chromatogr. B.* **686,** (1996) 27-34.

[4] M. Yunus, H. H. Siddiqui, P. Bagga, M. A. Ali, K. Singh, A simple UV spectrophotometric method for the determination of flupenthixol dihydrochloride in bulk and pharmaceutical formulations, *IJPSR* **2,** (2011) 2152-2155.

[5] S. K. Acharjya, P. Panda, P. Mallick, K. R. Kumar, Spectrophotometric methods for simultaneous estimation of flupentixol dihydrochloride and melitracen hydrochloride in combined tablet dosage form, *J. Chem. Pharm. Res.* **2,** (2010) 158-171.

[6] J. Che, Q. Meng, Z. Chen, C. San, Y. Hou, Y. Cheng, Validation of a sensitive LC/MS/MS method for simultaneous quantitation of flupentixol and melitracen in human plasma, *J. Pharmaceut. Biomed.* **45,** (2007) 785-792.

[7] P. Xu, H. D. Li, Y. G. Zhu, B. M. Chen, N. Ma, Y. L. Xie, B. K. Zhang, Validated liquid-liquid extraction and LC-ESI-MS method for the determination of melitracen in human plasma, *Chromatographia* **67,** (2008) 935-939.

[8] X. C. Zuo, B. K. Zhang, B. M. Chen, S. G. Liu, G. P. Yang, S. K. Liu, S. Q. Liu, Z. J. Huang, H. Yuan, LC-ESI-MS determination of flupentixol in human plasma, *Chromatographia* **69,** (2009) 301-305.

[9] K. A. Bakeev, *Process analytical technology: spectroscopic tools and implementation strategies for the chemical and pharmaceutical industries,* Wiley, West Sussex, 2010.
[10] E. Skibsted, S. B. Engelsen, *Spectroscopy for process analytical technology (PAT)* in: *Encyclopedia of Spectroscopy and Spectrometry* (2010) 2651-2661.
[11] S. S. Thosar, R. A. Forbess, N. K. Ebube, Y. X. Chen, R. L. Rubinovitz, M. S. Kemper, G. E. Reier, T. A. Wheatley, A. J. Shukla, A comparison of reflectance and transmittance near-infrared spectroscopic techniques in determining drug content in intact tablets, *Pharm. Dev. Technol.* **6,** (2001) 19-29.
[12] J. Christensen, L. Nørgaard, R. Bro, S. B. Engelsen, Multivariate autofluorescence of intact food systems, *Chem. Rev.* **106,** (2006) 1979-1994.
[13] A. L. Pomerantsev, O. Y. Rodionova, Process analytical technology: a critical view of the chemometricians, *J. Chemometr.* **26,** (2012) 299-310.
[14] J. C. Alves, R. J. Poppi, Simultaneous determination of acetylsalicylic acid, paracetamol and caffeine using solid-phase molecular fluorescence and parallel factor analysis, *Anal. Chim. Acta* **642,** (2009) 212-216.
[15] C. K. Lai, C. C. Cooney, Application of a fluorescence sensor for miniscale on-line monitoring of powder mixing kinetics, *J. Pharm. Sci.* **93,** (2004) 60-70.
[16] C. K. Lai, A. Zahari, B. Miller, W. E. Katstra, M. J. Cima, C. L. Cooney, Nondestructive and on-line monitoring of tablets using light-induced fluorescence technology, *Aaps PharmSciTech* **5,** (2004) E3.
[17] C. K. Lai, D. Holt, J. C. Leung, C. L. Cooney, G. K. Raju, P. Hansen, Real time and noninvasive monitoring of dry powder blend homogeneity, *Aiche J.* **47,** (2001) 2618-2622.
[18] S. M. Hassan, F. Belal, F. Ibrahim, F. A. Aly, Fluorometric determination of some thioxanthene derivatives in dosage forms, *Talanta* **36,** (1989) 557-560.
[19] F. A. Aly, Difference spectrophotometric determination of some pharmaceutically important thioxanthene derivatives in dosage forms, *Microchim. Acta* **110,** (1993) 187-192.
[20] I. A. Shehata, S. M. El-Ashry, M. A. El-Sherbeny, D. T. El-Sherbeny, F. Belal, Fluorimetric determination of some thioxanthene derivatives in dosage forms and biological fluids, *J. Pharmaceut. Biomed.* **22,** (2000) 729-737.
[21] H. D. Dell, J. Fiedler, R. Kamp, Fluorimetrische Bestimmung geringer Mengen von Thioxanthenen durch Spaltung zu Thioxanthon bzw. dessen Derivaten, *Fresen. J. Anal. Chem.* **253,** (1971) 357-360.
[22] A. B. Moreira, H. P. M. Oliveira, T. D. Z. Atvars, I. L. T. Dias, G. O. Neto, E. A. G. Zagatto, L. T. Kubota, Direct determination of paracetamol in powdered pharmaceutical samples by fluorescence spectroscopy, *Anal. Chim. Acta* **539,** (2005) 257-261.
[23] A. B. Moreira, I. L. T. Dias, G. O. Neto, E. A. G. Zagatto, L. T. Kubota, Solid-phase fluorescence spectroscopy for the determination of acetylsalicylic acid in powdered pharmaceutical samples, *Anal. Chim. Acta* **523,** (2004) 49-52.
[24] A. B. Moreira, I. L. T. Dias, G. O. Neto, E. A. G. Zagatto, M. M. C. Ferreira, L. T. Kubota, Solid-phase spectrofluorimetric determination of acetylsalicylic acid and caffeine in pharmaceutical preparations using partial least-squares multivariate calibration, *Talanta* **67,** (2005) 65-69.
[25] R. Domike, S. Ngai, C. L. Cooney, Light induced fluorescence for predicting API content in tablets: Sampling and error, *Int. J. Pharm.* **391,** (2010) 13-20.
[26] M. M. Karim, C. W. Jeon, H. S. Lee, S. M. Alam, S. H. Lee, J. H. Choi, S. O. Jin, A. K. Das, Simultaneous determination of acetylsalicylic acid and caffeine in pharmaceutical formulation by first derivative synchronous fluorimetric method, *J. Fluoresc.* **16,** (2006) 713-721.
[27] M. del Olmo, C. Diez, A. Molina, I. de Orbe, J. L. Vilchez, Resolution of phenol, o-cresol, m-cresol and p-cresol mixtures by excitation fluorescence using partial least-squares (PLS) multivariate calibration, *Anal. Chim. Acta* **335,** (1996) 23-33.
[28] A. Navalon, R. Blanc, M. del Olmo, J. L. Vilchez, Simultaneous determination of naproxen, salicylic acid and acetylsalicylic acid by spectrofluorimetry using partial least-squares (PLS) multivariate calibration, *Talanta* **48,** (1999) 469-475.
[29] A. B. Moreira, I. L. T. Dias, G. O. Neto, E. A. G. Zagatto, L. T. Kubota, Simultaneous spectrofluorimetric determination of paracetamol and caffeine in pharmaceutical preparations in solid-phase using partial least squares multivariate calibration, *Anal. Lett.* **39,** (2006) 349-360.
[30] J. C. G. Esteves da Silva, J. M. M. Leitão, F. S. Costa, J. L. A. Ribeiro, Detection of verapamil drug by fluorescence and trilinear decomposition techniques, *Anal. Chim. Acta* **453,** (2002) 105-115.
[31] J. M. M. Leitão, J. C. Esteves da Silva, A. J. Girón, A. M. de la Peña, Optimization of verapamil drug analysis by excitation-emission fluorescence in combination with second-order multivariate calibration, *J. Fluoresc.* **18,** (2008) 1065-1076.
[32] A. García-Reiriz, P. C. Damiani, M. J. Culzoni, H. C. Goicoechea, A. C. Olivieri, A versatile strategy for achieving the second-order advantage when applying different artificial neural networks to non-linear

second-order data: Unfolded principal component analysis/residual bilinearization, *Chemometr. Intell. Lab.* **92,** (2008) 61-70.
[33] Y. Ni, Y. Lai, S. Kokot, Fluorescence spectral analysis for the discrimination of complex, similar mixtures with the aid of chemometrics, *Appl. Spectrosc.* **66,** (2012) 810-819.
[34] K. Villez, K. Steppe, D. J. W. De Pauw, Use of unfold PCA for on-line plant stress monitoring and sensor failure detection, *Biosyst. Eng.* **103,** (2009) 23-34.
[35] S. Wold, K. Esbensen, P. Geladi, Principal component analysis, *Chemometr. Intell. Lab.* **2,** (1987) 37-52.
[36] S. Wold, H. Martens, H. Wold, The multivariate calibration-problem in chemistry solved by the PLS method, *Lect. Notes Math.* **973,** (1983) 286-293.
[37] L. Nørgaard, A. Saudland, J. Wagner, J. P. Nielsen, L. Munck, S. B. Engelsen, Interval partial least-squares regression (iPLS): A comparative chemometric study with an example from near-infrared spectroscopy, *Appl. Spectrosc.* **54,** (2000) 413-419.
[38] K. H. Esbensen, D. Guyot, F. Westad, L. P. Houmøller, *Multivariate data analysis, in practice, an introduction to multivariate data analysis and experimental design,* CAMO AS, Oslo, 2002, 19-74.
[39] I. C. H. *Guideline, Validation of analytical procedures: text and methodology Q2 (R1),* IFPMA*: Geneva* (2005).
[40] R. Bro, PARAFAC. Tutorial and applications, *Chemometr. Intell. Lab.* **38,** (1997) 149-171.
[41] J. R. Lakowicz, *Principles of fluorescence spectroscopy,* Springer, New York, 2006.
[42] D. A. Skoog, F. J. Holler, S. R. Crouch, *Instrumental analysis,* Brooks/Cole, Cengage Learning, Belmont, 2007.
[43] S. Warnecke, Å. Rinnan, M. Allesø, S. B. Engelsen, Measurement of active content in escitalopram tablets by a nearinfrared transmission spectroscopy model that encompasses batch variability, *J. Pharm. Sci.* (2013) 1268-1280.

DEPARTMENT OF FOOD SCIENCE
FACULTY OF SCIENCE · UNIVERSITY OF COPENHAGEN
PHD THESIS 2014 · ISBN 978-87-7611-701-6

SOLVEIG WARNECKE

New PAT tools for assessing content uniformity, sampling error, and degree of crystallinity in pharmaceutical tablets

The pharmaceutical industry faces considerable challenges due to an increasing complexity of products, greater competition in the generic drug arena, and higher regulatory demands to ensure safe and effective pharmaceutical products. Process analytical technology (PAT) tools can provide knowledge of the pharmaceutical drug, both during development and throughout the production. The usage of PAT tools is encouraged by the regulatory authorities, and therefore the interest in new and improved PAT tools is increasing. The main purpose of introducing Quality by Design (QbD) and PAT in pharmaceutical production is to introduce innovation in the full scale production and to continuously increase the knowledge of the pharmaceutical processes, products, and how they relate to each other, so it is possible to produce pharmaceutical products at a high and consistent quality. This gives benefits to the consumer, the regulatory authorities, and the pharmaceutical manufacturers.

The PAT tools include a wide range of disciplines, including process analyzers (e.g. spectroscopic sensors), multivariate statistical analysis (e.g. chemometric data treatment), process control, continuous improvement, and knowledge management. The real advantage of PAT tools lay in the combination of the different disciplines. This could be spectroscopy-based process analyzer that monitors the pharmaceutical product including latent factors that could influence on the final product quality. Chemometric data treatment can then be used to extract the relevant information from the data, and process control can ensure low variation in the final product quality. This can help to optimize the production, allow real-time product release, and potentially replace the expensive, destructive, and time consuming laboratory testing that is currently the standard practice in traditional pharmaceutical industry.

In this thesis, three spectroscopic PAT tools are investigated, near-infrared-, terahertz-, and fluorescence- spectroscopy. These techniques have been evaluated with chemometrics and theory of sampling. The first study focused on the critical but rather overlooked sampling uncertainty that exists in all analytical measurements. The sampling error was studied using an example involving near infrared transmission (NIT) spectroscopy to examine content of uniformity of escitalopram tablets. The second study investigated the potential use of terahertz time domain spectroscopy (THz-TDS) to quantify crystallinity in binary mixtures of amorphous and crystalline lactose. Finally, the third study investigated the use of fluorescence spectroscopy to simultaneously predict two APIs in a tablet formulation: flupentixol (FLU) in low dosage and melitracen (MEL).

SL grafik